DISSERTATION

PREDICTIVE MODELS OF INDIVIDUAL TREE HEALTH: THE UTILITY OF UNCREWED AERIAL SYSTEM DATA TO INFORM FOREST MANAGEMENT

Submitted by

Lauren E. Lad

Department of Forest and Rangeland Stewardship

In partial fulfillment of the requirements

For the Degree of Doctor of Philosophy

Colorado State University

Fort Collins, Colorado

Spring 2025

Doctoral Committee:

Advisor: Wade T. Tinkham
Co-Advisor: Camille Stevens-Rumann

Alistair M.S. Smith
Melanie K. Vanderhoof
Jody C. Vogeler

ABSTRACT

PREDICTIVE MODELS OF INDIVIDUAL TREE HEALTH: THE UTILITY OF UNCREWED AERIAL SYSTEM DATA TO INFORM FOREST MANAGEMENT

Informed forest management is an essential tool for increasing forest resilience as global climate change increases the frequency and severity of disturbances. Drought and fire are inherent components of natural forest ecosystems, yet the increase in their occurrence combined with increasing severity threatens forest recovery pathways and their ability to sequester carbon. Fire is an essential disturbance that regulates both local and global ecosystem processes and functions. In forests of the United States, fire exclusion during the 20th century drove increases in vegetation density and connectivity, while altering ecosystem composition and structure. As a result of this increase in forest density and fuels, the U.S. has experienced increases in the severity, size, and frequency of wildfires, and drought. Fuels treatments in the form of mechanical thinning and prescribed fire provide opportunities to reduce forest density and fuels, research treatment effectiveness, and reduce the risk of catastrophic fires. Remote sensing allows researchers to collect spatially continuous data on forest conditions both before and after treatments, to study treatment-based impacts. Uncrewed aerial systems (UAS), specifically, provide a tool with user-controlled temporal and spatial resolutions. These systems enable the collection of multispectral and three-dimensional data, via structure from motion (SfM) or LiDAR, allowing researchers to examine changes to structure, composition, and health at ultra-high-resolution. The research within this dissertation focuses on combining pre- and post-treatment multispectral and structural data to

assess individual tree health and changes to that health induced by disturbances. Chapter 2 investigates the utility of band-equivalent reflectance (BER) data from a consumer-grade multispectral UAS camera to predict sapling drought stress in western white pine (*Pinus monticola*) and Douglas-fir (*Pseudotsuga menziesii* var. *glauca*) through a controlled laboratory experiment. The results demonstrate that BER data can reliably detect physiological stress under controlled conditions, providing a strong foundation for using low-cost remote sensing to monitor tree health. Chapter 3 evaluates the transferability of the lab-developed BER models to mature ponderosa pine (*Pinus ponderosa*) and Douglas-fir forests in northern Colorado. This chapter evaluates the models' ability to predict relative drought stress in natural forests and explores the development of site-specific models to improve accuracy. Results reveal that while lab-based models provide valuable insights, field-developed models significantly enhance predictive performance, emphasizing the importance of adapting methodologies to specific field conditions and species. Chapter 4 quantifies the impact of compounding drought stress and fire, of varied intensities, on sapling physiology and mortality for western white pine and Douglas-fir. This chapter modeled the interaction of sapling drought stress and fire intensity on mortality using a dose-response strategy and pre-fire physiological and morphological characteristics. Results demonstrate that increasing drought stress results in higher post-fire mortality compared to less-stressed saplings subjected to the same fire intensity, regardless of species. Chapter 5 examines our ability to predict individual tree crown volume scorch in longleaf pine (*Pinus palustris*) forests treated with prescribed fire. This chapter assesses the impacts of data collection timing, inclusion of pre-fire data, and spectral range on model accuracy. The results of this chapter demonstrate that crown volume scorch can be successfully

modeled using post-fire imagery as soon as one-day post-fire, with any sensor that includes red-green-blue data. This collection of research advances our understanding on the use of UAS data for modeling forest health. The models of relative drought stress could be integrated with forest structure and composition metrics to inform site-based thinning to optimize post-treatment stand resilience. Further, scorch classification models could be used to examine patterns of fire effects, providing critical feedback about prescribed fire ignition patterns. These models have the potential to be integrated into operational forestry practices and can provide actionable insights to guide management that promotes forest resilience and disturbance recovery.

ACKNOWLEDGEMENTS

I would like to extend my unwavering gratitude to my advisors, Dr. Wade Tinkham and Dr. Camille Stevens-Rumann for their insights, time, patience, and support over the last 5 years. Thank you both for the opportunities you have provided, the knowledge you have instilled in me, and for helping me grow as a scientist. Wade, thank you for continuing to advise me through a job change and for always being ready to talk about the latest rugby matches. Camille, thank you for adopting me into your lab and providing me with a renewed sense of community. I will forever aspire to have the same impact on the people around me that you have had on me.

I would like to thank my committee, Alistair, Melanie, and Jody for their support and guidance. My research would not have been possible without the opportunities you provided or the conversations we shared. You have been influential in shaping the way I think about research. I would also like to thank Dr. Chad Hoffman for providing me with invaluable opportunities both to conduct and discuss research and for helping me see from new perspectives.

I am thankful for the lab mates who helped me along the way. Neal, Laura, Casey, George, and Katarina, thank you for the laughs in the office and the support in the field. To the members of the grad student office, thank you for the distractions, potlucks, and discussions.

DEDICATION

To Nash for being my rock, my lighthouse, my best friend. To my mom who instilled a love of trees and curiosity in me. To my dad who showed me the beauty in the everyday, the art in the mundane. To the friends who remind me where I came from and push me towards where I am going.

TABLE OF CONTENTS

CHAPTER 1 – UAS FOR DISTURBANCE MONITORING: APPLICATIONS AND LIMITATIONS

1.1 Introduction

Forests are an indispensable global resource that help regulate biogeochemical cycling (Bonan, 2008), provide ecosystem services, and support biodiversity (Mori et al., 2016). Forest ecosystems are essential sequesters and contributors in the carbon and water cycles, improving global resilience to climate change (Bonan, 2008; Mina et al., 2022). As climate change increases the frequency, severity, and extent of disturbances such as wildfire (Abatzoglou & Williams, 2016), it promotes feedback loops that reinforce alterations to the timing, retention, and availability of moisture as part of the precipitation regime through increasing temperatures that elevate evapotranspiration (Bolinger et al., 2023). These interacting alterations to natural disturbance cycles are testing the limits of forests' ecological resilience and potentially pushing ecosystems down alternative successional pathways that move systems into a new regime of behavior (Holling, 1973; Anderson-Teixeria et al., 2013; Lucash et al., 2018). Thus, the proactive management of these systems is essential for maintaining global resilience to current and future disturbances and ensuring critical forest ecosystem services are maintained.

The management of forest ecosystems is a complex balance of ecological, economic, social, and cultural objectives. Decisions regarding how and when to manage forests, specifically in the United States, may be informed by structured decision-making, participatory approaches using working groups with varied backgrounds (Aplet et al., 2014), economic drivers such as timber production (Kolo et al., 2020), or by ecological drivers such as climate change resilience (North et al., 2021) and ecosystem service protection (Blattert et al., 2017).

These varied, and sometimes competing, drivers of forest management may be employed individually or in combination with one another, usually with the goal of optimizing forest longevity. That longevity, however, may be defined dissimilarly by different affected entities. For this dissertation, forest longevity refers to the management of forests with the intention of maintaining forest cover and improving or maintaining resilience to disturbances. Thus, forest management to improve this longevity is informed by ecological pressures and the physiology of the species being managed.

As a result of anthropogenic climate change, the frequency, intensity, and severity of wildfires are predicted to increase (Westerling et al., 2006). These changes will alter the observed variability and range of ecological disturbances across the western U.S., and the world. In Colorado, temperature increases may lead to overall decreases in mean annual precipitation and are likely to alter the volume and timing of snow melt and increase the duration, intensity, and spatial extent of droughts (Lukas et al., 2014). Temperature-driven drought, quantified by vapor-pressure deficit, affects the ability of vegetation to photosynthesize and, when sustained, can lead to hydraulic failure or carbon starvation (Adams et al., 2017). Although adapted to semi-arid environments, even species like *Pinus ponderosa* are at risk for drought-induced physiological stress as these landscapes are projected to face more severe and extensive droughts than what existed historically (Partelli-Feltrin et al., 2020). This risk compounds *Pinus ponderosa's* vulnerability to other disturbances such as bark-beetles (Kolb et al., 2019) and wildfire (Pile et al., 2019). Drought-stressed trees are more vulnerable to fire-induced mortality because compounding disturbances can stress trees beyond their adapted level of resilience (Johnstone et al., 2016). Beyond the immediate effects of drought on

fire intensity and severity, extreme drought in the first post-disturbance year also affects the ability of species to regenerate in the years following fire (Young et al., 2018; Guz et al., 2021). Proactive management can promote tree resilience to disturbances. Specifically, reduced stand density is associated with increased growth rates, decreased drought sensitivity (Andrews et al., 2020), lower mortality rates from drought and bark beetles (Restaino et al., 2019), and improved soil moisture availability (Andrews et al., 2020). Forest thinning can be further optimized by retaining trees with better growth form and crown vigor, as these trees often show improved resilience to disturbance (Vernon et al., 2023). Prescribed fire can strategically target the reduction of understory fuels to further increase a site's resilience to future disturbances (Fitzgerald, 2005, Kerns & Day, 2018, Kupfer et al., 2022). This highlights a need for understanding both pre- and post-disturbance forest conditions so that managers can understand divergences between pre- and post-disturbance forest composition.

Forest composition and condition are shaped by the interactions of environmental gradients and disturbances which are often characterized by the resultant mortality, change in species dominance, or change in species composition. These conditions inform forest management, which may be motivated by data collected at multiple scales. Field-survey data such as stem maps may be used to monitor forest condition and composition either at single time points or through time, but often are limited in their spatial extent (Gratzer et al., 2004). Plot-based samples are the most common forest monitoring technique and may be employed using a variety of approaches, making them adaptable to diverse research and management questions, and allowing the sampling to be tailored to specific systems (Burkhart et al., 2018). However, these approaches focus on post-disturbance observations and often lack pre-

disturbance data, which are helpful for contextualizing the impacts directly attributable to a disturbance (White et al., 2023). Further, post-disturbance recovery in most forested systems is highly dependent not only on the severity of disturbance, but on pre-disturbance community composition (Seidl et al., 2014). Additionally, as manual field data collection is labor intensive, efforts are typically limited in their spatial extent and therefore, may overlook important forest conditions, especially in larger projects. As disturbances are projected to increase in frequency, it will be important to prioritize and optimize novel monitoring strategies capable of fully informing and evaluating management decisions.

The combination of pre- and post-fire field and remote sensing data provides an opportunity for differenced metrics that describe the changes directly induced by fires. In pre-fire environments, remote sensing indices have been used to describe conditions such as drought, vegetation vigor, forest species composition and density, and to estimate fuel loading and arrangement (Lentile et al., 2006). In post-fire environments, remote sensing indices have been used to describe conditions such as vegetation consumption, short- and long-term vegetation mortality, and changes to soil properties (Lentile et al., 2006). The combination of pre- and post-fire indices can be used to describe the ecological change undergone during fires at broader scales than those able to be described by field methods alone. Overall, remote sensing of pre- and post-fire environments offers a basis for describing the physiological changes which fires induce.

Passive remote sensing, such as that collected by Landsat or Sentinel-2, can capture multispectral imagery that allows researchers to examine vegetation spectral changes before and after disturbances to describe disturbance-induced stress. The most common passive

remote sensing indices that evaluate drought-induced physiological changes include the Normalized Difference Vegetation Index (NDVI) and the Normalized Difference Wetness Index (NDWI). These indices use a combination of spectral channels to highlight vegetation robustness, water-stress, and a myriad of disturbance effects and interactions (Le et al., 2023). Specifically, a differenced NDVI (dNDVI) has been used to describe vegetation robustness before and after fires by accounting for pre-fire reflectance and the resultant post-fire change to reflectance (Escuin, Navarro, & Fernández, 2007). Another set of remote sensing indices were developed to describe fire severity and include things such as the Normalized Burn Ratio (NBR) (Lentile et al., 2006). These indices were designed to describe fire severity using satellites with resolutions from 30 m to 1 km. These relatively coarse scales average across multiple plants and background substrates (e.g., soil, litter, rock) making it difficult to isolate the spectral signal from the plant functional group of interest. Therefore, while this resolution is useful for describing landscape scale changes it is limited in its applicability to plant-level analysis.

Satellite-based remote sensing by commonly utilized satellites, like MODIS, Landsat, and Sentinel-2, is challenged by the sensor's temporal resolution (1 to 16 days) and spatial resolution (10 m to 1 km), which tend to inversely vary with each other. These limitations can make it difficult to assess forest health and wildfire severity as the spatial details captured or the date of capture may not align with project objectives or the timing of fires (Lentile et al., 2006). Light detection and ranging (LiDAR) systems have been used to assess fine-scale structural parameters such as canopy cover and individual tree crown profiles (Ma et al., 2018). However, repeated LiDAR acquisitions are costly and potentially prohibitively expensive for small-scale projects or for change detection studies (Hummel et al., 2011). Uncrewed aerial

systems (UAS) offer a potential solution to these limitations as the temporal resolution can be controlled by users and repeated flights come at a lower cost than manned aircraft using either optical sensors or active sensors like LiDAR (Christensen, 2015). Furthermore, UASs offer ultra-high-resolution imagery at 1-5 cm resolution and can efficiently collect 10s to 100s of acres per day (Perez-Rodriguez et al., 2019; Perez-Rodriguez et al., 2020). These data can then be used in individual tree detection and extraction scripts to provide assessments of forest structure and composition that can be adapted into forest management plans (Creasy et al., 2021). Integration of UAS monitoring for forest resilience management could combine existing and emergent techniques to provide rapid near-census assessments of tree-level structure, health, and disturbance effects.

UAS are emerging as a prominent tool to cover the gap in data acquisition between field observations and moderate scale remote sensing (1,000s to 10,000s of acres). Between 2012 and 2022, 99 papers focused on the use of UAS data for forest health monitoring (Ecke et al., 2022). The growth in UAS applications is attributed to user-controlled temporal resolution, ultra-high-resolution imagery, cost-efficiency, and flexibility that is not readily matched by other remote sensing options. However, spatial coverage is limited by battery life, with most systems able to collect 10 to 100 acres in a single flight, so UAS-based research should focus on site-specific questions. Stand scale monitoring has often been the focus of existing UAS forest health assessments. Most forest health assessment papers focus on conifers (70%), while only 19.7% of papers focus on drought or fire (Ecke et al., 2022). Significant contributions in these areas include Hernández-Clemente et al. (2012) and D'Odorico et al. (2021) that examined carotenoid content using a green band index and the photochemical reflectance index (PRI),

respectively. Fraser & Congalton (2021) also successfully identified forest health, however, their work focused on New England mixed conifer and broadleaf forests. There is a significant gap in UAS forest health assessments in both the southeastern and southwestern United States, despite the Southeast comprising 90% of the prescribed burn area over the last decade (Cummins et al., 2023), and the Southwest experiencing widespread drought along with a significant increase in the number of large wildfires and total area burned (Ager et al., 2018). In addition to the spatial gap in forest health assessments, few papers have focused on multi-temporal monitoring of forest health (Ecke et al., 2022). Forests are dynamic ecosystems with constantly changing conditions, thus single time points cannot capture the variability of forest conditions, highlighting a need for forest health assessments based on multiple time points. Thus, this dissertation focuses on the southeastern and western US and incorporates data from multiple collection dates to model individual tree health and track changes to that health.

The overall objective of this dissertation is to build upon the existing applications of UAS imagery in forestry to understand how multispectral data can be used to identify individual tree stress. I aim to improve our understanding of the best approaches for summarizing individual tree spectral values, the timing of UAS data collection both pre- and post-management, and the importance of pre-fire data for contextualizing disturbance effects. This dissertation will provide valuable information on our ability to use UAS for forest and disturbance monitoring and aims to improve our understanding of how UAS data can be applied to identify tree-level health metrics.

In Chapter 2 I examine how band equivalent reflectance (BER) of a consumer-grade multispectral UAS camera could be used to predict sapling drought-stress in western white pine

(*Pinus monticola* Douglas ex D. Don) and Douglas-fir (*Pseudotsuga menziessii* (Mirb.) Franco var. *glauca* (Beissn.) Franco) in a laboratory experiment. In Chapter 3, I examine whether those lab-developed models can be applied to mature ponderosa pine (*Pinus ponderosa* Lawson & C. Lawson) and Douglas-fir forests to identify relative drought conditions at sites in northern Colorado. Then, I developed site-specific models of relative tree stress using field data. In Chapter 4, drought-stressed saplings from Chapter 2 were subjected to varying levels of fire radiative energy (FRE) to understand how compounding drought and fire affect sapling physiology and post-fire recovery. Sapling drought stress was then used to model the fire intensity-mortality dose-response relationship. By first testing spectral-based models in a controlled setting, then applying them to natural forests, I expand upon existing knowledge on the scalability of lab-based models and demonstrate the importance of choosing the appropriate spectral summarization approach. Further, by focusing on species that are ecologically significant to western U.S. forests, I explore the feasibility of model transferability. These chapters advance the application of UAS models from controlled laboratory settings to operational forestry practices aiming to improve forest resilience to drought, and compounding drought and fire.

In Chapter 5, I examine how the timing of collection, inclusion of pre-fire data, and choice of spectral range impact the prediction accuracy of crown volume scorch in a longleaf pine (*Pinus palustris* Mill.) forest treated with prescribed fire. The objective of this chapter is to evaluate how timing, pre-fire data, and modeling approach impact model performance and accuracy. This work contributes to our understanding of multi-temporal forest assessments and the adaptation of UAS imagery to model disturbance effects. This chapter outlines a practical,

low-cost approach to collecting and processing UAS imagery to classify tree damage, with applications in evaluating the success of prescribed burns and informing ignition strategies for future burns. Ultimately, this chapter demonstrates how UAS-derived data can be used to optimize fire management practices and support adaptive management in fire-prone ecosystems.

The successful application of the models developed in this dissertation will provide crucial information on the health status of trees affected by disturbances and improve managers' confidence in their treatment approaches. These spectral models can be applied to accurately predict individual tree stress (i.e., relative foliar moisture content and crown volume scorch) resulting from multiple disturbance types and across multiple conifer species. This capability will enable managers to tailor management actions to site-specific conditions, allowing them to mitigate tree stress and improve overall site resilience. Further, this dissertation provides a valuable framework for researchers in the UAS space. Specifically, we discuss best practices for collecting, processing, and applying UAS data for forest disturbance monitoring. This work demonstrates how ultra-high resolution spectral data can be leveraged into actionable metrics that inform both immediate management actions and long-term monitoring approaches. This dissertation bridges the gap between emerging remote sensing techniques and actionable forestry applications to improve our ability to prepare our forests for a changing climate.

1.2 References

Abatzoglou, J. T., & Williams, A. P. (2016). Impact of anthropogenic climate change on wildfire across western US forests. *Proceedings of the National Academy of Sciences*, *113*(42), 11770–11775. https://doi.org/10.1073/pnas.1607171113

Adams, H. D., Zeppel, M. J., Anderegg, W. R., Hartmann, H., Landhäusser, S. M., Tissue, D. T., Huxman, T. E., Hudson, P. J., Franz, T. E., Allen, C. D., Anderegg, L. D., Barron-Gafford, G. A., Beerling, D. J., Breshears, D. D., Brodribb, T. J., Bugmann, H., Cobb, R. C., Collins, A. D., Dickman, L. T., … McDowell, N. G. (2017). A multi-species synthesis of physiological mechanisms in drought-induced tree mortality. *Nature Ecology & Evolution, 1*(9), 1285–1291. https://doi.org/10.1038/s41559-017-0248-x

Ager, A. A., Palaiologou, P., Evers, C. R., Day, M. A., & Barros, A. M. G. (2018). Assessing Transboundary Wildfire Exposure in the Southwestern United States. *Risk Analysis*, *38*(10), 2105–2127. https://doi.org/10.1111/risa.12999

Anderson-Teixeira, K. J., Miller, A. D., Mohan, J. E., Hudiburg, T. W., Duval, B. D., & DeLucia, E. H. (2013). Altered dynamics of forest recovery under a changing climate. *Global Change Biology*, *19*(7), 2001–2021. https://doi.org/10.1111/gcb.12194

Andrews, C. M., D'Amato, A. W., Fraver, S., Palik, B., Battaglia, M. A., & Bradford, J. B. (2020). Low stand density moderates growth declines during hot droughts in semi-arid forests. *Journal of Applied Ecology*, *57*(6), 1089–1102. https://doi.org/10.1111/1365-2664.13615

Aplet, G, Brown, P, Briggs, J. Mayben, S, Edwards, D, and Cheng, T. (2014). Collaborative implementation of forest landscape restoration in the Colorado Front Range. Technical Brief CFRI-TB-1403, Colorado Forest Restoration Institute, Colorado State University, Fort Collins, Colorado.

Blattert, C., Lemm, R., Thees, O., Lexer, M. J., & Hanewinkel, M. (2017). Management of ecosystem services in mountain forests: Review of indicators and value functions for model based multi-criteria decision analysis. *Ecological Indicators*, *79*, 391–409. https://doi.org/10.1016/j.ecolind.2017.04.025

Burkhart, H. E., Avery, T. E., & Bullock, B. P. (2018). Forest Measurements (6th Edition). Waveland Press, Long Grove, Illinois, United States.

Bolinger, R., Lukas, J., Schumacher, R., & Goble, P. (2023). Climate change in Colorado. https://hdl.handle.net/10217/237323

Bonan, G. B. (2008). Forests and Climate Change: Forcings, Feedbacks, and the Climate Benefits of Forests. *Science*, *320*(5882), 1444–1449. https://doi.org/10.1126/science.1155121

Christensen, B. R. (2015). Use of UAV or Remotely Piloted Aircraft and Forward-Looking Infrared in Forest, Rural and Wildland Fire Management: Evaluation Using Simple Economic Analysis. *New Zealand Journal of Forestry Science,* 45(1). https://doi.org/10.1186/s40490-015-0044-9

Creasy, M. B., Tinkham, W. T., Hoffman, C. M., & Vogeler, J. C. (2021). Potential for individual tree monitoring in ponderosa pine dominated forests using unmanned aerial system structure from motion point clouds. *Canadian Journal of Forest Research*, *51*(8), 1093–1105. https://doi.org/10.1139/cjfr-2020-0433

Cummins, K., Noble, J., Varner, J. M., Robertson, K. M., Hiers, J. K., Nowell, H. K., & Simonson, E. (2023). The Southeastern U.S. Prescribed Fire Permit Database: Hot Spots and Hot Moments in Prescribed Fire across the Southeastern U.S.A. *Fire*, *6*(10), Article 10. https://doi.org/10.3390/fire6100372

D'Odorico, P., Schönbeck, L., Vitali, V., Meusburger, K., Schaub, M., Ginzler, C., Zweifel, R., Velasco, V. M. E., Gisler, J., Gessler, A., & Ensminger, I. (2021). Drone-based physiological index reveals long-term acclimation and drought stress responses in trees. *Plant, Cell & Environment*, *44*(11), 3552–3570. https://doi.org/10.1111/pce.14177

Ecke, S., Dempewolf, J., Frey, J., Schwaller, A., Endres, E., Klemmt, H.-J., Tiede, D., & Seifert, T. (2022). UAV-Based Forest Health Monitoring: A Systematic Review. *Remote Sensing*, *14*(13), Article 13. https://doi.org/10.3390/rs14133205

Escuin, S., Navarro, R., & Fernández, P. (2007). Fire severity assessment by using NBR (Normalized Burn Ratio) and NDVI (Normalized Difference Vegetation Index) derived from LANDSAT TM/ETM images. *International Journal of Remote Sensing, 29(*4), 1053-1073. https://doi.org/10.1080/01431160701281072

Fitzgerald, S. A. (n.d.). *Fire Ecology of Ponderosa Pine and the Rebuilding of Fire-Resilient Ponderosa Pine Ecosystems*.

Gratzer, G., Canham, C., Dieckmann, U., Fischer, A., Iwasa, Y., Law, R., Lexer, M. J., Sandmann, H., Spies, T. A., Splechtna, B. E., & Szwagrzyk, J. (2004). Spatio-temporal development of forests – current trends in field methods and models. *Oikos*, *107*(1), 3–15. https://doi.org/10.1111/j.0030-1299.2004.13063.x

Guz, J., Gill, N. S., & Kulakowski, D. (2021). Long-term empirical evidence shows post-disturbance climate controls post-fire regeneration. *Journal of Ecology*, *109*(12), 4007–4024. https://doi.org/10.1111/1365-2745.13771

Hernández-Clemente, R., Navarro-Cerrillo, R. M., & Zarco-Tejada, P. J. (2012). Carotenoid content estimation in a heterogeneous conifer forest using narrow-band indices and PROSPECT + DART simulations. *Remote Sensing of Environment*, *127*, 298–315. https://doi.org/10.1016/j.rse.2012.09.014

Hummel, S., Hudak, A. T., Uebler, E. H., Falkowski, M. J., & Megown, K. A. (2011). A comparison of accuracy and cost of LiDAR versus stand exam data for landscape management on the Malheur National Forest. *Journal of Forestry, 109*(5), 267-273. https://doi.org/10.1093/jof/109.5.267

Johnstone, J. F., Allen, C. D., Franklin, J. F., Frelich, L. E., Harvey, B. J., Higuera, P. E., Mack, M. C., Meentemeyer, R. K., Metz, M. R., Perry, G. L. W., Schoennagel, T., & Turner, M. G. (2016). Changing disturbance regimes, ecological memory, and forest resilience. *Frontiers in Ecology and the Environment, 14(*7), 369–378. https://doi.org/10.1002/fee.1311

Kerns, B. K., & Day, M. A. (2018). Prescribed fire regimes subtly alter ponderosa pine forest plant community structure. *Ecosphere. 9(12): E02529-.*, *9*, e02529. https://doi.org/10.1002/ecs2.2529

Key, C. H., Benson, N. C. (2003). The composite burn index (CBI): field rating of burn severity. US Geological Survey Northern Rocky Mountain Science Center. U.S. Department of the Interior, Geological Survey, Northern Rocky Mountain Science Center.

Kolb, T., Keefover-Ring, K., Burr, S. J., Hofstetter, R., Gaylord, M., & Raffa, K. F. (2019). Drought-Mediated Changes in Tree Physiological Processes Weaken Tree Defenses to Bark Beetle Attack. *Journal of Chemical Ecology*, *45*(10), 888–900. https://doi.org/10.1007/s10886-019-01105-0

Kolo, H., Kindu, M., & Knoke, T. (2020). Optimizing forest management for timber production, carbon sequestration and groundwater recharge. *Ecosystem Services*, *44*, 101147. https://doi.org/10.1016/j.ecoser.2020.101147

Kupfer, J. A., Lackstrom, K., Grego, J. M., Dow, K., Terando, A. J., & Hiers, J. K. (2022). Prescribed fire in longleaf pine ecosystems: Fire managers' perspectives on priorities, constraints, and future prospects. *Fire Ecology*, *18*(1), 27. https://doi.org/10.1186/s42408-022-00151-6

Le, T. S., Harper, R., & Dell, B. (2023). Application of Remote Sensing in Detecting and Monitoring Water Stress in Forests. *Remote Sensing*, *15*(13), Article 13. https://doi.org/10.3390/rs15133360

Lentile, L. B., Holden, Z. A., Smith, A. M., Falkowski, M. J., Hudak, A. T., Morgan, P., . . . Benson, N. C. (2006). Remote Sensing Techniques to Assess Active Fire Characteristics and Post-Fire Effects. International Journal of Wildland Fire, 15(3), 319. https://doi.org/10.1071/wf05097

Lucash, M. S., Scheller, R. M., Sturtevant, B. R., Gustafson, E. J., Kretchun, A. M., & Foster, J. R. (2018). More than the sum of its parts: How disturbance interactions shape forest dynamics under climate change. *Ecosphere*, *9*(6), e02293. https://doi.org/10.1002/ecs2.2293

Lukas, J., Barsugli, J., Doesken, N., Rangwala, I., & Wolter, K. (2014, August). Climate Change in Colorado: A Synthesis to Support Water Resources Management and Adaptation.

Ma, Q., Hu, T., Su, Y., Guo, Q., Battles, J. J., & Kelly, M. (2018). Individual Tree Level Forest Fire Assessment Using Bi-temporal LiDAR Data. *IGARSS 2018 - 2018 IEEE International Geoscience and Remote Sensing Symposium*. https://doi.org/10.1109/igarss.2018.8519445

Mina, M., Messier, C., Duveneck, M. J., Fortin, M.-J., & Aquilué, N. (2022). Managing for the unexpected: Building resilient forest landscapes to cope with global change. *Global Change Biology*, *28*(14), 4323–4341. https://doi.org/10.1111/gcb.16197

Mori, A. S., Lertzman, K. P., & Gustafsson, L. (2017). Biodiversity and ecosystem services in forest ecosystems: A research agenda for applied forest ecology. *Journal of Applied Ecology*, *54*(1), 12–27. https://doi.org/10.1111/1365-2664.12669

North, M. P., York, R. A., Collins, B. M., Hurteau, M. D., Jones, G. M., Knapp, E. E., Kobziar, L., McCann, H., Meyer, M. D., Stephens, S. L., Tompkins, R. E., & Tubbesing, C. L. (2021). Pyrosilviculture needed for landscape resilience of dry western United States forests. *Journal of Forestry, 119*(5), 520–544. https://doi.org/10.1093/jofore/fvab026

Pile, L. S., Meyer, M. D., Rojas, R., Roe, O., & Smith, M. T. (2019). Drought Impacts and Compounding Mortality on Forest Trees in the Southern Sierra Nevada. *Forests*, *10*(3), Article 3. https://doi.org/10.3390/f10030237

Partelli-Feltrin, R., Johnson, D.M., Sparks, A.M., Adams, H.D., Kolden, C.A., Nelson, A.S., Smith, A.M.S (2020). Drought Increases Vulnerability of Pinus ponderosa Saplings to Fire-Induced Mortality. *Fire, 3*(4), 56. https://doi.org/10.3390/fire3040056

Pérez-Rodríguez, L. A., Quintano, C., Fernández-Manso, A., Calvo, L., Marcos, E., & Fernández-Guisuraga, J. M. (2020). Evaluation of prescribed fires from unmanned aerial vehicles (UAVs) imagery and machine learning algorithms. *Remote Sensing, 12*(8), 1295. https://doi.org/10.3390/rs12081295

Pérez-Rodríguez, L. A., Quintano, M. del C., García-Llamas, P., Fernández-García, V., Taboada, A., Fernández-Guisuraga, J. M., Marcos, E., Suarez-Seoane, S., Calvo, L., & Fernández-Manso, A. (2019). Using Unmanned Aerial Vehicles (UAV) for forest damage monitoring in south-western Europe. In E. J. Ientilucci (Ed.), *Imaging Spectrometry XXIII: Applications, Sensors, and Processing* (p. 22). SPIE. https://doi.org/10.1117/12.2531265

Seidl, R., Rammer, W., & Spies, T. A. (2014). Disturbance legacies increase the resilience of forest ecosystem structure, composition, and functioning. *Ecological Applications : A Publication of the Ecological Society of America*, *24*(8), 2063–2077. https://doi.org/10.1890/14-0255.1

Vernon, M. J., Johnston, J. D., Stokely, T. D., Miller, B. A., & Woodruff, D. R. (2023). Mechanical thinning restores ecological functions in a seasonally dry ponderosa pine forest in the inland Pacific Northwest, USA. *Forest Ecology and Management 546*, 121371. https://doi.org/10.1016/j.foreco.2023.121371

Westerling, A. L., Hidalgo, H. G., Cayan, D. R., & Swetnam, T. W. (2006). Warming and earlier spring increase western U.S. Forest wildfire activity. *Science, 313*(5789), 940-943. https://doi.org/10.1126/science.1128834

White, J. C., Hermosilla, T., & Wulder, M. A. (2023). Pre-fire measures of boreal forest structure and composition inform interpretation of post-fire spectral recovery rates. *Forest Ecology and Management*, *537*, 120948. https://doi.org/10.1016/j.foreco.2023.120948

Young, D. J. N., Werner, C. M., Welch, K. R., Young, T. P., Safford, H. D., & Latimer, A. M. (2019). Post-fire forest regeneration shows limited climate tracking and potential for drought-induced type conversion. *Ecology*, *100*(2), e02571. https://doi.org/10.1002/ecy.2571

CHAPTER 2 – EVALUATING PREDICTIVE MODELS OF TREE FOLIAR MOISTURE CONTENT FOR APPLICATION TO MULTISPECTRAL UAS DATA: A LABORATORY STUDY [1]

2.1 Introduction

Foliar moisture content (FMC) is a key indicator of vegetation health and influences individual plant resilience to weather, climatic variability, and disturbances such as insects, disease, and fire [1,2]. Further, foliar moisture content changes seasonally and daily based on evapotranspiration and water loss, or through precipitation and water uptake [1–3]. Beyond indicating the relative ratio of dry and wet plant material, foliar moisture content informs estimates of fire risk and rate of spread [4]. Additionally, foliar moisture plays a key role in the feedback loops of disturbances, such as bark beetles, by influencing the likelihood of infestation and resources available for defense following infestation [5]. Water stress on trees in California, US, recently resulted in >100 million trees succumbing to beetle infestation due to reduced defense mechanisms related to foliar moisture [6]. Lower limit thresholds of foliar moisture also indicate when vegetation is vulnerable to disturbance-induced damage and mortality [7]. Lower foliar moisture content values are related to decreased resilience and increased mortality from both fire and insects [8,9]. Conventional measures of FMC require the collection of foliage from each plant and a comparison of the foliage's dry and wet weight [4,10], providing a sample of the data to represent an entire population. The need to oven-dry specimens can delay the applicability of foliar moisture observations after collection, which

[1] Chapter published as: Lad, L. E., Tinkham, W. T., Sparks, A. M., & Smith, A. M. S. (2023). Evaluating Predictive Models of Tree Foliar Moisture Content for Application to Multispectral UAS Data: A Laboratory Study. *Remote Sensing*, *15*(24), Article 24. https://doi.org/10.3390/rs15245703

limits its use for rapid hazard assessment applications [7]. Although in other parts of the fuel stratum (i.e., woody debris, duff, and litter), there has been the development of rapid sensing systems [11] and research to understand the drivers of moisture content [12,13], limited research has focused on foliar moisture content [3]. As such, there is limited capacity to collect rapid, spatially continuous measures of FMC, particularly at scales and extents relevant to management decision-making (i.e., 10 s of hectares).

One alternative method of assessing FMC continuously and across larger areas is the use of aircraft and satellite-based remote sensing [14]. The Normalized Difference Moisture Index (NDMI), which uses near-infrared (NIR) and short-wave infrared (SWIR) spectral bands, is used to monitor drought because of the index's sensitivity to changes in plant water content [15]. Originally, this index was named the Normalized Difference Water Index (NDWI) but is generally referred to by NDMI following the development of a different NDWI index by McFeeters (1996) [16]. The NDMI was developed using laboratory measurements of reflectance and has since demonstrated its utility in characterizing vegetation drought stress in diverse ecosystems including forested areas [15] and peatlands [17]. At multiple scales and across several conifer species, NDMI and red edge spectral wavelengths have been demonstrated to have a significant correlation with plant water content [18,19]. Seong et al. (2015) used NDMI to assess drought stress in forests in Korea and found that areas with increased NDMI values, indicative of drought-stress, experienced large forest fires, thus showing a causal effect between low FMC and higher fire risk [20]. From satellite observations, NDMI has been demonstrated as a better predictor of live FMC than the more commonly applied Normalized Difference Vegetation Index (NDVI) [21], suggesting its potential for improving coarse-scale management of drought in

forests. However, application of NDMI through satellite-based remote sensing is limited due to its coarse spatial and temporal resolutions. Landsat and Sentinel-2 satellites collect imagery at 30 m and 20 m spatial resolution, respectively, and at 16- and 5-day return intervals. Quantifying FMC using moderate spatial resolution imagery can be problematic because spectral reflectance from individual pixels is a mixture of canopy and understory components, which makes FMC estimation at the plant level challenging. Further, the low (relative to UAS) temporal resolution of these satellites limits the timely assessment of FMC, which varies diurnally [1]. These limitations in resolution restrict its application to inform management decisions that require rapid, timely information such as responding to wildfire incidents or informing early warning systems [7].

At the other end of the spatial resolution spectrum, fine-scale laboratory and field experiments can provide insight into stress impacts on individual plant physiology, growth, and mortality. Several studies have used toxicological dose-response experiments to assess how varying levels of stressors, such as drought and fire, affect conifer sapling physiology and whether these changes can be detected using remote sensing data. Sparks et al. (2016) evaluated the impact of increasing fire radiative energy (FRE), or the total radiative heat flux from surface fires, on *Pinus contorta* var. *latifolia* and *Larix occidentalis* saplings and whether physiological responses could be accurately quantified using foliar spectral reflectance [22]. They found that the change in NDVI (dNDVI) from pre- to post-fire could accurately quantify metrics of physiological stress including reduced net photosynthesis and chlorophyll fluorescence [22]. Other spectral indices such as the Photochemical Reflectance Index (PRI) [23] have also been shown to accurately quantify tree stress. Specifically, Sparks et al. [24] observed

that PRI accurately quantified reductions in net photosynthesis and chlorophyll fluorescence in *Pinus monticola* and *Pseudotsuga menziesii* saplings subjected to fires of varying intensity [24]. Additionally, Partelli-Feltrin et al. [8] examined the interaction of drought-stressed ponderosa pine (*Pinus ponderosa* Lawson and C. Lawson) saplings and FRE doses in a laboratory, finding that drought-stressed saplings died at lower FRE doses than well-watered saplings. These studies demonstrate the utility of fine-scale laboratory experiments for examining linkages between spectral indices derived from foliar spectral reflectance (i.e., NDVI, PRI) and plant physiological metrics (i.e., net photosynthesis, chlorophyll fluorescence, FMC) [8]. Based on previous laboratory studies, there is a clear linkage between pre-fire conifer sapling water stress and a sapling's resilience to fire induced tree mortality [8,22]. However, few tree species and size classes have been assessed, restricting the application of these findings to inform management decision-making processes.

Uncrewed aerial systems (UAS) offer a potential bridge between fine-scale laboratory and field sampling efforts and satellite-derived landscape-scale assessments by providing fine-spatial resolution continuous data at the forest-stand scale [25]. Prior to 2023, UAS were commonly described as unmanned aerial systems, but a change in terminology by the United States Pentagon and the United States National Oceanic and Atmospheric Administration (NOAA) in late 2022 led to the widely adopted shift from unmanned to uncrewed. Specifically, UAS have demonstrated their ability to characterize individual tree attributes, including stem diameter and height, in fire-adapted moderate canopy closure *Pinus ponderosa* forests and provide users with control of the temporal resolution of imagery [26]. A growing range of UAS sensors, such as the MicaSense Dual-Camera (MicaSense, Seattle, WA, USA), provide spectral

information not available on Landsat and Sentinel, including three red edge bands [27,28]. These narrower red edge bands can facilitate early detection of physiological stress and improve the scale of stress-detection through increased spatial resolution compared to satellite imagery [29]. Using high-resolution satellite imagery from RapidEye, Eitel et al. [19] showed that a spectral index using wavelengths in the red edge was able to accurately identify stressed trees in a pinon–juniper woodland 16 days earlier than NDVI, highlighting the utility of red edge spectra for early stress detection. NDVI, and other indices derived from NIR, red, green, and blue spectral bands, have strong potential to predict stress when used as training data in random forest and support vector machine classification models [30]. When comparing a UAS-derived NDVI and National Agricultural Imagery Program imagery for classifying trees into five health classes, the UAS data out-predicted NAIP by 14.97% [30]. However, while indices such as NDVI have proven utility in detecting forest stress, these indices may not be sensitive to the rapid changes in tree moisture that result from environmental stressors [31]. Thus, this study examines a variety of remotely sensed indices to identify which indices may produce robust predictions of drought stress and status.

In this study, the overall objective was to assess if band equivalent reflectance (BER) of a consumer-grade multispectral UAS camera could be used to predict FMC and sapling drought-stress, defined here as saplings with an FMC lower than 120%, for two western United States conifer species: western white pine (*Pinus monticola* Douglas ex D. Don) and Douglas-fir (*Pseudotsuga menziessii* (Mirb.) Franco var. *glauca* (Beissn.) Franco). To address this objective, directly measured FMC of saplings (n = 123) at varying levels of drought stress was collected concurrently with sapling foliar spectral reflectance acquired with a spectroradiometer. This

spectral reflectance data were used as input data for classification and regression models to predict FMC and drought stress status.

2.2 Materials and Methods

2.2.1 Saplings and Study Treatments

Saplings were grown in a climate-controlled greenhouse at the University of Idaho, Moscow, Idaho. Detailed information on sapling growth and storage is described by Smith et al. [32]. A total of 62 western white pine and 61 Douglas-fir saplings were grown for 2 years in 9.5-L pots in the greenhouse before being relocated to the Idaho Fire Initiative for Research and Education (IFIRE) combustion laboratory. Once at the IFIRE lab, both species were randomly divided into a control and three drought groups to provide a range of FMC (Table 2.1). Before the experiment, all seedlings were watered to field capacity daily; then, beginning 25 days before spectral reflectance and FMC measurements, the three drought groups had water withheld for progressively shorter intervals, while the control was watered to field capacity daily. Specifically, water was withheld from Group 3 for 25 days, 19 days for Group 2, and 14 days for Group 1. The 25-day total water withhold period was chosen based on a previous droughting trial that showed significant drought induced mortality starting at this time period. There were three fewer Douglas-fir saplings in the control group due to pre-study mortality. Prior to drought treatments, average (±SE) root collar diameters were 1.7 ± 0.03 cm and 2.1 ± 0.05 cm, and mean heights were 0.82 ± 0.02 m and 1.0 ± 0.02 m for *P. monticola* and *P. menziessii*, respectively.

Table 2.1: Sample size for each drought stress group showing average foliar moisture content (SD) for each group.

Species	Control—0 Days		Group 1—14 Day Drought		Group 2—19 Day Drought		Group 3—25 Day Drought	
	FMC (%)	Sample Size	FMC (%)	Sample Size	FMC (%)	Sample Size	FMC (%)	Sample Size
western white pine	173.69 (17.61)	14	168.78 (19.97)	16	158.25 (18.33)	16	52.40 (55.09)	16
Douglas-fir	148.90 (10.47)	13	158.53 (19.32)	16	103.23 (57.62)	16	19.92 (15.70)	16

2.2.2 Data Collection and Processing

For each of the 123 saplings, we collected foliar spectral reflectance using an ASD FieldSpec Pro spectroradiometer (Malvern Panalytical Ltd., Malvern, UK) equipped with the mineral probe attachment. Each of these measurements represents the average of 10 measurements that the instrument rapidly collects. This spectroradiometer collects measurements at wavelengths between 350 and 2500 nm and has a spectral resolution of 3 nm between 350 and 1000 nm and 10 nm between 1000 and 2500 nm. Prior to export, the data are resampled to 1 nm by the instruments' software, resulting in 2151 spectral bands. Three measurements were acquired in the top 1/3 of the canopy of each sapling, each being the result of 10 rapidly averaged collections by the ASD probe. For each spectral sample, ~5 cm^2 of foliage was positioned between a background object of known reflectance and a mineral probe attachment. Radiance measurements were calibrated using a 100% reflective Lambertian Spectralon panel (Labsphere Inc., North Sutton, NH, USA) prior to the measurement of each new sapling, following Sparks et al. [22]. During the processing of each sapling, ~5 g of needles were collected randomly throughout the top 1/3 of the canopy and immediately had their wet sample weight recorded (±0.01 g). These foliar samples were then oven-dried for 24 h at 100

degrees C and weighed again to acquire their dry weight. Finally, FMC was calculated using the difference between the dry and wet weights of the needles (Equation (1), Figure 2.1) [4].

$$\text{Foliar Moisture Content} = \frac{\text{wet weight (g)} - \text{dry weight (g)}}{\text{dry weight (g)}} \times 100 \quad (1)$$

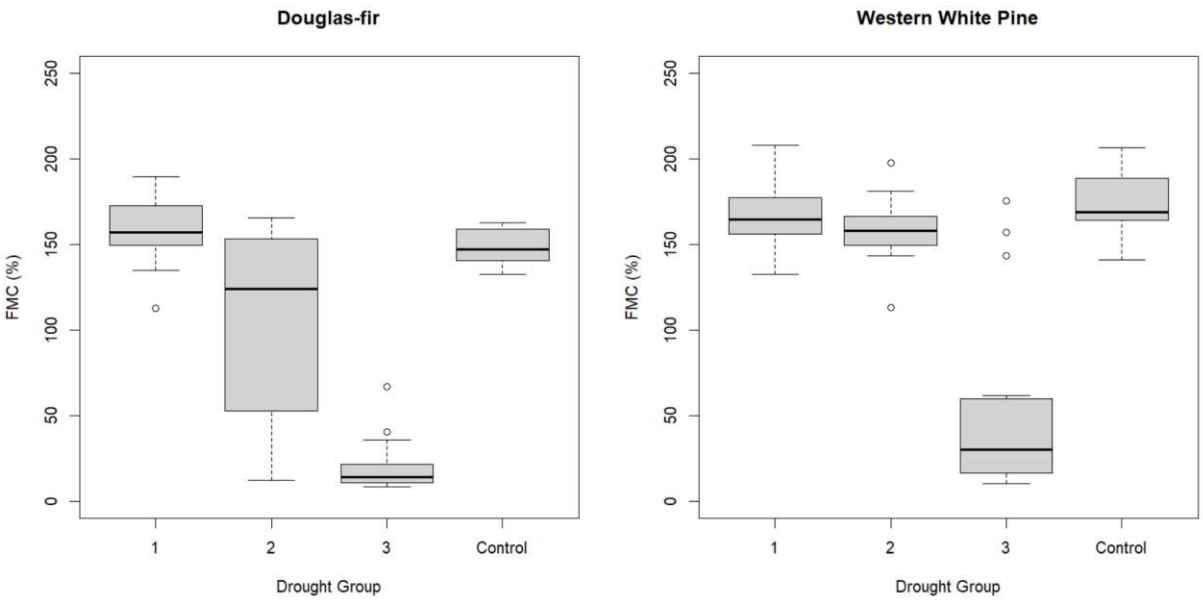

Figure 2.1: Boxplots of foliar moisture content (FMC; %) for each drought group and each species. Within each boxplot, horizontal lines represent the median, the box shows the first and third quartiles, the whiskers represent the maximum and minimum values within 1.5 times the interquartile range, and dots represent outliers.

The three canopy reflectance measurements acquired for each sapling were averaged (Figure 2.2) and converted to band equivalent reflectance (BER) [33,34] of the 10 spectral bands of the MicaSense Dual-Camera system through convolving the spectra with the percent transmissivity values associated with these bands. This transmissivity function enabled the calculation of a single reflectance value for each band representative of the theoretical reflectance value that would be sensed by the MicaSense Dual-Camera system [27]. Using the 10-band values for each sapling, we calculated several spectral indices that have been demonstrated to be useful for predicting various measures of vegetation health (Table 2.2).

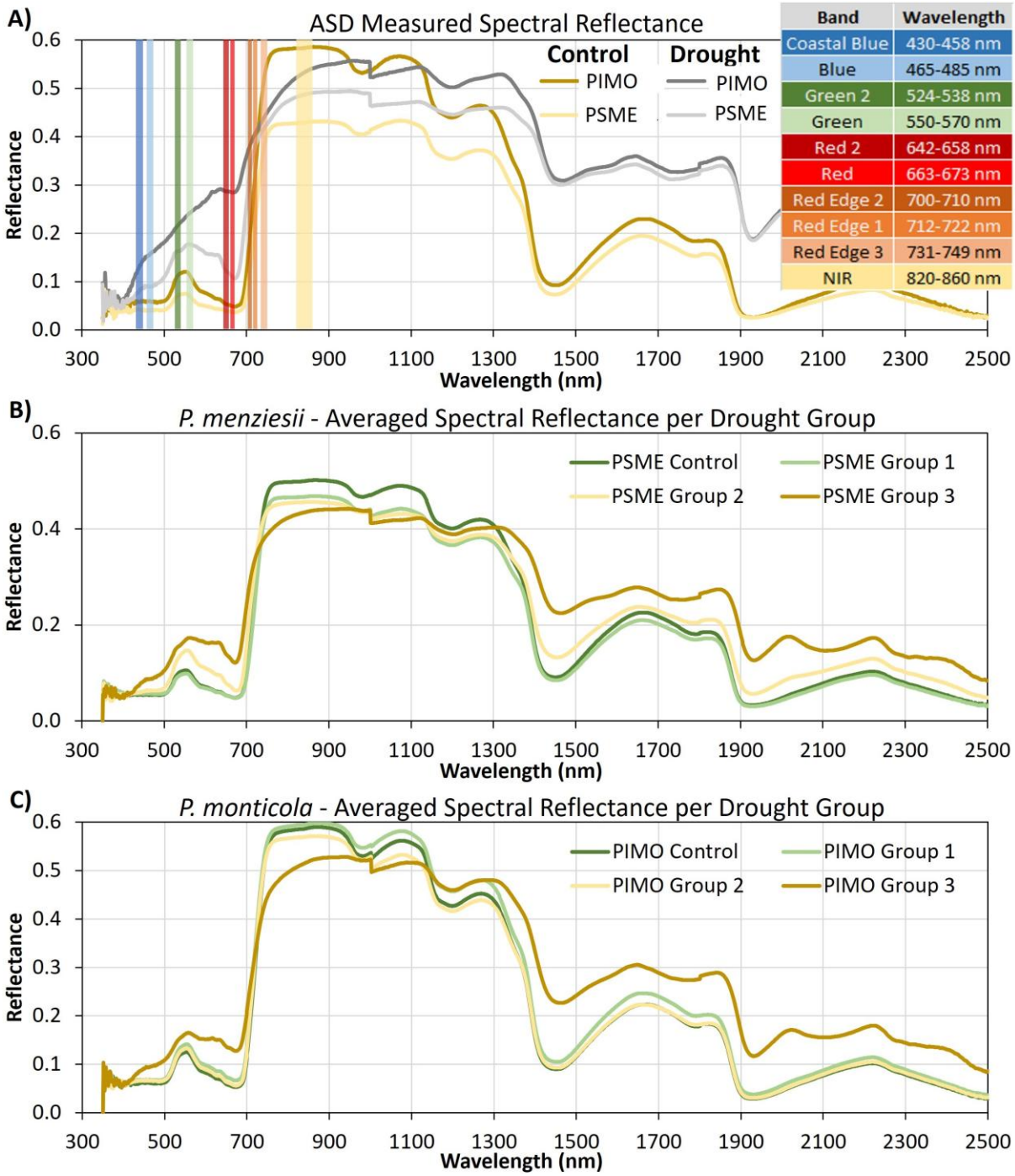

Figure 2.2: Spectroradiometer-measured foliar spectral reflectance of (A) two saplings in the droughted groups in gray (P. monticola FMC: 10.2%; P. menziesii FMC: 8.8%) and two saplings in the control group in yellow (P. monticola FMC: 140.5%; P. menziesii FMC: 140.5%; P. menziesii FMC: 142%). The vertical-colored bars show the 10 spectral bands available on the Micasense Dual-Camera sensor. The associated table colors match the spectral bands and report the range of wavelengths covered by each band. (B) Averaged spectral reflectance of each drought group for western white pine. (C) Averaged spectral reflectance of each drought group for Douglas-fir.

Additionally, one novel index was tested for this study, the foliar moisture content index (FMCI), by examining the gaps in the spectral response curves of drought-stressed versus healthy saplings using similar methods to those employed by Gao (1996; Table 2.2, Figure 2.3) [15]. Specifically, we utilized the spectral separation between healthy and drought-stressed vegetation present in the red edge 3 and NIR channels. This provided 20 predictor variables to test in our models (tree species, 10 spectral bands, and 9 spectral indices).

Table 2.2: Spectral indices derived from the 10 spectral bands available with the MicaSense Dual Camera system, along with the formulation and examples of their previous application.

Index	**Index Name**	**Equation**	**Main Application**
NDVI	Normalized Difference Vegetation Index	$\frac{NIR - Red}{NIR + Red}$	Chlorophyll content/Plant greenness [35]
NDVI2	Normalized Difference Vegetation Index 2	$\frac{NIR - Red_2}{NIR + Red_2}$	Not commonly used; Chlorophyll content/Plant greenness
GNDVI	Green Normalized Difference Vegetation Index	$\frac{NIR - Green}{NIR + Green}$	Photosynthetic activity/ greenness [36]
GNDVI2	Green Normalized Difference Vegetation Index 2	$\frac{NIR - Green_2}{NIR + Green_2}$	Not commonly used
NDRE	Normalized Difference Red Edge	$\frac{NIR - Red\ Edge_1}{NIR + Red\ Edge_1}$	Plant health of mature plants [37]
GRVI	Green Ratio Vegetation Index	$\frac{NIR}{Green}$	Phenological indicator [38]
NDWI	Normalized Difference Water Index	$\frac{Green - NIR}{Green + NIR}$	Water content of water bodies [16]
PRI	Physiological Reflectance Index	$\frac{Green_2 - Green}{Green_2 + Green}$	Crop health monitoring [39]
FMCI	Foliar Moisture Content Index	$\frac{Red\ Edge_3 - NIR}{Red\ Edge_3 + NIR}$	Developed for this study

2.2.3 Model Development

We developed classification and regression-based models to predict drought stress and FMC using the spectral predictor variables as inputs. Prior to model development, we examined predictor variable collinearity (Figure 2.3), and for predictor pairs that had a correlation of >70%, we removed the variable with lower correlation with FMC. The remaining predictors

were evaluated for variable importance using the varImpPlot function in the randomForest package [40] within R statistical software version 4.1.0 [41,42]. This two-step process resulted in five predictor variables which included (in order of importance): NDVI2, red edge 3, PRI, FMCI, and species. For all models, both classification and regression, input data were randomly split into training (70%) and validation (30%) subsets.

Both a random forest classification model (RFCM) and a logistic classification model (LCM) were developed using the training dataset to predict whether saplings were drought-stressed or healthy based on a threshold of above or below 120% FMC. This FMC threshold was used as it represents the approximate moisture content where shrub and tree foliage become more receptive to fire spread [43,44]. We tested these models as the RFCM allows for increased model complexity while the LCM provides more interpretable results. The RFCM was developed using the randomForest package [40] in the R statistical software. The RFCM was run using the five selected predictor variables, with seed 1002 and using 199 decision trees. The LCM was developed using base R and the glm function [41]. Variable selection for the LCM was performed using forward and backward stepwise selection to identify the subset of variables that minimized the Akaike Information Criterion (AIC) in the MASS package [45]. We assessed classification accuracy using confusion matrices calculated between the validation dataset and the model classification results. We report three commonly used accuracy metrics: overall accuracy, omission error and commission error.

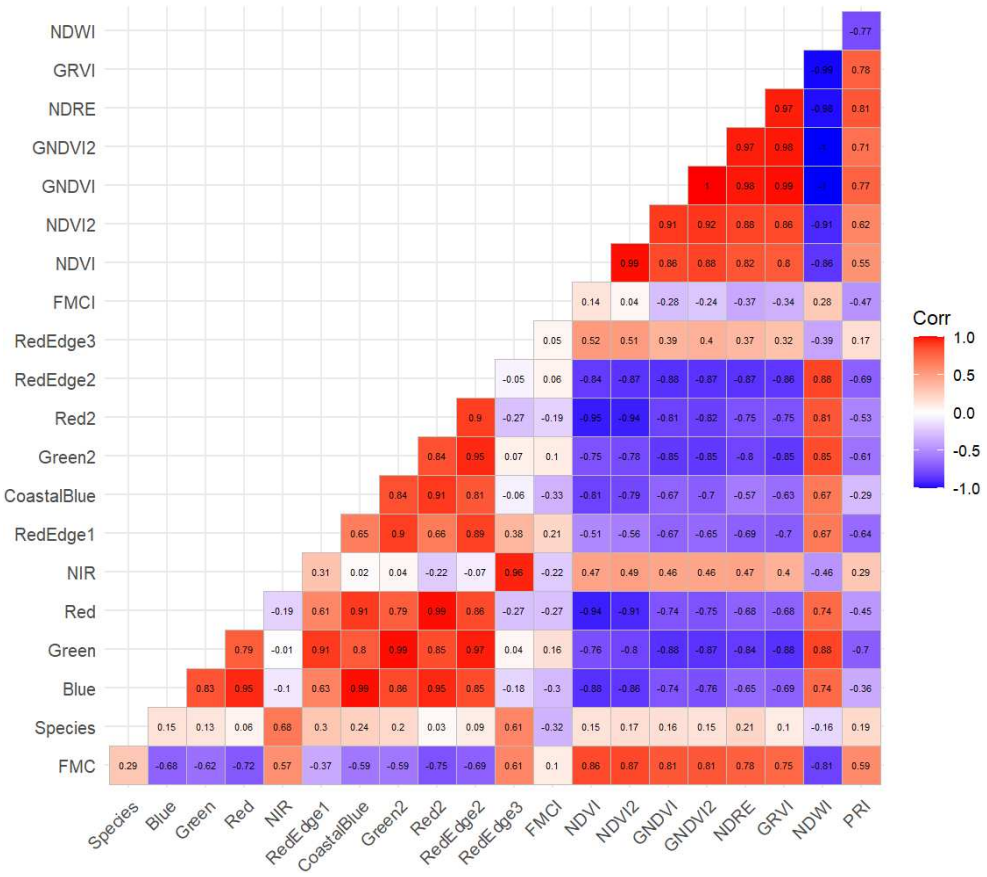

Figure 2.3: Correlation between the 20 predictor variables and foliar moisture content (FMC). For variables with >70% correlation we removed the variables with lower correlation to FMC.

Predictions of FMC as a continuous response were made by developing a set of simple linear models (SLRM), a multiple linear model (MLRM), and a random forest regression model (RFRM). For the SLRM, we compared five univariate models using each predictor variable: NDVI2, red edge 3, FMCI, PRI, and species. For the MLRM, variable selection was conducted using ordinary least squares forward and backstep stepwise selection to identify the variable subset that minimized AIC from the olsrr package in R [46]. Bootstrapping with 100 repetitions was used to resample the training and validation data to avoid overfitting for all of the SLRMs and the MLRM. The RFRM was developed following the same steps as the classification version, with the only difference being the use of FMC as a continuous response variable. Model

performance was assessed using linear regression analysis between the observed FMC and model predicted FMC. Residual standard error and the coefficient of determination (r^2) were computed and used to evaluate the relationship 'goodness of fit'.

2.3 Results

2.3.1 Foliar Moisture and Spectral Variation

Visual comparison of the FMC between the species and across the drought groups shows similar trends with a few small differences (Figure 2.1). The western white pine had both wetter and more variable FMC in all but Drought Group 2 compared to the Douglas-fir. A more continuous distribution of FMC was achieved by the Douglas-fir drought groups, largely due to the wide range of values in Drought Group 2 (Figure 2.1). However, the western white pine resulted in a wider total range of FMC, but with a notable gap in FMC values from ~60% to ~125%.

The spectral response curves varied between species, with western white pine having higher reflectance from ~750–1300 nm compared to Douglas-fir for all drought groups (Figure 2.2B,C). However, the mean reflectance of drought groups varied more for Douglas-fir than western white pine. Spectral separation was only apparent in the green (550–570 nm) and green 2 (524–538 nm) bands for the longest duration drought group (Group 3). For both species, the greatest spectral separation across the drought groups occurred in the NIR (820–860 nm), followed by the red (663–673 nm) and red 2 (642–658 nm) bands (Figure 2). Although outside the spectral bands tested in this study, the shortwave infrared portion of the spectrum also exhibited strong separation of the drought groups for both species.

Evaluation of the 20 predictor variables for collinearity showed that NDVI2 was the strongest single predictor, but that it was highly colinear with several other terms (Figure 2.3). Because of high correlation (>|70%|) with NDVI2, the following predictors were removed from analysis, including coastal blue, blue, green, green 2, red, red edge 2, NDVI, GNDVI, GNDVI2, NDRE, GRVI, and NDWI.

2.3.2 Classification Models

The RFCM retained the NDVI2, PRI, red edge 3, and FMCI. In the final set of predictor variables, species was removed due to its low variable importance. The RFCM had an R^2 of 85.41 and produced a mean square error (MSE) of 0.049, with balanced classification errors between the two classes (Table 2.3). When the RFCM was tested against the validation data, the model resulted in a final overall classification accuracy of 94.44%, with drought-stressed saplings having an omission error of 9.09% and a commission error of 9.09%, while healthy saplings had an omission error of 4.0% and a commission error of 4.0%.

Table 2.3: Confusion matrices of the predicted versus observed class for the random forest classification model (RFCM) and logistic classification model (LCM) using the validation data. Overall accuracies were 94.44% and 97.22% for the RFCM and LCM, respectively.

		Reference Class		
Random Forest		**Drought-Stressed**	**Healthy**	**Commission Error**
Predicted Class	Drought-Stressed	10	1	9.09%
	Healthy	1	24	4.00%
	Omission Error	9.09%	4.00%	
Logistic Regression				
Predicted Class	Drought-Stressed	11	0	0.00%
	Healthy	1	24	4.00%
	Omission Error	8.33%	0.00%	

Prediction accuracy of the LCM was 96.55% for the training data (Table 2.3) and, when tested against the validation data, an overall classification accuracy of 97.22% was achieved.

Omission errors of 8.33% for the drought-stressed saplings and 0% for the healthy saplings and commission errors of 0% for the drought-stressed saplings and 4.0% for the healthy saplings were observed. When developing the LCM, species was the only predictor variable removed during the stepwise variable selection process (Table 2.4). Since a true r^2 cannot be calculated for LCMs, we calculated McFadden's r^2, which has values ranging from 0 to 1, and achieved a value of 0.84. Any McFadden r^2 values over 0.4 demonstrate a strong model fit to the data and high predictive power [47]. The RFCM and the LCM misclassified the same sapling, with the RFCM misclassifying an additional sapling (Table 2.3). One drought-stressed Douglas-fir sapling (FMC: 112%) was confused as healthy by both models. For the RFCM, one healthy western white pine sapling (FMC: 132%) was confused as drought-stressed.

Table 2.4: Logistic classification model (LCM) coefficients. The Z-value is the regression coefficient divided by the standard error.

	Coefficient	**Standard Error**	**Z-Value**	***p*-Value**
Intercept	43.63	18.07	2.41	<0.05
NDVI2	−11.68	7.50	−1.55	0.12
Red edge 3	−89.16	39.14	−2.28	<0.05
FMCI	−115.01	53.35	−2.16	<0.05
PRI	−147.73	56.94	−2.60	<0.05

2.3.3 Regression Models

The best-performing SLRM used NDVI2 as the predictor variable and resulted in an adjusted R^2 of 73.41 ($p < 0.05$) with a residual standard error of 33.08 (Table 2.5). For this model, each 0.1 increase in NDVI2 resulted in a 26.0% increase in FMC. Comparison of predicted SLRM versus observed FMC showed strong general relationships but with the greatest prediction errors in the middle of the range of FMC values (Figure 2.4A). The NDVI2

SLRM explained more than twice as much of the variation in FMC compared to any of the other SLRMs tested.

Table 2.5: Predictor variable results from five simple linear regression models (SLRM).

Predictor Variable	Intercept	Coefficient (SE)	*p*-Value	Residual Standard Error	Adjusted r^2
NDVI2	13.17	267.66 (17.47)	<0.05	33.08	73.41
Red edge 3	−135.46	1504.39 (223.94)	<0.05	52.32	33.91
FMCI	28.13	375.90 (323.54)	0.25	63.18	0.41
PRI	158.16	1732.76 (255.01)	<0.05	52.12	34.44
Species	101.56	36.28 (13.19)	<0.05	61.52	7.09

The MLRM used 100 bootstrap repetitions for resampling, and the OLS stepwise variable selection informed the removal of species. The final MLRM removed species as a predictor and resulted in a final adjusted r^2 of 82.62 ($p < 0.05$) with a residual standard error of 26.77 (Table 2.6). When testing the model against the validation dataset, we achieved an r^2 of 84.57 ($p < 0.05$) with a residual standard error of 25.05. The MLRM represented an ~19% improvement in the model residual standard error over the best SLRM. Each of the spectral indices showed a positive response, indicating that increases in any of the spectral index values resulted in increased FMC prediction (Table 2.6). Comparison of MLRM predictions to observed values showed mostly normally distributed residuals throughout the data range, but 3.4% of samples were predicted to have negative FMC values (Figure 2.4B). The RFRM used NDVI2, red edge 3, FMCI, and PRI as predictors and had an r^2 of 75.32 and a root mean square error of 31.37 (Figure 2.4C). Inspection of the RFRM predicted versus observed values showed slightly greater

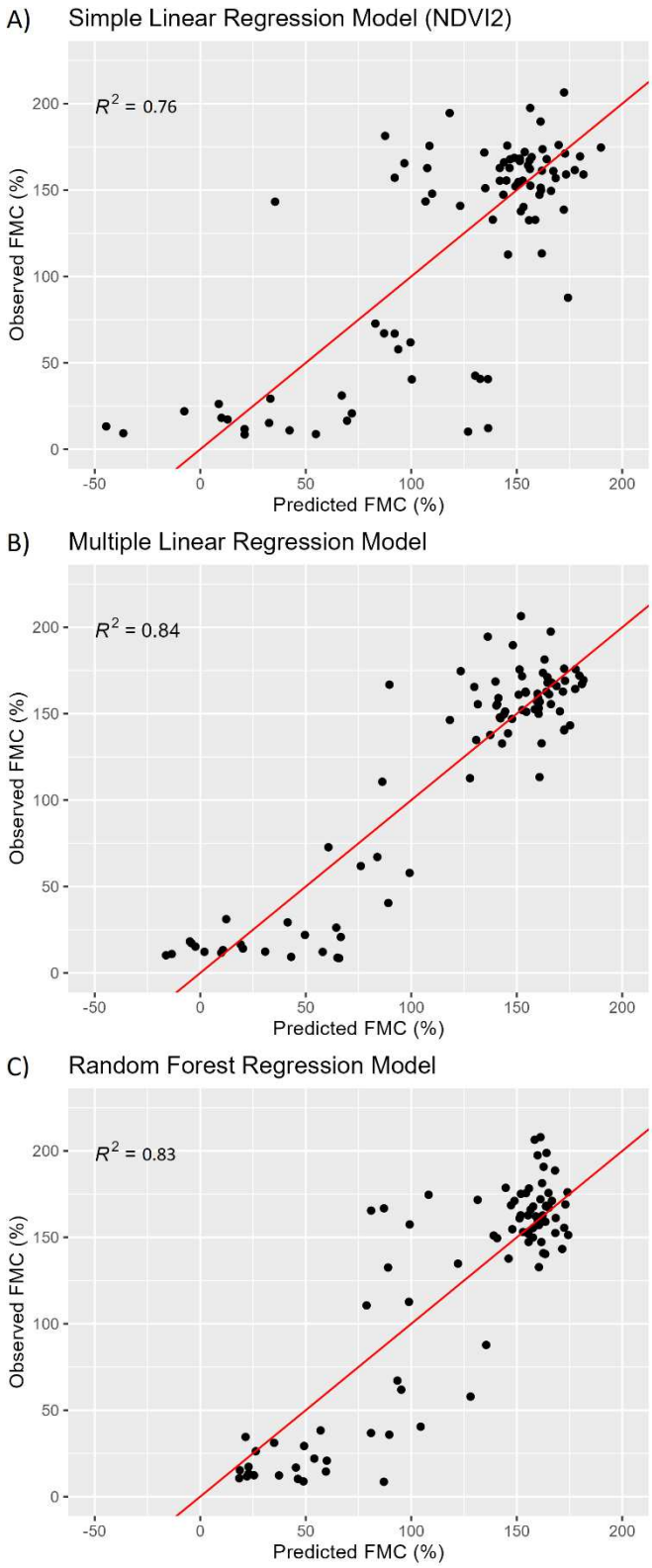

Figure 2.4: Predicted versus observed foliar moisture content (FMC) for (A) the simple linear model (SLM) using NDVI2, (B) the multiple linear regression model (MLRM), and (C) the random forest regression model. The red line in each panel shows the 1:1 relationship.

variation in prediction accuracy in the middle of the dataset compared to the MLRM but eliminated the negative predictions seen from the MLRM (Figure 2.4C).

Table 2.6: Multiple linear regression model (MLRM) output table.

	Coefficient	**Standard Error**	**T Value**	***p*-Value**	**AIC**
Intercept	−226.61	41.18	−5.50	<0.05	-
NDVI2	138.64	21.39	6.48	<0.05	860.96
Red edge 3	611.92	149.30	4.10	<0.05	850.84
FMCI	851.31	159.19	5.38	<0.05	833.78
PRI	1039.63	202.10	5.14	<0.05	854.59

2.4 Discussion

The strongest-performing drought stress classification and FMC regression models were the LCM and the MLRM, with an overall accuracy of 96.55% and r^2 of 82.62, respectively. Both models used NDVI2, PRI, red edge 3, and FMCI as their predictor variables. The MLRM model explained 82.6% of the variation but produced a residual standard error of 26.7% FMC. While this error level is fairly consistent in an absolute sense throughout the tested range of FMC values, the relative magnitude of the error is going to be exacerbated at lower FMC levels. While the model captures the general trend in FMC, it may struggle to differentiate trees near the critical 120% FMC level. The high accuracy of the LCM indicates that a consumer-grade UAV sensor, such as the MicaSense Dual-Camera, could accurately predict the drought status of Douglas-fir and western white pine. The results also suggest that this approach could be used to assess the drought stress status of other tree species and potentially be scaled across landscapes in combination with coarser-resolution imagery with further study. The MLRM could have applications where there is a need to assess conifer physiology, ignition risk, and/or susceptibility to insects and disease. The fact that the tested species represent both short- and

long-needle conifers, which did not impact model performance, is promising for the potential transference of these relationships to other conifer species. However, more studies are needed with additional conifer species in both controlled laboratory and natural forest settings to understand if these relationships are similar across species and scale to older and larger trees.

The models developed in this study use existing spectral indices, and combined with the high model accuracy, suggests that UAVs equipped with similar sensors could improve the spatial resolution and scale of FMC predictions. To the authors' knowledge, no prior studies exist which quantify the foliar moisture content and drought stress of conifers using a UAS; however, Blanco et al. [48] were able to quantify cherry tree leaf water potential (r^2 = 0.67) using UAS-derived NDVI. Studies in agricultural systems have achieved root mean square error values as low as 1% when predicting maize FMC using data from a similar UAS multispectral sensor to that tested in this study [49]. Previous studies predicting FMC in grasslands have achieved r^2 values of 0.91 using MODIS imagery at 500 m spatial resolution [50], while models of FMC using hyperspectral data have predicted FMC of forest canopies using the normalized difference infrared index and achieved an r^2 of 0.9 [51]. However, these hyperspectral data, part of the NASA HyspIRI Mission, have not yet been launched, precluding their immediate application [51]. While a range of success has been found in predicting FMC across various ecosystems from moderate resolution sensors [52–56], these sensors are unable to provide the individual tree-level information needed for management decisions related to promoting resistance and resilience to disturbances at the stand-level.

Our MLRM and LCM models both retained NDVI2, PRI, red edge 3, and FMCI as significant predictors. NDVI2 and FMCI are not widely used indices and the authors could not

identify any papers using either index for tree health assessments. However, NDVI2 is only slightly different from NDVI in that it uses the second red band (red 2) available on the MicaSense Dual-Camera sensor, which is narrower and covers the lower part of the Sentinel-2a red band. This narrowing of the band spectral range might account for the increased performance over satellite-based observations as changes in reflectance are averaged over smaller channels. Similar to NDVI, we would expect NDVI2 to have higher values for vegetation with lower red reflectance, assuming NIR reflectance remains constant. NDVI2 uses lower wavelengths of red light and occurs in a region where there is a larger difference in reflectance between healthy and drought-stressed saplings (Figure 2.2). This narrower band allows us to detect smaller changes in moisture, similar to the increased accuracy seen by Hunt et al. [51] when using hyperspectral imagery. Since FMCI was developed for this study by examining the spectral reflectance signatures of a drought-stressed and healthy sapling, it was expected that FMCI would help predict continuous and classified FMC response variables. However, FMCI had lower explanatory power for predicting FMC than the other final four predictors. This reduced explanatory power is likely due to inconsistent shifts in the red edge 3 band between the two species across the range of FMC. PRI was originally developed for the assessment of agricultural vegetation vigor and moisture and appears to have significant explanatory potential for conifer tree health status [24,57]. Sensors that incorporate short-wave infrared bands would likely result in improved accuracy in predicting FMC as shortwave infrared reflectance is highly responsive to water content in foliage [15,58]. However, current cameras for UAS that operate in the SWIR are costly, potentially limiting the ability for managers to acquire such sensors. As these sensors become more broadly available it would be worth considering SWIR bands in the

prediction of FMC from UAS platforms. Such bands when applied through hyperspectral remote sensing have provided substantial improvements in predicting FMC [51]. Finally, the red edge 3 band covers a spectral range not available on conventional satellite-based sensors. This spectral range has high reflectance for healthy saplings and lower reflectance for drought-stressed saplings but, compared to other bands and indices used in this study, has relatively low variance across our samples (range of 0.13). Since light is reflected by living vegetation in this red edge 3 channel, consistent differences in reflectance represent potential biologic indicators that can be exploited for predicting FMC.

Modeling results suggest that UAS equipped with sensors like the MicaSense Dual-Camera system could be used for identifying vegetation stress as it relates to changes in FMC. In prescribed fire planning and fire behavior modeling, FMC is an important input and influences manager expectations of fire effects [59]. Additionally, drought-status has a strong correlation in many conifer species with bark beetle susceptibility [60]. Since FMC varies across and within vegetation types and within individual tree crowns, the flexibility of our random forest models may be beneficial for capturing this range of conditions. While our random forest models performed slightly worse than the logistic and multiple linear models, most other UAS studies of foliar moisture have shown that machine-learning strategies achieve the highest model accuracy [49]. Operational field deployment of these methods will need to be flexible enough to overcome vertical and horizontal gradients in FMC within individual tree crowns associated with shadowing and solar angles that impact both reflectance and FMC. Our models were developed based on an average of three FMCs collected randomly across sapling tree crowns. In mature forests, data summarization strategies will need to be explored to account

for variation in the multiple pixels within a single tree crown to accurately characterize the mean or median FMC. Within western US dry conifer forests, reasonable success has been achieved at delineating individual tree crowns from UAS-derived canopy height models [61]. The resulting individual tree crown polygons could be used to isolate the spectra for a single tree for applying models similar to those developed in this study. Successful deployment of such individual tree drought monitoring models holds potential to inform forest thinning operations aiming to improve forest drought resilience. Future work should focus on applying a suite of predictive models in mature forests across a range of site conditions to examine the ability of different models to reliably predict individual tree crown FMC.

2.5 Conclusions

Using spectroradiometer-derived band equivalent reflectance of a multispectral consumer-grade UAS camera, we were able to accurately predict FMC and drought stress status (FMC < 120%) for western white pine and Douglas-fir saplings. While these models were developed using spectroradiometer derived data, the high FMC prediction accuracy using band equivalent reflectance of a UAS sensor suggests that accurate FMC quantification using UAS is possible; however, this study should be repeated using UAS-collected imagery. The logistic model developed in this study to classify stressed and non-stressed saplings had high overall classification accuracy for both species and could be beneficial for land managers seeking to incorporate drought status information when planning prescribed fire or other silvicultural treatments. Similarly, the multiple linear regression model used to predict FMC could aid efforts needing rapid and spatially extensive FMC observations of saplings or mature trees to understand patterns of drought stress within and among forest stands. Specifically, this model

could aid in assessing tree-level physiological responses to different growing environments or treatment designs. While the FMC results in this study are promising, these models need further testing using UAS-derived data across a range of tree sizes and species to determine their applicability and transferability across conifer forests experiencing drought.

2.6 References

1. Keyes, C.R. Foliar Moisture Contents of North American Conifers. In *Fuels Management-How to Measure Success: Conference Proceedings, Portland, OR, USA, 28–30 March 2006*; Proceedings RMRS-P-41; Andrews, P.L., Butler, B.W., Eds.; U.S. Department of Agriculture, Forest Service, Rocky Mountain Research Station: Fort Collins, CO, USA, 2006; pp. 395–399.
2. Martin-Stpaul, N.; Ruffault, J.; Pimont, F.; Dupuy, J. Chapter 2-Fuel Management Live Fuel Moisture Content: Variability, Predictability and Impact on Fire Behavior and Activity. In *Advances in Forest Fire Research 2018*; Coimbra University Press: Coimbra, Portugal, 2018.
3. Jolly, W.; Johnson, D. Pyro-Ecophysiology: Shifting the Paradigm of Live Wildland Fuel Research. *Fire* 2018, *1*, 8. https://doi.org/10.3390/fire1010008.
4. Jolly, W.M.; Hadlow, A.M. A Comparison of Two Methods for Estimating Conifer Live Foliar Moisture Content. *Int. J. Wildland Fire* **2012**, *21*, 180. https://doi.org/10.1071/WF11015.
5. McNichol, B.H.; Clarke, S.R.; Faccoli, M.; Montes, C.R.; Nowak, J.T.; Reeve, J.D.; Gandhi, K.J.K. 6—Relationships between Drought, Coniferous Tree Physiology, and Ips Bark Beetles under Climatic Changes. In *Bark Beetle Management, Ecology, and Climate Change*; Gandhi, K.J.K., Hofstetter, R.W., Eds.; Academic Press: Cambridge, MA, USA, 2022; pp. 153–194, ISBN 978-0-12-822145-7.
6. Hansen, M.E.; Bentz, B.J.; Vandygriff, J.C.; Garza, C. Factors associated with bark beetle infestations of Colorado Plateau ponderosa pine using repeatedly-measured field plots. *For. Ecol. Manag.* **2023**, *545*, 121307. https://doi.org/10.1016/j.foreco.2023.121307.
7. Smith, A.M.S.; Kolden, C.A.; Tinkham, W.T.; Talhelm, A.F.; Marshall, J.D.; Hudak, A.T.; Boschetti, L.; Falkowski, M.J.; Greenberg, J.A.; Anderson, J.W.; et al. Remote Sensing the Vulnerability of Vegetation in Natural Terrestrial Ecosystems. *Remote Sens. Environ.* **2014**, *154*, 322–337. https://doi.org/10.1016/j.rse.2014.03.038.
8. Partelli-Feltrin, R.; Johnson, D.M.; Sparks, A.M.; Adams, H.D.; Kolden, C.A.; Nelson, A.S.; Smith, A.M.S. Drought Increases Vulnerability of Pinus Ponderosa Saplings to Fire-Induced Mortality. *Fire* **2020**, *3*, 56. https://doi.org/10.3390/fire3040056.
9. Robbins, Z.J.; Xu, C.; Aukema, B.H.; Buotte, P.C.; Chitra-Tarak, R.; Fettig, C.J.; Goulden, M.L.; Goodsman, D.W.; Hall, A.D.; Koven, C.D.; et al. Warming Increased Bark Beetle-Induced Tree Mortality by 30% during an Extreme Drought in California. *Glob. Change Biol.* **2022**, *28*, 509–523. https://doi.org/10.1111/gcb.15927.
10. Smith, A.M.S.; Tinkham, W.T.; Roy, D.P.; Boschetti, L.; Kremens, R.L.; Kumar, S.S.; Sparks, A.M.; Falkowski, M.J. Quantification of Fuel Moisture Effects on Biomass Consumed Derived from Fire Radiative Energy Retrievals. *Geophys. Res. Lett.* **2013**, *40*, 6298–6302. https://doi.org/10.1002/2013GL058232.
11. Robichaud, P.R.; Gasvoda, D.S.; Hungerford, R.D.; Bilskie, J.; Ashmun, L.E.; Reardon, J. Measuring Duff Moisture Content in the Field Using a Portable Meter Sensitive to Dielectric Permittivity. *Int. J. Wildland Fire* **2004**, *13*, 343. https://doi.org/10.1071/WF03072.
12. Hyde, J.C.; Smith, A.M.S.; Ottmar, R.D. Properties Affecting the Consumption of Sound and Rotten Coarse Woody Debris in Northern Idaho: A Preliminary Investigation Using Laboratory Fires. *Int. J. Wildland Fire* **2012**, *21*, 596. https://doi.org/10.1071/WF11016.

13. Talhelm, A.F.; Smith, A.M.S. Litter Moisture Adsorption Is Tied to Tissue Structure, Chemistry, and Energy Concentration. *Ecosphere* **2018**, *9*, e02198. https://doi.org/10.1002/ecs2.2198.
14. Chuvieco, E.; Cocero, D.; Aguado, I.; Palacios, A.; Prado, E. Improving Burning Efficiency Estimates through Satellite Assessment of Fuel Moisture Content. *J. Geophys. Res. Atmos.* **2004**, *109,* D14S07. https://doi.org/10.1029/2003JD003467.
15. Gao, B. NDWI—A Normalized Difference Water Index for Remote Sensing of Vegetation Liquid Water from Space. *Remote Sens. Environ.* **1996**, *58*, 257–266. https://doi.org/10.1016/S0034-4257(96)00067-3.
16. McFeeters, S.K. The Use of the Normalized Difference Water Index (NDWI) in the Delineation of Open Water Features. *Int. J. Remote Sens.* **1996**, *17*, 1425–1432. https://doi.org/10.1080/01431169608948714.
17. Meingast, K.M.; Falkowski, M.J.; Kane, E.S.; Potvin, L.R.; Benscoter, B.W.; Smith, A.M.S.; Bourgeau-Chavez, L.L.; Miller, M.E. Spectral Detection of Near-Surface Moisture Content and Water-Table Position in Northern Peatland Ecosystems. *Remote Sens. Environ.* **2014**, *152*, 536–546. https://doi.org/10.1016/j.rse.2014.07.014.
18. Stimson, H.C.; Breshears, D.D.; Ustin, S.L.; Kefauver, S.C. Spectral Sensing of Foliar Water Conditions in Two Co-Occurring Conifer Species: Pinus Edulis and Juniperus Monosperma. *Remote Sens. Environ.* **2005**, *96*, 108–118. https://doi.org/10.1016/j.rse.2004.12.007.
19. Eitel, J.U.H.; Vierling, L.A.; Litvak, M.E.; Long, D.S.; Schulthess, U.; Ager, A.A.; Krofcheck, D.J.; Stoscheck, L. Broadband, Red-Edge Information from Satellites Improves Early Stress Detection in a New Mexico Conifer Woodland. *Remote Sens. Environ.* **2011**, *115*, 3640–3646. https://doi.org/10.1016/j.rse.2011.09.002.
20. Seong, N.; Seo, M.; Lee, K.-S.; Lee, C.; Kim, H.; Choi, S.; Han, K.-S. A Water Stress Evaluation over Forest Canopy Using NDWI in Korean Peninsula. *Korean J. Remote Sens.* **2015**, *31*, 77–83. https://doi.org/10.7780/kjrs.2015.31.2.3.
21. Roberts, D.A.; Dennison, P.E.; Peterson, S.H.; Rechel, J. Use of Normalized Difference Water Index for Monitoring Live Fuel Moisture. *Int. J. Remote Sens.* **2006**, *26*, 1035–1042. https://doi.org/10.1080/0143116042000273998.
22. Sparks, A.; Kolden, C.; Talhelm, A.; Smith, A.; Apostol, K.; Johnson, D.; Boschetti, L. Spectral Indices Accurately Quantify Changes in Seedling Physiology Following Fire: Towards Mechanistic Assessments of Post-Fire Carbon Cycling. *Remote Sens.* **2016**, *8*, 572. https://doi.org/10.3390/rs8070572.
23. Gamon, J.A.; Peñuelas, J.; Field, C.B. A Narrow-Waveband Spectral Index That Tracks Diurnal Changes in Photosynthetic Efficiency. *Remote Sens. Environ.* **1992**, *41*, 35–44. https://doi.org/10.1016/0034-4257(92)90059-S.
24. Sparks, A.M.; Blanco, A.S.; Wilson, D.R.; Schwilk, D.W.; Johnson, D.M.; Adams, H.D.; Bowman, D.M.J.S.; Hardman, D.D.; Smith, A.M.S. Fire Intensity Impacts on Physiological Performance and Mortality in *Pinus monticola* and *Pseudotsuga menziesii* Saplings: A Dose–Response Analysis. *Tree Physiol.* **2023**, *43*, 1365–1382. https://doi.org/10.1093/treephys/tpad051.
25. Pérez-Rodríguez, L.A.; Quintano, C.; García-Llamas, P.; Fernández-García, V.; Taboada, A.; Fernández-Guisuraga, J.M.; Marcos, E.; Suárez-Seoane, S.; Calvo, L.; Fernández-Manso, A. Using Unmanned Aerial Vehicles (UAV) for Forest Damage Monitoring in South-Western

Europe. In *Imaging Spectrometry XXIII: Applications, Sensors, and Processing*; SPIE: Bellingham, WA, USA, 2019.
26. Swayze, N.C.; Tinkham, W.T.; Vogeler, J.C.; Hudak, A.T. Influence of Flight Parameters on UAS-Based Monitoring of Tree Height, Diameter, and Density. *Remote Sens. Environ.* **2021**, *263*, 112540. https://doi.org/10.1016/j.rse.2021.112540.
27. MicaSense. Available online: https://micasense.com/dual-camera-system/ (accessed on 15 September 2020).
28. European Space Agency. Available online: https://sentinel.esa.int/web/sentinel/user-guides/sentinel-2-msi/resolutions/spectral (accessed on 17 March 2023).
29. Dash, J.P.; Watt, M.S.; Pearse, G.D.; Heaphy, M.; Dungey, H.S. Assessing Very High Resolution UAV Imagery for Monitoring Forest Health during a Simulated Disease Outbreak. *ISPRS J. Photogramm. Remote Sens.* **2017**, *131*, 1–14. https://doi.org/10.1016/j.isprsjprs.2017.07.007.
30. Fraser, B.T.; Congalton, R.G. Monitoring Fine-Scale Forest Health Using Unmanned Aerial Systems (UAS) Multispectral Models. *Remote Sens.* **2021**, *13*, 4873. https://doi.org/10.3390/rs13234873.
31. D'Odorico, P.; Schönbeck, L.; Vitali, V.; Meusburger, K.; Schaub, M.; Ginzler, C.; Zweifel, R.; Velasco, V.M.E.; Gisler, J.; Gessler, A.; et al. Drone-Based Physiological Index Reveals Long-Term Acclimation and Drought Stress Responses in Trees. *Plant Cell Environ.* **2021**, *44*, 3552–3570. https://doi.org/10.1111/pce.14177.
32. Smith, A.M.S.; Sparks, A.M.; Kolden, C.A.; Abatzoglou, J.T.; Talhelm, A.F.; Johnson, D.M.; Boschetti, L.; Lutz, J.A.; Apostol, K.G.; Yedinak, K.M.; et al. Towards a New Paradigm in Fire Severity Research Using Dose–Response Experiments. *Int. J. Wildland Fire* **2016**, *25*, 158. https://doi.org/10.1071/WF15130.
33. Trigg, S.; Flasse, S. An Evaluation of Different Bi-Spectral Spaces for Discriminating Burned Shrub-Savannah. *Int. J. Remote Sens.* **2001**, *22*, 2641–2647. https://doi.org/10.1080/01431160110053185.
34. Smith, A.M.S.; Wooster, M.J.; Drake, N.A.; Dipotso, F.M.; Falkowski, M.J.; Hudak, A.T. Testing the Potential of Multi-Spectral Remote Sensing for Retrospectively Estimating Fire Severity in African Savannahs. *Remote Sens. Environ.* **2005**, *97*, 92–115. https://doi.org/10.1016/j.rse.2005.04.014.
35. Rouse, J.W.; Haas, R.H.; Schell, J.A.; Deering, D.W. Monitoring Vegetation Systems in the Great Plains with ERTS. *NASA Spec. Publ*. **1974**, *351*, 309.
36. Perez Castillo, C.J. Determination of Biophysical Variables Using Remote Sensing Techniques. Ph.D. Thesis, The University of Nebraska—Lincoln, Lincoln, NE, USA, 1998.
37. Kostrzewski, M.A. Determining the Feasibility of Collecting High-Resolution Ground-Based Remotely Sensed Data and Issues of Scale for Use in Agriculture. Ph.D. Thesis, The University of Arizona, Tucson, AZ, USA, 2000.
38. Shibayama, M.; Salli, A.; Häme, T.; Iso-Iivari, L.; Heino, S.; Alanen, M.; Morinaga, S.; Inoue, Y.; Akiyama, T. Detecting Phenophases of Subarctic Shrub Canopies by Using Automated Reflectance Measurements. *Remote Sens. Environ.* **1999**, *67*, 160–180. https://doi.org/10.1016/S0034-4257(98)00082-0.

39. Gamon, J.A.; Serrano, L.; Surfus, J.S. The Photochemical Reflectance Index: An Optical Indicator of Photosynthetic Radiation Use Efficiency across Species, Functional Types, and Nutrient Levels. *Oecologia* **1997**, *112*, 492–501. https://doi.org/10.1007/s004420050337.
40. Liaw, A.; Wiener, M. Classification and Regression by randomForest. *R News* **2002**, *2*, 18–22.
41. R: A Language and Environment for Statistical Computing. Available online: https://www.R-project.org/ (accessed on 15 January 2022).
42. Genuer, R.; Poggi, J.-M.; Tuleau-Malot, C. Variable Selection Using Random Forests. *Pattern Recognit. Lett.* **2010**, *31*, 2225–2236. https://doi.org/10.1016/j.patrec.2010.03.014.
43. Live Fuel Moisture Content (NWCG). Available online: https://www.nwcg.gov/publications/pms437/fuel-moisture/live-fuel-moisture-content (accessed on 15 November 2021).
44. Fire Behavior Field Reference Guide, PMS 437|NWCG. Available online: https://www.nwcg.gov/publications/pms437 (accessed on 15 November 2022).
45. Venables, B.; Ripley, B. *Modern Applied Statistics with S*; Springer: Berlin/Heidelberg, Germany, 2002.
46. Olsrr: Tools for Building OLS Regression Models. Available online: https://CRAN.R-project.org/package=olsrr (accessed on 17 March 2023).
47. McFadden, D. Regression-Based Specification Tests for the Multinomial Logit Model. *J. Econom.* **1987**, *34*, 63–82. https://doi.org/10.1016/0304-4076(87)90067-4.
48. Blanco, V.; Blaya-Ros, P.J.; Castillo, C.; Soto-Vallés, F.; Torres-Sánchez, R.; Domingo, R. Potential of UAS-Based Remote Sensing for Estimating Tree Water Status and Yield in Sweet Cherry Trees. *Remote Sens.* **2020**, *12*, 2359. https://doi.org/10.3390/rs12152359.
49. Ndlovu, H.S.; Odindi, J.; Sibanda, M.; Mutanga, O.; Clulow, A.; Chimonyo, V.G.P.; Mabhaudhi, T. A Comparative Estimation of Maize Leaf Water Content Using Machine Learning Techniques and Unmanned Aerial Vehicle (UAV)-Based Proximal and Remotely Sensed Data. *Remote Sens.* **2021**, *13*, 4091. https://doi.org/10.3390/rs13204091.
50. Yebra, M.; Chuvieco, E.; Riaño, D. Estimation of Live Fuel Moisture Content from MODIS Images for Fire Risk Assessment. *Agric. For. Meteorol.* **2008**, *148*, 523–536. https://doi.org/10.1016/j.agrformet.2007.12.005.
51. Hunt Jr, E.R.; Wang, L.; Qu, J.J.; Hao, X. Remote Sensing of Fuel Moisture Content from Canopy Water Indices and Normalized Dry Matter Index. *JARS* **2012**, *6*, 061705. https://doi.org/10.1117/1.JRS.6.061705.
52. Urban, M.; Berger, C.; Mudau, T.E.; Heckel, K.; Truckenbrodt, J.; Onyango Odipo, V.; Smit, I.P.J.; Schmullius, C. Surface Moisture and Vegetation Cover Analysis for Drought Monitoring in the Southern Kruger National Park Using Sentinel-1, Sentinel-2, and Landsat-8. *Remote Sens.* **2018**, *10*, 1482. https://doi.org/10.3390/rs10091482.
53. Hu, X.; Ren, H.; Tansey, K.; Zheng, Y.; Ghent, D.; Liu, X.; Yan, L. Agricultural Drought Monitoring Using European Space Agency Sentinel 3A Land Surface Temperature and Normalized Difference Vegetation Index Imageries. *Agric. For. Meteorol*. **2019**, *279*, 107707. https://doi.org/10.1016/j.agrformet.2019.107707.
54. Wang, L.; Quan, X.; He, B.; Yebra, M.; Xing, M.; Liu, X. Assessment of the Dual Polarimetric Sentinel-1A Data for Forest Fuel Moisture Content Estimation. *Remote Sens.* **2019**, *11*, 1568. https://doi.org/10.3390/rs11131568.

55. Kaiser, P.; Buddenbaum, H.; Nink, S.; Hill, J. Potential of Sentinel-1 Data for Spatially and Temporally High-Resolution Detection of Drought Affected Forest Stands. *Forests* **2022**, *13*, 2148. https://doi.org/10.3390/f13122148.
56. Shorachi, M.; Kumar, V.; Steele-Dunne, S.C. Sentinel-1 SAR Backscatter Response to Agricultural Drought in The Netherlands. *Remote Sens.* **2022**, *14*, 2435. https://doi.org/10.3390/rs14102435.
57. Hernández-Clemente, R.; Navarro-Cerrillo, R.M.; Suárez Barranco, M.D.; Morales Iribas, F.; Zarco-Tejada, P.J. Assessing Structural Effects on PRI for Stress Detection in Conifer Forests. *Remote Sens. Environ.* **2011**, *115*, 2360–2375. https://doi.org/10.1016/j.rse.2011.04.036.
58. Ollinger, S.V. Sources of Variability in Canopy Reflectance and the Convergent Properties of Plants. *New Phytol.* **2011**, *189*, 375–394. https://doi.org/10.1111/j.1469-8137.2010.03536.x.
59. Baeza, M.J.; De Luís, M.; Raventós, J.; Escarré, A. Factors Influencing Fire Behaviour in Shrublands of Different Stand Ages and the Implications for Using Prescribed Burning to Reduce Wildfire Risk. *J. Environ. Manag.* **2002**, *65*, 199–208. https://doi.org/10.1006/jema.2002.0545.
60. Kolb, T.; Keefover-Ring, K.; Burr, S.J.; Hofstetter, R.; Gaylord, M.; Raffa, K.F. Drought-Mediated Changes in Tree Physiological Processes Weaken Tree Defenses to Bark Beetle Attack. *J. Chem. Ecol.* **2019**, *45*, 888–900. https://doi.org/10.1007/s10886-019-01105-0.
61. Creasy, M.B.; Tinkham, W.T.; Hoffman, C.M.; Vogeler, J.C. Potential for individual tree monitoring in ponderosa pine-dominated forests using unmanned aerial system structure from motion point clouds. *Can. J. For. Res.* **2021**, *51*, 1093–1105. https://doi.org/10.1139/cjfr-2020-0433.

CHAPTER 3 – UAS CLASSIFICATION OF DROUGHT STRESS IN PONDEROSA PINE AND DOUGLAS-FIR

3.1 Introduction

Anthropogenic climate change is projected to increase the severity and intensity of drought across the southwestern United States (Cook et al., 2015), impacting western conifer forests through increasing temperatures, precipitation deficits (Cook et al., 2018), and decreasing soil water storage (Liu et al., 2019, Bolinger et al., 2023). Between 2000 and 2019 CE, southwestern North America experienced its second driest two decades since 800 CE, resulting in a regional megadrought (Williams et al., 2020). This region is projected to experience continued trends of increasing temperatures coupled with variable precipitation (Bolinger et al., 2023). Temperature-driven decreases in soil water availability and higher plant water demand are contributing to plant-level physiological stress that reduces resilience to current and future drought (Breshears et al., 2005, Williams et al., 2012). Drought-induced physiological stress in trees reduces their resilience to fire and insect attacks (Sparks et al., 2024). Lower water availability affects trees by reducing foliar moisture content, nutrient uptake, and sap flux, all of which contribute to a tree's ability to withstand disturbances (Kreuzwieser & Gessler, 2010, Ryan, 2011). Drought stress is being compounded by stand density increases relative to historic norms (Mast et al., 1998) due to a legacy of fire suppression over the last century (Littell et al., 2016), which increases forest water demands and further stresses trees (Zhang et al., 2019). These compounding climate and management-

induced demands on moisture availability make forests increasingly susceptible to drought-, fire-, and insect-induced mortality (Williams et al., 2013).

The interaction of drought and stand density stressors contribute to elevated levels of mortality that can drive increases in fine, dead woody fuel accumulation (Ruthrof et al., 2016). Furthermore, increasing temperatures are driving decreases in surface fuel moisture, increasing the likelihood of ignition, fire hazard, and extreme fire days (Alexander & Cruz, 2013, Flannigan et al., 2015). Reduced moisture in both surface and canopy fuels increase the likelihood of fires transitioning from surface and ground fires into ladder fuels and the overstory, resulting in crown fires. Alterations to the drought, fire, and pest disturbance regimes, when coupled with persistent drought in an era of climate change, may facilitate changes to forest successional pathways that result in ecosystem conversion following disturbance-induced mortality (Batllori et al., 2020, Coop et al. 2020). Thus, forest managers must consider the current climate and the projected increase in hot, dry conditions, and work to maintain forest resilience in the face of increasing and compounding disturbances.

A major indicator of water availability in forests is foliar moisture content. Foliar moisture content (FMC) responds to vegetation health and is a surrogate for individual plant resilience to weather, climatic oscillations, and disturbances (Keyes, 2006, Zhang et al., 2019, Sparks et al., 2024). Further, FMC changes daily based on evapotranspiration and water loss, or through precipitation and water uptake (Groover, 2017). Beyond indicating the relative water content in plant material, FMC provides an estimate of fire risk and rate of spread (Jolly & Hadlow, 2012). Conventional measures of foliar moisture require the collection of foliage from each plant and a comparison of the foliage's dry and wet weight (Jolly & Hadlow, 2012),

providing a sample of data to represent an entire population. The need to sample individual plants and oven-dry specimens limits data extent and delays the availability of foliar moisture observations after collection. As such, there is limited capacity to collect rapid, spatially continuous measures of foliar moisture, particularly across management scales (i.e., 10s to 100s hectares).

Satellite-based remote sensing can supplement field data collection to provide landscape-scale assessments of ecosystem stress (Lentile et al., 2006). Landsat (30 m resolution) and Sentinel-2 (10-20 m resolution), for example, are multispectral satellites that have been used to monitor vegetation condition (Humagain et al., 2017, Hogland et al., 2019, Phiri et al., 2020). Plant water status is commonly assessed using spectral indices like the Normalized Difference Vegetation Index (NDVI, Rouse, 1974), Normalized Difference Water Index (NDWI, Gao, 1996), or thermal imagery (Pierce et al., 1990). These moderate-resolution satellite sensors average spectral data across multiple species, vegetation strata, and substrates within a single pixel, smoothing plant and species level variation (Lentile et al., 2006). Thus, forest managers cannot easily leverage this moderate spatial resolution to inform management decisions about which trees to retain or cut during thinning operations.

Uncrewed Aerial Systems (UAS) offer a potential solution to these limitations as the temporal resolution can be controlled by users and the high spatial resolution imagery can be smaller than 3 cm (Perez-Rodriguez et al., 2019). Recent advances in UAS tree-level mapping have been successful in creating near-census maps of tree locations, heights, and diameters at breast height (DBHs) in dry, more open canopy conifer forests (Swayze et al., 2021, Tinkham et al., 2022). As these techniques become refined, UAS estimates of basal area and tree density

achieve precisions of 5% to 10% (Tinkham & Woolsey, 2024) and spatial patterns match field collected data (Hanna et al., 2024). Additionally, several studies have attempted to use UAS multispectral and thermal imagery to estimate FMC or similar vegetation moisture and health metrics for agricultural and crop tree (i.e., cherry, olive, citrus, and chestnut trees) applications with varying success (Ezenne et al., 2019, Blanco et al., 2020, Garza et al., 2020, Grulke et al., 2020, Padua et al., 2020, Marques et al., 2023). In a Northeastern United States forest, Fraser & Congalton (2021) were able to classify between healthy, disturbed through either disease or pests, and degraded trees with 71% accuracy. In a European mixed-conifer forest, Abdollahnejad & Panagiotidis (2020) used multispectral imagery and a support vector machine classifier to classify leaf discoloration as an indicator of health with 84.7% accuracy. These studies show promise for tree-health assessments from UAS multispectral remote sensing, but no studies have examined the disturbance-adapted mixed-conifer forests of the Rocky Mountains, which are particularly at risk for future drought events.

Previous work on individual conifer tree FMC remote sensing used a laboratory setting to develop models to classify drought-stress status and predict continuous FMC from the spectral bands available on a consumer-grade multispectral UAS camera for both a short-needle and long-needle conifer species (Lad et al., 2023). This previous effort examined western white pine and Douglas fir at various levels of drought stress to classify drought status and predict FMC (Lad et al., 2023). Similar to studies monitoring crop FMC, Lad et al. (2023) found that indices such as the NDVI (Normalized Difference Vegetation Index) and PRI (Photochemical Reflectance Index), along with the red edge spectral range (700-720 nm) were the strongest predictors in modeling drought-stress in both short- and long-needle western conifers. Previous

studies have also found PRI to be sensitive to real-time changes in photochemical efficiency (D'Odorico et al., 2021; Vicca et al., 2016), highlighting its utility for assessing tree health changes. Further, Sparks et al. (2016) found that a pre- and post-burning differenced NDVI quantified vegetation stress and burn severity with a high correlation to photosynthetic activity (r^2=0.73-0.85) following a laboratory burn. These modeling approaches, while promising, need to be validated through testing in mature forests of varying densities and drought conditions. Specifically, scaling these models to mature trees may present challenges to accurate quantification of FMC resulting from intra-tree variability or shadowing of lower branches.

Drought events, which decrease FMC, are and will continue to be a driving force of forest health and disturbance risk and recovery, underscoring its importance as a metric to describe forest conditions and to inform management actions. However, no comprehensive methods have yet been validated to predict tree-level FMC in forests. Lad et al. (2023) found that a logistic regression and multiple linear regression model using NDVI, PRI, and red edge spectra were effective in identifying drought stress of saplings in a laboratory setting. Thus, this study will test these models in two mature mixed-conifer forests in northern Colorado. Using the models developed by Lad et al. (2023) we explored the question: Can laboratory-developed models of drought stress be used to identify the gradient of drought stress in a mixed-species conifer forest?

3.2 Methods

3.2.1 Study Area and Field Data Collection

To capture a gradient of FMC, this study was conducted at field sites with varying management histories and topographic complexities. The Estes Park (EP) site was dominated by a northwesterly aspect on a 7-60% slope covering 4.2 hectares and was hand thinned in 2012 to create an open mixed-conifer stand of ponderosa pine (*Pinus ponderosa* Lawson & C. Lawson) and Douglas-fir (*Pseudotsuga menziesii* (Mirb.) Franco var. *glauca* (Beissn.) Franco). The Red Feather Lakes (RFL) site was an untreated 6.0 hectare area of open mixed-conifer forest of ponderosa pine and Douglas-fir on a hill (slope=1-65%) with all aspects covered and featuring exposed rocky outcroppings (Figure 3.1).

Figure 3.1: UAS flight boundaries and derived true color imagery of the A) Red Feather Lakes (RFL) site and B) Estes Park (EP) site with the ESRI Outdoor base map. The northern star on the inset map is the Red Feather Lakes site and the southern star is the Estes Park site.

We calculated mean annual temperature (T, °C) and mean annual precipitation (P, mm) using mean monthly values from PRISM (Parameter elevation Regression on Independent Slopes Model) 30-year normals (1991-2020) at 800 m resolution. These annual means allow us

to characterize typical climatic site conditions. At RFL and EP, mean annual temperatures are 5.6°C and 7.9°C while mean annual precipitation was 444.7 mm and 525.1 mm, respectively. The precipitation received during the sampling year, 2023, was 503.7 mm at RFL and 564.3 mm at EP.

Prior to FMC monitoring, field survey trees were selected by randomly generating 50 points at each site, with the nearest dominant or codominant ponderosa pine or Douglas-fir tree identified for sampling. Limiting the survey to dominant and codominant trees was done to ensure reliable extraction from the UAS point cloud to allow for the testing of these drought models. The sample trees had their height, diameter at breast height (DBH), crown base height (CBH), and species recorded, along with their location using an Emlid Reach RS2+ real-time kinematic GPS (Emlid Tech Kft, Budapest, Hungary).

Each site was sampled two times, for a total of four collection dates (July 25, July 27, September 18, and October 16) and 200 foliar moisture samples (Table 3.1). On each collection date, needle collection began at approximately 10:00 am and continued until 12:00 pm when UAS flights were conducted. Following UAS flights, any remaining trees were sampled, with all moisture samples collected within 2 hours of the UAS acquisition. Needle collection for each tree involved using loppers on an extending pole to clip bundles of needles in each cardinal direction and at varying heights. A minimum of four bundles were clipped from each tree and placed in a weighed and labeled plastic bag and stored in a cooler until they could be processed in the lab that afternoon. Variations in tree height and CBH meant that some samples could only be collected from the lower and middle third of the crown of some individuals. Testing was done on a subsample (n=50) of trees where FMC could be assessed in the lower, middle, and

upper third of individual crowns, with a paired t-test showing no significant differences between FMC at different heights (p=0.12).

Table 3.1: Mean (standard deviation) of sample trees across the two study sites along with dates of the FMC collections. DBH: diameter at breast height, CBH: canopy base height.

Site	ponderosa pine			Douglas-fir			First Collection			Second Collection		
	DBH (cm)	Height (m)	CBH (m)	DBH (cm)	Height (m)	CBH (m)	Julian Date	Temp (°C)	VPD (hPA)	Julian Date	Temp (°C)	VPD (hPA)
Estes Park (EP)	29.4 (7.7)	13.9 (2.2)	3.5 (1.0)	30.7 (12.4)	14.4 (3.5)	2.0 (1.0)	153	21.8	4.5-30.6	206	15.2	4.6-22.2
Red Feather Lakes (RFL)	29.0 (11.3)	10.2 (3.1)	2.4 (1.2)	22.3 (6.8)	9.3 (2.9)	0.7 (0.5)	151	21.9	5.3-35.2	234	7.1	1.4-10.3

In the lab, bundles were removed from their plastic bag, needles and cones were stripped from the branch, and only the needles were added back to the bag. The wet needle weight for each tree was measured by subtracting the weight of the plastic bag from the weight of the needles in the bag. All wet weights were recorded within six hours of field sample collection. Then, needles were transferred to paper bags and dried in an oven at 105 degrees Fahrenheit for at least 48 hours, or until the dry weight had stabilized (Matthews, 2010). Once dry, the dry weight of each sample was measured by weighing the dried needles on a tared scale. All weights were recorded using an OHAUS scale with a precision of 0.01 grams (OHAUS Corporation, Parsippany, NJ, USA). The FMC of each sample was calculated using Equation 1 (Jolly & Hadlow, 2012).

$$Foliar\ Moisture\ Content = \frac{(Wet\ Weight - Dry\ Weight)}{Dry\ Weight}\ x\ 100 \quad [1]$$

UAS flights were conducted as close to 12:00 as possible to align with the sun's peak and reduce shadowing in the imagery. Acquisitions were conducted using a DJI Matrice 210V2 (DJI, Shenzhen, China) with a Micasense 10-band Dual-Camera system attached (Micasense, Seattle,

WA, USA) and lasted an average of 20 minutes at each site. Prior to takeoff and immediately after landing, manual captures were taken of the Micasense reflectance panels. These images allowed us to capture 100% reflectance and were used to correct inconsistencies in lighting during the flights. All flights used a serpentine flight pattern at 90 m above ground level and a speed of 6 m s^{-1} with 85% forward and 80% cross-track image overlap. The Micasense system captured 10-band multispectral imagery (Table 3.2) at 6.3 cm resolution. Ten ground control points (GCPs) were used at each site to ensure spatial accuracy of image alignment. These GCPs were chosen based on visibility from above, spacing across the sites, and had their locations recorded using an Emlid Reach RS2+ real-time kinematic GPS (Emlid Tech Kft, Budapest, Hungary). The GCPs had a reported average horizontal and vertical root mean square error of 0.038 m and 0.077 m, respectively.

Table 3.2: List of bands available on the Micasense Dual-Camera System and the wavelengths covered by each band.

MicaSense Band	MicaSense λ
Blue	430-458 nm
Blue 2	465-485 nm
Green	550-570 nm
Green 2	524-538 nm
Red	663-673 nm
Red 2	642-658 nm
Red Edge 1	712-722 nm
Red Edge 2	700-710 nm
Red Edge 3	731-749 nm
Near Infrared	820-860 nm

3.2.2 UAS Image Processing

For each of the seven acquisitions, UAS images were processed in Agisoft Metashape version 1.6.4 (Agisoft LLC., St. Petersburg, Russia) using the Structure from Motion algorithm with Mild Depth Map Filtering and High-Quality generation parameters. These settings were used to maximize individual tree extraction accuracy based on the findings of Tinkham and

Swayze (2021). Photos of the reflectance panels were used to calibrate image spectral reflectance and correct for lighting inconsistencies due to clouds and sun angle.

The GCP locations were imported to Metashape and iteratively georeferenced using a minimum of 10 photos per GCP, resulting in a median (s.d.) root mean square error of 7.3 (5.2) cm, 5.8 (3.5) cm, and 0.8 (0.5) cm for X, Y, and Z locations, respectively across all sites and collections. Once GCPs were georeferenced, UAS photos were aligned to produce approximately 5-8 million tie points as well as an orthomosaic and dense point cloud with information for the 10 spectral bands attached. The orthomosaics had a final pixel resolution of 6.3 cm. Before export, pixel and point values were converted from digital number to reflectance by dividing each band value by 32,768 following the recommendation of the camera manufacturer (MicaSense Seattle, WA, USA). Then, orthomosaics and point clouds were exported as GeoTiffs and LAS files, respectively, for each flight date in the North American Datum 1983 UTM Zone 13 North (NAD83, UTM 13N) projected coordinate system. These data were then imported into R for analysis.

3.2.3 UAS Tree Extraction

To extract individual trees and tree crowns, point clouds and orthomosaics were processed in RStudio version 4.3.2 (R Core Team, 2022). Following the point cloud processing steps from Tinkham & Woolsey (2024), point clouds were processed using the cloud2trees package (Woolsey, 2024) which integrates the lasR (Roussel, 2024) and lidR packages (Roussel et al., 2020, Roussel & Auty, 2024). First, raw point clouds were denoised which involved classifying isolated points and dropping them, as well as duplicate points, from the point cloud. Then, we classified ground points and generated a digital terrain model (DTM) with 1.0 m

resolution using Delaunay triangulation and pit fill. This allowed us to height normalize the point cloud and generate a canopy height model (CHM) at 0.10 m resolution. To locate individual trees, we used a variable window function [Equation 2] as proposed by Creasy et al. (2021) and the locate_trees function from the lidR package to identify all tree tops that were at least 2 meters tall. Then, we delineated tree crowns using the marker-controlled watershed function of the ForestTools package (Plowright, 2024). Finally, we spatially joined the tree tops with the tree crowns following the methods of Tinkham et al. (2022). The outputs of these steps included a CHM and DTM raster, individual tree crown polygons, and tree location points which included the calculated height and DBH.

$$Variable\ Window\ Radius = 0.3 + CHM\ Value * 0.1 \quad [2]$$

The tree location points were spatially matched to field-collected tree locations following the methods of Tinkham et al. (2022). This spatial matching process used a maximum search distance of 5 m and a maximum height error of 4 m to identify the nearest UAS trees to the field trees using the sf package (Pebesma, 2018). The UAS tree within the search distance with the smallest height error was then assigned to the field tree as a match. These matches were used with the st_intersects function from the sf package to extract the nearest individual tree crown polygon. Then, using the individual tree crown polygons and 10-band orthomosaics, we derived each pixel's spectral values for each of the 10 bands within each crown polygon using the exact_extract function of the exactextractr package (Baston, 2024; Figure 3.2). These values were normalized to the reflectance scale by dividing each cell value for a given band by the global maximum of that respective band (Micasense). Then, using the normalized cell values we calculated NDVI2 (Equation 3), PRI (Equation 4), and FMCI (Equation 5), and

extracted Red Edge 3 values for all pixels. Raster values within each tree crown polygon were further summarized as the mean, median, 10th, 20th, 25th, 30th, 40th, 60th, 70th, 75th, 80th, and 90th percentile band and index values. The summarized raster values were then tested as predictor variables in the multiple linear regression model developed by Lad et al. (2023). We also evaluated species, Julian date, and site as potential predictor variables.

$$NDVI2 = \frac{NIR-Red2}{NIR+Red2} \quad [3]$$

$$PRI = \frac{Green2-Green}{Green2+Green} \quad [4]$$

$$FMCI = \frac{RedEdge3-NIR}{RedEdge3+NIR} \quad [5]$$

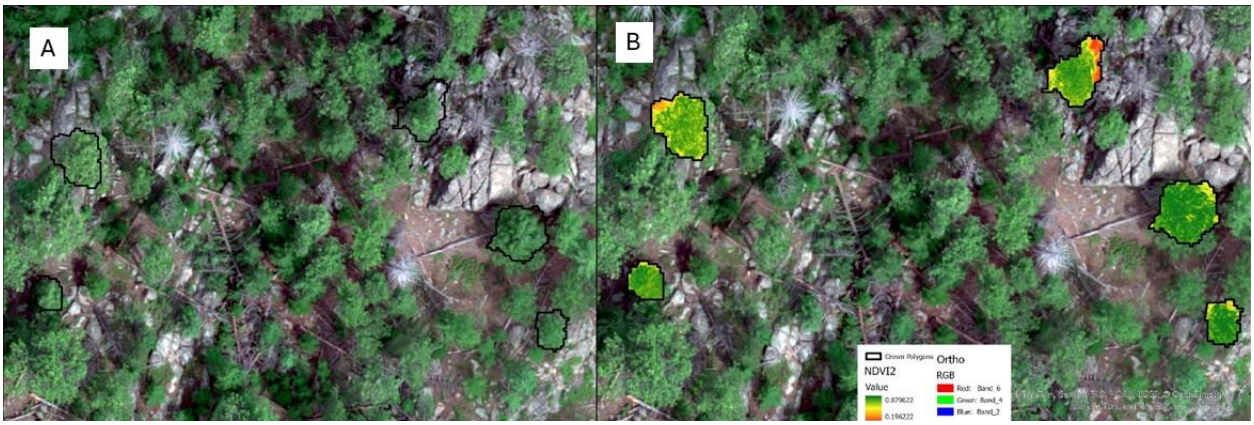

Figure 3.2: Extracted tree polygons showing A) true color imagery and B) their calculated Normalized Difference Vegetation Index 2 (NDVI2) value on top of UAS-derived true color imagery of the Red Feather Lakes (RFL) site. The within tree crown polygons pixels were used to calculate mean, median, and every 10th-90th percentile values as potential predictors of tree foliar moisture content.

3.2.4 Modeling and Data Analysis

After summarizing predictor variables by tree crown, we tested the lab developed Multiple Linear Regression Model (MRLM; Equation 6) from Lad et al. (2023) which used NDVI2, PRI, FMCI, and the RedEdge3 band as predictor variables for FMC. We used the stats package in

base R (R Core Team, 2023) and tested the Lad et al. (2023) model using each of the 12 crown summarization techniques (i.e., mean, median, 10, 20, 25, 30, 40, 60, 70, 75, 80, 90 percentile) with the model's four variables (NDVI2, PRI, FMCI, RedEdge3). We compared the accuracy of the 12 versions of the MLRM in predicting observed FMC using Pearson's correlation, mean error (ME), and root mean square error (RMSE). Pearson's correlation was used to evaluate the strength of the linear relationship between predicted and observed FMC values, providing insight into how well the model captures overall variance in FMC. To assess systematic bias in model predictions, we performed a paired t-test comparing the mean observed FMC to the mean model-predicted FMC. Additionally, we examined the model's ability to rank trees by relative drought stress using Spearman's rank correlation. Unlike Pearson's correlation, which assumes a linear relationship, Spearman's correlation assesses monotonic relationships and is robust to non-linearity. This allowed us to determine how well the model preserves the relative ordering of trees based on their FMC values

$$FMC\% = -226.61 + 138.64 \times NDVI2 + 611.92 \times RedEdge3 + 851.31 \times FMCI + 1039.63 \times PRI \quad [6]$$

To identify potential differences between the lab model and the optimal prediction of FMC using field scale data, we also fit a series of new multiple linear regression models using the UAS-derived tree-level spectral bands and indices, along with species and Julian date to predict FMC. We first fit Random Forest models to each of the 12 sets of summarization metrics (e.g., 10th, 20th, 30th percentile, etc.) to identify the set of metrics best suited to predict FMC using the RandomForest R package (Liaw & Wiener, 2002). The models included the tree-level summary metrics for the ten spectral bands and nine spectral indices (19 variables). These spectral indices included NDVI, NDVI2, PRI, FMCI, Normalized Difference Wetness Index (NDWI;

Equation 7), Green Normalized Difference Vegetation Index (GNDVI; Equation 8), and Normalized Difference Red Edge (NDRE; Equation 9). The best Random Forest regression model was identified as the model with the greatest variance explained (R^2).

$$NDWI = \frac{Green-NIR}{Green+NIR} \quad [7]$$

$$GNDVI = \frac{NIR-Green}{NIR+Green} \quad [8]$$

$$NDRE = \frac{NIR-RedEdge1}{NIR+RedEdge1} \quad [9]$$

For the set of metrics from the highest performing Random Forest model, we tested variable correlation to remove any highly (i.e., >70%) collinear variables. When two variables were highly correlated, we first retained variables that have previously demonstrated success in modeling FMC. For instance, since NDVI2 was a significant predictor of FMC in Lad et al. (2023), we retained NDVI2 over NDVI. This reduced set of non-collinear predictors was then used to construct a multiple linear regression model in R using the stats package (R Core Team, 2023). The model was reduced using a forward-backward stepwise approach to minimize the Akaike Information Criterion (AIC) using the olsrr R package (Hebbali, 2020). This approach identified the most parsimonious model while retaining key predictors of FMC. To quantify uncertainty and assess model consistency, we estimated predictor coefficients and their 95% confidence intervals using bootstrapping with 1,000 repetitions (boot package; Davison & Hinkley, 1997; Canty & Ripley, 2022). To evaluate the practical utility of the final model, we ranked the model-predicted and field-observed FMC values from lowest to highest and categorized trees into two groups based on their rank percentiles. Specifically, we assessed the model's ability to correctly classify trees within the most drought-stressed subset by dividing the dataset at thresholds of

10%, 20%, 30%, 40%, and 50% of the lowest FMC values. This analysis was designed to simulate how a forest manager might use the model to prioritize trees for targeted intervention, ensuring that the method effectively identifies the most drought-stressed individuals.

3.3 Results

Field-collected FMC was approximately normally distributed when examined across all sites and dates (Figure 3.3). The observed FMC values ranged from 73% to 126%, with an average of 98.4%. FMC across the four dates was bimodally distributed, but the range of FMC values tended to narrow through time. Additionally, the FMC values at EP tended to be higher when compared to RFL, and there were generally higher values for Douglas-fir than ponderosa pine (Figure 3.3).

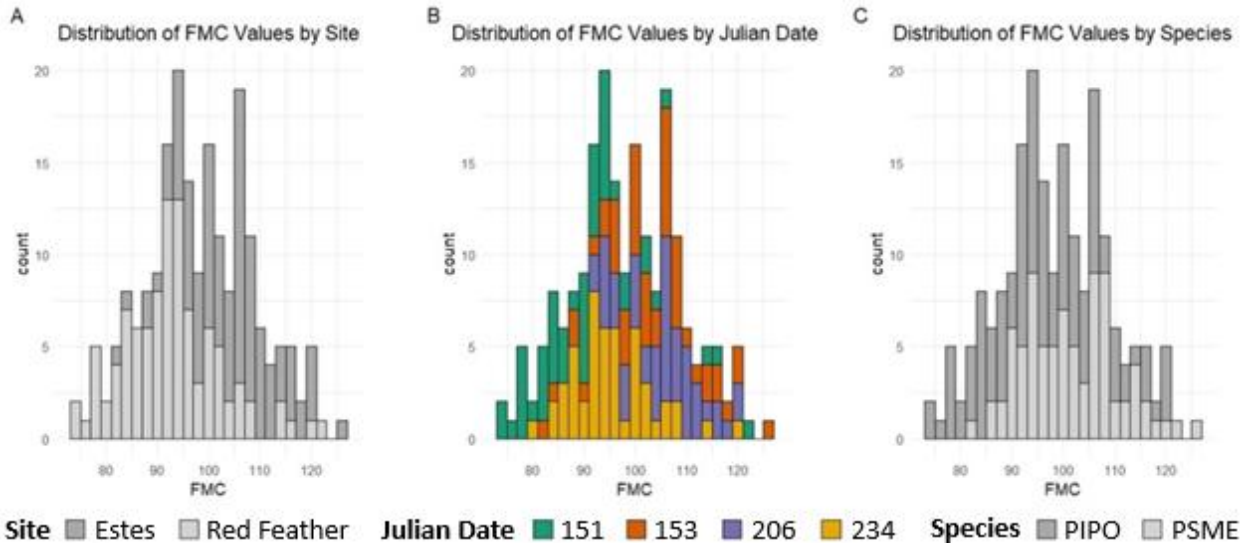

Figure 3.3: Histograms of foliar moisture content values across the four collections at the Red Feather Lakes (RFL) and Estes Park (EP) sites separated into A) distribution by site, B) distribution by Julian date, and C) distribution by species.

Spectral reflectance of bands and indices were also compared across Julian dates to examine the importance of the collection date (Figure 3.4). Most spectral bands exhibited low

variation between Julian dates, except for the first data collection which consistently had greater reflectance levels. Within a single collection date, bands in the red and red edge portion of the spectrum featured greater variability and wider interquartile ranges than bands with shorter wavelengths. The near-infrared indices (NDVI2 and FMCI) exhibited lower mean values for the RFL collections (first and last Julian date) compared to the EP collections, with there being much more consistency in the PRI values between dates, but less within site variation.

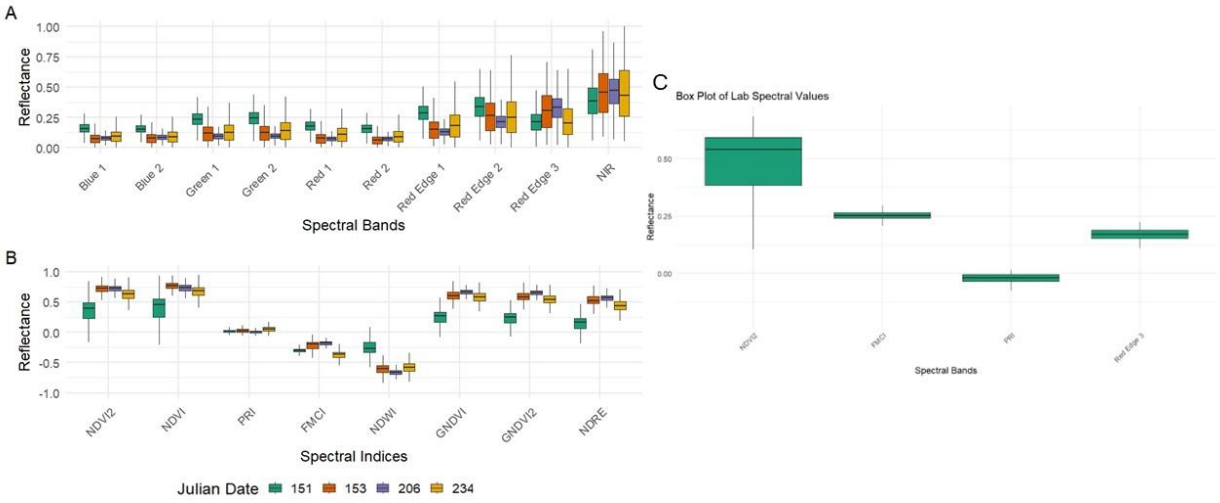

Figure 3.4: Boxplot of A) spectral band and B) index distribution within surveyed tree crowns colored by Julian Date. C) Box plot of spectral predictors from Lad et al. (2023).

Comparing the 12 sets of MLRM predictions from Lad et al. (2023) against observed FMC values found that the mean summarization approach achieved the highest Pearson's correlation, while the 90th percentile achieved the lowest ME and RMSE (Table 3.3). A paired t-test of the observed and predicted values found no significant difference between means ($p=0.57$) using the 90th percentile technique, but the mean technique was significantly different ($p<0.05$). Across the 12 summarized models, the correlation generally remained stable but using lower percentiles of within canopy values had higher correlation and there was a slight decline in correlation at higher percentiles. However, the ME and RMSE decrease with the use

of higher percentiles, suggesting an increase in accuracy of the predicted values. Testing the ranking of the predicted FMC values from the mean and 90th percentile models against the observed rankings using the Spearman's rank correlation showed that both models similarly captured the gradient of FMC values (Figure 3.5).

Table 3.3: Accuracy of each summarization metric tested in applying the multiple linear regression model from Lad et al. (2024).

Summarization Technique	**Pearson's Correlation**	**Mean Error**	**Root Mean Square Error**
Mean	0.437	203.77	238.44
Median	0.414	197.08	237.00
10th Percentile	0.421	411.86	431.77
20th Percentile	0.422	345.18	368.12
25th Percentile	0.423	317.33	342.09
30th Percentile	0.421	291.50	318.50
40th Percentile	0.417	242.94	275.42
60th Percentile	0.412	153.16	202.91
70th Percentile	0.409	109.54	173.04
75th Percentile	0.408	86.89	159.92
80th Percentile	0.405	63.14	148.40
90th Percentile	0.398	5.53	135.66

The lack of high accuracy in the lab-developed MLRM could be the result of scaling and summarization mismatches. In the lab, pure individual sapling spectral values were collected using three plant probe samples across the crown, while in the field, tree spectral values were collected as pixels across the entire crown, with values primarily reflecting the top 2D profile of the crown. To account for the mixture of foliage, branch, and background substrate captured in the UAS pixels, we attempted to account for these collection approach differences by testing summarization techniques. However, the UAS imagery also contended with greater spectral variability in mature crowns as, even within extracted polygons, there are differences in crown shading/illumination. This all contributes to the relatively narrow spectral distribution of the

laboratory saplings (Figure 3.4 C) compared to the UAS imagery (Figure 3.4 A & B). The young needles (i.e., less than two years old) on the laboratory saplings likely reflect more light (Rock et al., 1994) compared to the older (i.e., up to five years old) needles assessed in the field. Comparing the lab spectral data from Lad et al. (2023) against this study's UAS data shows a much lower and narrower range of near-infrared values from the lab data. The lack of variability in the training data for the lab MLRM likely contributed to a lack of model fit when predicting using field values that featured higher levels of variability, as well as higher reflectance values in general.

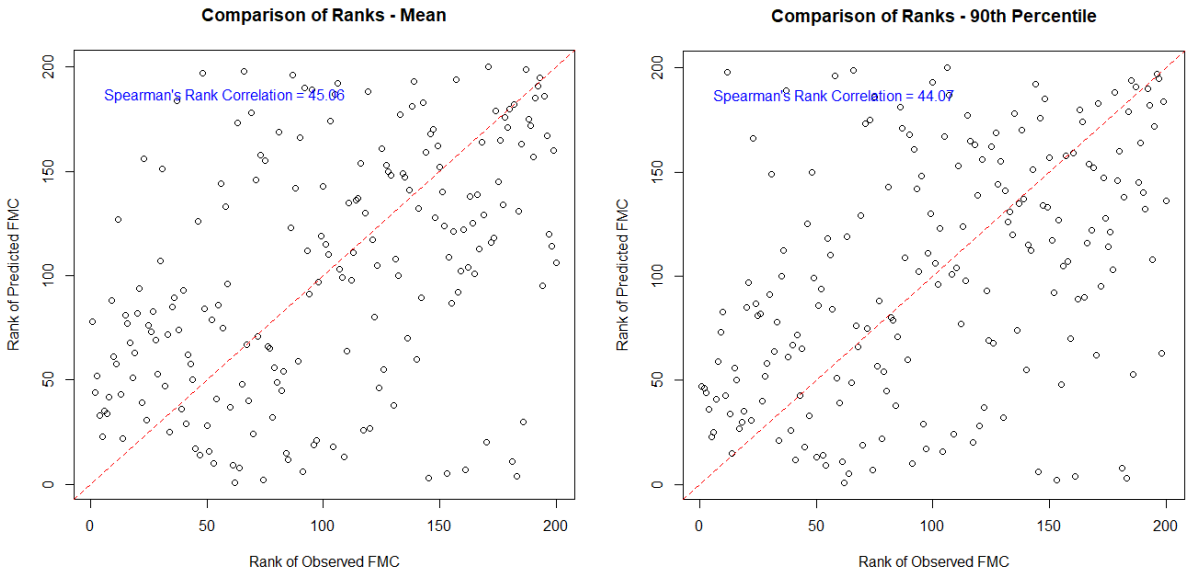

Figure 3.5: Observed versus predicted foliar moisture content (FMC) ranks from the two highest performing multiple linear regression models, based on Lad et al. (2023) using, (a) the mean spectral values per crown, and (b) the 90th percentile spectral values per crown.

The random forest model identified that using the 80th percentile of tree level summarized spectral bands and indices provided the most predictive power. In our testing of summarization approaches, species was a significant predictor of FMC in ten out of twelve of the random forest models, highlighting its utility. The final reduced multiple linear regression

model developed on the field data retained species and the within crown 80th percentile values of NDVI2 and FMCI as predictors and resulted in an adjusted R^2 of 31.02 ($p<0.05$) with a residual standard error of 8.98% FMC (Table 3.4, Figure 3.6). Predicted FMC increased as the index score increased for both NDVI2 and FMCI (Figure 3.7). Additionally, species was significant with Douglas-fir increasing the intercept by 4.2% FMC over ponderosa pine.

Table 3.4: Final reduced multiple linear regression model output table.

	Coefficient	Confidence Interval	Standard Error	T value	p-value
Intercept	89.71	75.59, 100.74	4.38	20.50	<0.05
Douglas-fir	4.20	1.15, 6.68	1.31	3.22	<0.05
NDVI2_p80	23.67	10.75, 41.67	4.67	5.07	<0.05
FMCI_p80	35.58	21.75, 55.62	8.72	4.43	<0.05

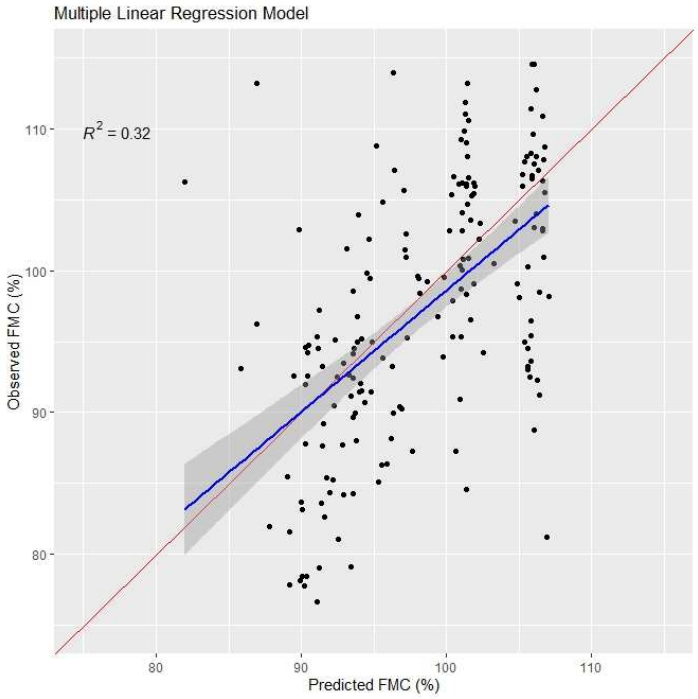

Figure 3.6: Observed and predicted foliar moisture content from a multiple linear regression model using Species and the 80th percentile values of NDVI2 and FMCI as predictor variables.

To test the utility of the model in thresholding the predictions to inform management decisions, we ranked the predicted and observed values and subset them into binary classes representing the lower 50% of FMC and higher 50% of FMC. This single split achieved an

accuracy of 75.5% with bin standard errors of 2.9% each. Repeating this process to include splits identifying the 10%, 20%, 30%, 40%, and 50% most drought stressed trees resulted in an average accuracy of 81.40%, with accuracy declining from 89.8% for the 10/90 split to 75.5% for the 50/50 split. Similarly, the smaller bin identifying the more drought-stressed trees had an average class standard error of 2.2% that went from 1.3% to 2.9% as the bin increased from 10% to 50% of the predictions. The larger bin inversely declined from 3.8% to 2.9% as the bin decreased from 90% to 50%, with an average of 3.4%. Predicted bins were statistically significant (i.e., $p<0.05$) when identifying the 30%, 40%, and 50% most drought stressed trees, but not when the threshold was set to identify the 10% ($p=0.56$) or 20% ($p=0.17$) most drought stressed trees.

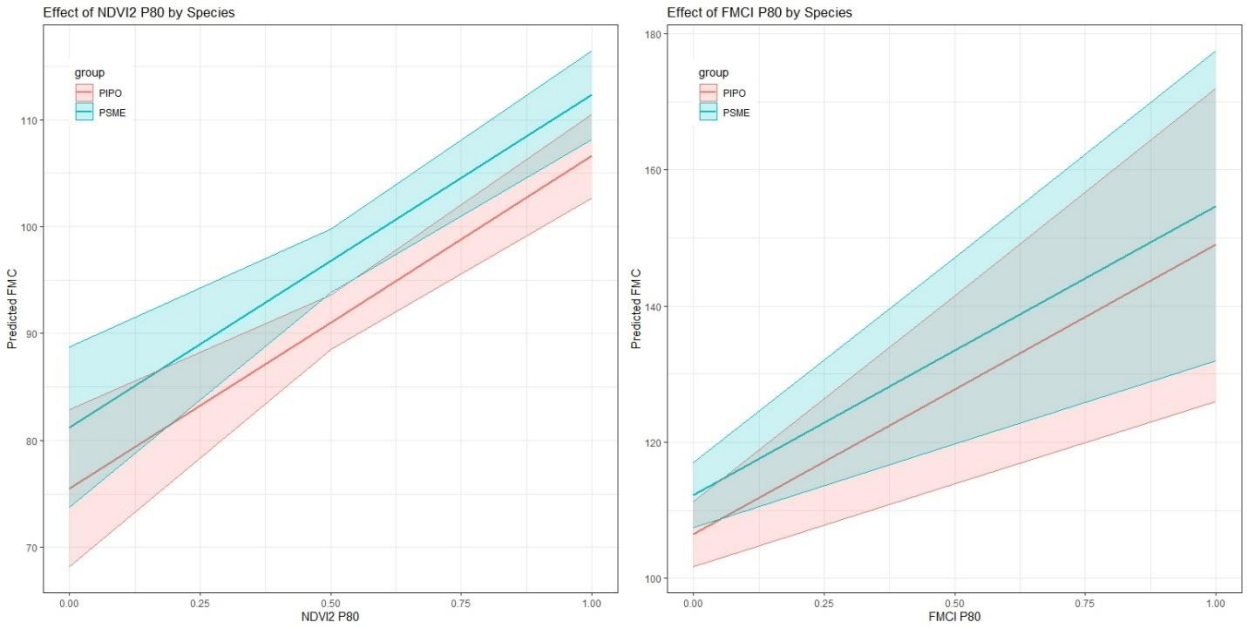

Figure 3.7: Predicted effects of the 80th percentile values of NDVI2 and FMCI in a multiple linear regression model separated by species. Shaded areas indicate 95% confidence intervals for predictions.

3.4 Discussion

3.4.1 Model Outcomes

When UAS derived values were applied to the prediction of FMC, the lab developed MLRM achieved relatively low prediction accuracy. The new multiple linear regression model fit to the UAS data successfully classified tress into higher vs lower drought-stress categories with = 81.4% accuracy. While exact predictions of FMC had a mean error of ~9%, it is likely more important to capture the gradient of drought-stress than precise values, as FMC is known to change rapidly in the field. For example, ponderosa pine has previously been shown to vary up to 34% diurnally in the summer with daily minima occurring in the morning and shortly after noon (Philpot, 1965). These temporal fluctuations mean that a prediction of FMC at a single time point may not necessarily represent the health of an individual tree. However, mid-day acquisitions minimize within-tree relative FMC, while reducing shadowing in imagery. FMC for Douglas-fir and ponderosa pine has been documented as between 100% and 130% in the summer with old foliage having values commonly under 100% (Keyes, 2006). However, our field observed average FMC across summer collection dates was 98%, with many trees below 90% FMC. The EP site had consistently higher FMC values, potentially resulting from this site being in a post-treatment condition, while the RFL site has high forest density and has not been treated or disturbed in the last 100 years.

While precise FMC prediction yielded low accuracies, our results suggest that rank-based thresholding provides an accurate decision-support tool for identifying the gradient of drought-stress. By converting continuous FMC predictions into binary classifications, we achieved high mean classification accuracy (81.4%), with the highest accuracy (89.8%) occurring

when identifying the most drought-stressed 10% of trees. Accuracy declined as the classification included a larger proportion of the drought-stressed trees, but remained statistically significant ($p < 0.05$) for identifying the 30%, 40%, and 50% most drought-stressed trees. This trend suggests that a rank-based classification approach could allow managers to effectively target trees most in need of intervention.

Our binary classification accuracy (stressed/not stressed) to identify the most drought-stressed trees was lower than previous studies attempting to classify tree health status using UAS multispectral imagery in orchards (healthy/unhealthy 97.5%; Jemaa et al, 2023), but similar to the accuracy achieved by other efforts in mixed broadleaf-conifer forests (live/dead/beetle infested 84.7%; Abdollahnejad & Panagiotidis, 2020), but no studies have thus far identified the relative health of western US mixed-conifer forests at the scale of individual trees. As UAS sensor technology and efforts to integrate hyperspectral, short-wave infrared, or thermal imagery continue to advance, model accuracy of FMC and other health metrics should continue to improve. Using a hyperspectral camera, for example, Näsi et al. (2018) classified bark beetle stress into health/infested/dead classes in an urban forest with 81% accuracy. Physiological indicators of tree health, such as stomatal conductance and leaf water potential, can also be modeled using hyperspectral and thermal imagery with crown temperature showing a strong correlation with stomatal conductance (Zarco-Tejada et al., 2012).

UAS shows strong potential for the early detection of tree moisture stress and models should consider ecosystem-specific physiology, such as species composition and morphology, as well as abiotic factors such as topography and hydrology (Ewane et al., 2023). Diverse applications of UAS imagery to inform vegetation health assessment can help support the

maintenance and restoration of forest resilience. Future research aiming to apply UAS imagery for tree health assessments should consider sensor cost, sensor spectral and spatial resolution, and site variability of biotic and abiotic factors when choosing the UAS that will be flown.

3.4.2 Management Implications

Forest FMC is an important indicator of forest resilience and the relative distribution of FMC within a site can highlight areas for targeted management actions. At our post-treatment site, Estes Park, mean FMC was 11% higher than at the untreated Red Feather Lakes site, consistent with previous studies that found a positive relationship between decreased stand density and increased moisture availability (Simonin et al., 2006, Andrews et al., 2020, Young et al., 2023). This increase in moisture availability also increases tree growth and decreases sensitivity to changing climate (Finley et al., 2019). Thus, our models of site-specific relative FMC could be applied to forest sites and provide managers with relative tree stress to inform targeted thinning and prescribed fire operations, resulting in subsequent increases in growth and improved resilience against drought.

One direct application of these models is in the wildland-urban interface (WUI), where the identification of drought-stressed trees can help prioritize their removal to increase the size of the defensible zone around homes and infrastructure. By mapping FMC across a WUI landscape, managers could target the most stressed individuals for removal, reducing both tree susceptibility to disturbances and fire risk near structures. Additionally, these models could support ongoing fire mitigation efforts by integrating near-real-time stress assessments into defensible space guidelines, helping refine vegetation management beyond standard distance-based thinning prescriptions.

Tree-level relative FMC, combined with tree size and spatial arrangement data, can also guide decision-making to achieve increases in the vertical and horizontal complexity of forests, while prioritizing the retention of the site's most resilient individuals (Churchill et al., 2013). The FMC rankings could be thought of as a weighting factor when identifying trees for removal or retention during thinning operations. Applying this model to assess where to enhance forest resilience supports stand-level adaptation that favors drought-tolerant trees while adjusting forest density to reduce competition. The model from this study could inform management actions including implementation of mechanical thinning and prescribed fire, which are most effective at reducing wildfire severity and effects when used in conjunction with one another, with potential reductions of fire severity of up to 72% compared to untreated areas (Davis et al., 2024). Models of relative FMC could be used to prioritize areas for mechanical thinning by focusing thinning on dense sites with high fuel loads and resource competition (Agee & Skinner, 2005). Additionally, these models could be used to evaluate sites post-thinning to examine changes to moisture content of the remaining trees (North et al., 2009). By connecting our model of tree-level FMC with ecologically-informed management, we can increase the information available for adaptive management that balances forest resilience and fire risk reduction.

A second application of these models is for monitoring treatment effectiveness. UAS data could be collected before thinning or prescribed fire treatments to detect the gradient of tree stress across a site, allowing managers to target the most stressed individuals. Following treatment, repeat UAS acquisitions could assess changes to FMC and evaluate treatment-induced improvements to forest moisture retention. By comparing pre- and post-treatment

FMC, managers could refine best practices for reducing competition, increasing drought resilience, and improving stand health.

In fire-dependent forests, prescribed fire is a useful management tool for reducing fuel availability and connectivity. Prescribed fire planning relies heavily on weather data which are used to make assumptions on fuel conditions and resultant fire behavior (Ryan et al., 2013). Integrating models of FMC into this planning process could provide data on live fuel moisture, improving fire behavior predictions. Relative FMC can fluctuate with weather (Keyes, 2006) and provides valuable information about fuel moisture levels and combustibility, which could guide ignition strategies, allowing managers to adjust ignition line distance to control fireline intensity based on burn-specific mortality objectives. By providing managers with near-real-time access to overstory fuel conditions, we can expand the information available to managers while they make fire planning decisions. Further, in areas with an increasing occurrence of short-interval fires, these models could be applied to assess the resilience of surviving trees after initial fires and inform thinning and refugia management to increase resistance to subsequent disturbances.

Informed management is important for maintaining and improving forest health, particularly as drought stress increasingly reduces tree productivity, growth, and carbon and nitrogen uptake (Joseph et al., 2020). Extreme drought can also drive widespread mortality events, particularly if the drought is prolonged (Allen et al., 2010). Climate stress is already exceeding species' physiological tolerance to drought, resulting in mortality, particularly in drier parts of species' ranges (Anderegg et al., 2019). The mortality of overstory trees can initially decrease crown fire potential, while increasing surface fire intensity (Stephens et al., 2018),

resulting in negative impacts on soil organic carbon (Boča et al., 2014; Gao et al., 2021). As climate change continues to push the bounds of forest resilience through drought stress and an increase in the occurrence of high-severity fires, forest management needs to anticipate future climatic pressures and adjust accordingly.

3.4.3 Limitations

While our model successfully identified the gradient of relative FMC and demonstrated utility for forest management applications, several limitations should be considered when applying these findings. This study was limited to two sites, each representing different management histories and stand structures. Expanding the number of sites and sampled trees could provide insight into the transference of these models across broader forest conditions. Additionally, species was an important predictor of FMC, meaning managers applying our model to aid in their prescription will need to consider the species on their site. Some studies have successfully classified tree species from UAS multispectral imagery achieving between 55.5% and 81.18% accuracies (Abdollahnegjad & Pangagiotidis, 2020, Grybas & Congalton, 2021), which may be applied using the same UAS data as those collected for FMC prediction. However, these studies focus on mixed broadleaf and conifer forests, highlighting a need for studies that conduct species classification in conifer-dominated forests.

Temporal variability in FMC presents another challenge. FMC is highly dynamic and can change significantly in response to short-term environmental conditions, such as diurnal fluctuations, seasonal precipitation, and drought stress (Keyes, 2006). At each site, greater FMC and spectral reflectance values were observed during the later collection date (Figure 3.3 B). In northern Colorado, late summer (i.e., July-September) precipitation is delivered by the North

American monsoon which provides crucial moisture for forests and plays an important role in the end of the fire season (Nauslar et al., 2018). The temporal variation in spectral reflectance highlights the importance of multiple collections to capture seasonal dynamics. This spectral variation is compounded by changing foliage, with older overwintered needles likely decreasing NIR reflectance in the spring, while new needles will have increased NIR reflectance (Rautianinen et al., 2018). Seasonal changes in needle spectra and variability in within-tree FMC are likely driven by tree biochemical and structural changes (Keyes, 2006, Rautiainen et al., 2018). This inverse relationship between needle age and NIR reflectance may smooth out seasonal dynamics in mature trees with multi-age needles, but more research is needed to understand these spectral and temporal dynamics in semi-arid systems. Overall, our data features variability in both observed FMC (Figure 3.3) and spectral reflectance (Figure 3.4 A) across sites and collection dates that reflect the heterogenous condition of mature forests. These seasonal and within-tree variations may complicate the application of static models for FMC prediction and highlight the importance of testing the relative persistence of how individual trees rank within a site's moisture gradient through time.

The feasibility of integrating UAS-derived FMC models into operational forest management also depends on logistical considerations, including the scale of data collection, image processing time, and computing resources required for model application. UAS surveys generate large datasets that require significant processing time and technical expertise, which may limit their practical use in large-scale forest assessments. Additionally, current UAS-based efforts are constrained by flight time and regulatory restrictions related to a pilot's line-of-sight to the aircraft may impact their effectiveness for characterizing larger extents within rugged

terrain. Intermediate-sized trees, often the primary targets for density reduction treatments, are also more likely to be shaded by the overstory, which could introduce challenges in accurately retrieving their spectral signatures.

Despite these limitations, our study demonstrates potential for UAS-derived models to inform targeted management actions, particularly for identifying drought-stressed trees and monitoring treatment effectiveness. Future research should focus on refining species classification methods, improving FMC models across broader temporal and spatial scales, and optimizing data processing workflows to enhance the operational feasibility of UAS-based forest health assessments.

3.5 Conclusions

Our analysis identified the most stressed trees at two sites in northern Colorado with ~80% accuracy, representing a significant advancement in the tools available for adaptive management in a semi-arid environment. As aridity is expected to increase in the coming years, this model provides valuable insights to guide targeted treatments aimed at enhancing forest resilience to future disturbances. Managers could integrate this model with site-specific knowledge and maps of tree composition and distribution to make fully informed decisions. By identifying areas with historically persistent openings, managers can pinpoint locations where infilling trees are likely drought-stressed due to soil moisture and nutrient limitations (Bond & Keeley, 2005). This would allow managers to prioritize areas for intervention and restoration while accounting for both overstory relative FMC, as well as underlying soil conditions. Future work should evaluate the accuracy of this model for predicting relative FMC of additional

species and in different elevation zones both within Colorado, and across the western United States.

3.6 References

Abatzoglou, J. T., & Williams, A. P. (2016). Impact of anthropogenic climate change on wildfire across western US forests. *Proceedings of the National Academy of Sciences*, *113*(42), 11770–11775. https://doi.org/10.1073/pnas.1607171113

Abdollahnejad, A., & Panagiotidis, D. (2020). Tree Species Classification and Health Status Assessment for a Mixed Broadleaf-Conifer Forest with UAS Multispectral Imaging. *Remote Sensing*, *12*(22), Article 22. https://doi.org/10.3390/rs12223722

A. Liaw and M. Wiener (2002). Classification and Regression by randomForest. *R News 2*(3), 18-22.

Agee, J. K., & Skinner, C. N. (2005). Basic principles of forest fuel reduction treatments. *Forest Ecology and Management*, *211*(1), 83–96. https://doi.org/10.1016/j.foreco.2005.01.034

Allen, C. D., Macalady, A. K., Chenchouni, H., Bachelet, D., McDowell, N., Vennetier, M., Kitzberger, T., Rigling, A., Breshears, D. D., Hogg, E. H. (Ted), Gonzalez, P., Fensham, R., Zhang, Z., Castro, J., Demidova, N., Lim, J.-H., Allard, G., Running, S. W., Semerci, A., & Cobb, N. (2010). A global overview of drought and heat-induced tree mortality reveals emerging climate change risks for forests. *Forest Ecology and Management*, *259*(4), 660–684. https://doi.org/10.1016/j.foreco.2009.09.001

Anderegg, W. R. L., Anderegg, L. D. L., & Huang, C. (2019). Testing early warning metrics for drought-induced tree physiological stress and mortality. *Global Change Biology*, *25*(7), 2459–2469. https://doi.org/10.1111/gcb.14655

Anderegg, W. R. L., Anderegg, L. D. L., Kerr, K. L., & Trugman, A. T. (2019). Widespread drought-induced tree mortality at dry range edges indicates that climate stress exceeds species' compensating mechanisms. *Global Change Biology*, *25*(11), 3793–3802. https://doi.org/10.1111/gcb.14771

Anderegg, W. R. L., Flint, A., Huang, C., Flint, L., Berry, J. A., Davis, F. W., Sperry, J. S., & Field, C. B. (2015). Tree mortality predicted from drought-induced vascular damage. *Nature Geoscience*, *8*(5), 367–371. https://doi.org/10.1038/ngeo2400

Andrews, C. M., D'Amato, A. W., Fraver, S., Palik, B., Battaglia, M. A., & Bradford, J. B. (2020). Low stand density moderates growth declines during hot droughts in semi-arid forests. *Journal of Applied Ecology*, *57*(6), 1089–1102. https://doi.org/10.1111/1365-2664.13615

Baston, D. exactextractr: fast extraction from raster datasets using polygons. R package version 0.10.0, https://github.com/isciences/exactextractr

Batllori, E., Lloret, F., Aakala, T., Anderegg, W. R. L., Aynekulu, E., Bendixsen, D. P., Bentouati, A., Bigler, C., Burk, C. J., Camarero, J. J., Colangelo, M., Coop, J. D., Fensham, R., Floyd, M. L., Galiano, L., Ganey, J. L., Gonzalez, P., Jacobsen, A. L., Kane, J. M., … Zeeman, B. (2020). Forest and woodland replacement patterns following drought-related mortality. *Proceedings of the National Academy of Sciences*, *117*(47), 29720–29729. https://doi.org/10.1073/pnas.2002314117

Blanco, V., Blaya-Ros, P. J., Castillo, C., Soto-Vallés, F., Torres-Sánchez, R., & Domingo, R. (2020). Potential of UAS-Based Remote Sensing for Estimating Tree Water Status and Yield in Sweet Cherry Trees. *Remote Sensing*, *12*(15), Article 15. https://doi.org/10.3390/rs12152359

Boča, A., Van Miegroet, H., & Gruselle, M.-C. (2014). Forest Overstory Effect on Soil Organic Carbon Storage: A Meta-analysis. *Soil Science Society of America Journal*, *78*(S1), S35–S47. https://doi.org/10.2136/sssaj2013.08.0332nafsc

Bolinger, R., Lukas, J., Schumacher, R., & Goble, P. (2023). Climate change in Colorado. https://hdl.handle.net/10217/237323

Bond, W. J., & Keeley, J. E. (2005). Fire as a global 'herbivore': The ecology and evolution of flammable ecosystems. *Trends in Ecology & Evolution*, *20*(7), 387–394. https://doi.org/10.1016/j.tree.2005.04.025

Breshears, D. D., Cobb, N. S., Rich, P. M., Price, K. P., Allen, C. D., Balice, R. G., Romme, W. H., Kastens, J. H., Floyd, M. L., Belnap, J., Anderson, J. J., Myers, O. B., & Meyer, C. W. (2005). Regional vegetation die-off in response to global-change-type drought. *Proceedings of the National Academy of Sciences*, *102*(42), 15144–15148. https://doi.org/10.1073/pnas.0505734102

Churchill, D. J., Larson, A. J., Dahlgreen, M. C., Franklin, J. F., Hessburg, P. F., & Lutz, J. A. (2013). Restoring forest resilience: From reference spatial patterns to silvicultural prescriptions and monitoring. *Forest Ecology and Management*, *291*, 442–457. https://doi.org/10.1016/j.foreco.2012.11.007

Cook, B. I., Ault, T. R., & Smerdon, J. E. (2015). Unprecedented 21st century drought risk in the American Southwest and Central Plains. *Science Advances*, *1*(1), e1400082. https://doi.org/10.1126/sciadv.1400082

Cook, B. I., Mankin, J. S., & Anchukaitis, K. J. (2018). Climate Change and Drought: From Past to Future. *Current Climate Change Reports*, *4*(2), 164–179. https://doi.org/10.1007/s40641-018-0093-2

Coop, J. D., Parks, S. A., Stevens-Rumann, C. S., Crausbay, S. D., Higuera, P. E., Hurteau, M. D., ... & Rodman, K. C. (2020). Wildfire-driven forest conversion in western North American landscapes. *BioScience*, *70*(8), 659-673. https://doi.org/10.1093/biosci/biaa061

Dash, J. P., Pearse, G. D., & Watt, M. S. (2018). UAV Multispectral Imagery Can Complement Satellite Data for Monitoring Forest Health. *Remote Sensing*, *10*(8), Article 8. https://doi.org/10.3390/rs10081216

Davis, K. T., Peeler, J., Fargione, J., Haugo, R. D., Metlen, K. L., Robles, M. D., & Woolley, T. (2024). Tamm review: A meta-analysis of thinning, prescribed fire, and wildfire effects on subsequent wildfire severity in conifer dominated forests of the Western US. *Forest Ecology and Management. 561: 121885.*, *581*, 121885. https://doi.org/10.1016/j.foreco.2024.121885

D'Odorico, P., Schönbeck, L., Vitali, V., Meusburger, K., Schaub, M., Ginzler, C., Zweifel, R., Velasco, V. M. E., Gisler, J., Gessler, A., & Ensminger, I. (2021). Drone-based physiological index reveals long-term acclimation and drought stress responses in trees. *Plant, Cell & Environment*, *44*(11), 3552–3570. https://doi.org/10.1111/pce.14177

Earles, J. M., North, M. P., & Hurteau, M. D. (2014). Wildfire and drought dynamics destabilize carbon stores of fire-suppressed forests. *Ecological Applications*, *24*(4), 732–740. https://doi.org/10.1890/13-1860.1

Ewane, E. B., Mohan, M., Bajaj, S., Galgamuwa, G. A. P., Watt, M. S., Arachchige, P. P., Hudak, A. T., Richardson, G., Ajithkumar, N., Srinivasan, S., Corte, A. P. D., Johnson, D. J., Broadbent, E. N., de-Miguel, S., Bruscolini, M., Young, D. J. N., Shafai, S., Abdullah, M. M., Jaafar, W. S.

W. M., … Cardil, A. (2023). Climate-Change-Driven Droughts and Tree Mortality: Assessing the Potential of UAV-Derived Early Warning Metrics. *Remote Sensing*, *15*(10), Article 10. https://doi.org/10.3390/rs15102627

Ezenne, G. I., Jupp, L., Mantel, S. K., & Tanner, J. L. (2019). Current and potential capabilities of UAS for crop water productivity in precision agriculture. *Agricultural Water Management*, *218*, 158–164. https://doi.org/10.1016/j.agwat.2019.03.034

Fajardo, A., Goodburn, J. M., & Graham, J. (2006). Spatial patterns of regeneration in managed uneven-aged ponderosa pine/Douglas-fir forests of Western Montana, USA. *Forest Ecology and Management*, *223*(1), 255–266. https://doi.org/10.1016/j.foreco.2005.11.022

Finley, K., & Zhang, J. (2019). Climate Effect on Ponderosa Pine Radial Growth Varies with Tree Density and Shrub Removal. *Forests*, *10*(6), Article 6. https://doi.org/10.3390/f10060477

Flannigan, M. D., Wotton, B. M., Marshall, G. A., de Groot, W. J., Johnston, J., Jurko, N., & Cantin, A. S. (2016). Fuel moisture sensitivity to temperature and precipitation: Climate change implications. *Climatic Change*, *134*(1), 59–71. https://doi.org/10.1007/s10584-015-1521-0

Fraser, B. T., & Congalton, R. G. (2021). Monitoring Fine-Scale Forest Health Using Unmanned Aerial Systems (UAS) Multispectral Models. *Remote Sensing*, *13*(23), Article 23. https://doi.org/10.3390/rs13234873

Gao, B. (1996). NDWI—A normalized difference water index for remote sensing of vegetation liquid water from space. *Remote Sensing of Environment*, *58*(3), 257–266. https://doi.org/10.1016/S0034-4257(96)00067-3

Gao, D., Joseph, J., Werner, R. A., Brunner, I., Zürcher, A., Hug, C., Wang, A., Zhao, C., Bai, E., Meusburger, K., Gessler, A., & Hagedorn, F. (2021). Drought alters the carbon footprint of trees in soils—Tracking the spatio-temporal fate of 13C-labelled assimilates in the soil of an old-growth pine forest. *Global Change Biology*, *27*(11), 2491–2506. https://doi.org/10.1111/gcb.15557

Garza, B. N., Ancona, V., Enciso, J., Perotto-Baldivieso, H. L., Kunta, M., & Simpson, C. (2020). Quantifying Citrus Tree Health Using True Color UAV Images. *Remote Sensing*, *12*(1), Article 1. https://doi.org/10.3390/rs12010170

Gergel, D. R., Nijssen, B., Abatzoglou, J. T., Lettenmaier, D. P., & Stumbaugh, M. R. (2017). Effects of climate change on snowpack and fire potential in the western USA. *Climatic Change*, *141*(2), 287–299. https://doi.org/10.1007/s10584-017-1899-y

Govi, D., Pappalardo, S. E., De Marchi, M., & Meggio, F. (2024). From Space to Field: Combining Satellite, UAV and Agronomic Data in an Open-Source Methodology for the Validation of NDVI Maps in Precision Viticulture. *Remote Sensing*, *16*(5), Article 5. https://doi.org/10.3390/rs16050735

Groover, A. (2017). Age-Related Changes in Tree Growth and Physiology. In John Wiley & Sons, Ltd (Ed.), *eLS* (1st ed., pp. 1–7). Wiley. https://doi.org/10.1002/9780470015902.a0023924

Grulke, N., Maxfield, J., Riggan, P., & Schrader-Patton, C. (2020). Pre-Emptive Detection of Mature Pine Drought Stress Using Multispectral Aerial Imagery. *Remote Sensing*, *12*(14), Article 14. https://doi.org/10.3390/rs12142338

Grybas, H., & Congalton, R. G. (2021). A Comparison of Multi-Temporal RGB and Multispectral UAS Imagery for Tree Species Classification in Heterogeneous New Hampshire Forests. *Remote Sensing*, *13*(13), Article 13. https://doi.org/10.3390/rs13132631

Hanna, L., Tinkham, W. T., Battaglia, M. A., Vogeler, J. C., Ritter, S. M., & Hoffman, C. M. (2024). Characterizing heterogeneous forest structure in ponderosa pine forests via UAS-derived structure from motion. *Environmental Monitoring and Assessment*, *196*(6), 530. https://doi.org/10.1007/s10661-024-12703-1

Harvey, B. J., Donato, D. C., & Turner, M. G. (2016). Burn me twice, shame on who? Interactions between successive forest fires across a temperate mountain region. *Ecology*, *97*(9), 2272–2282. https://doi.org/10.1002/ecy.1439

Hijmans R (2024). terra: Spatial Data Analysis. R package version 1.7-71. https://CRAN.R-project.org/package=terra

Hogland, J., Anderson, N., Affleck, D. L. R., & St. Peter, J. (2019). Using Forest Inventory Data with Landsat 8 Imagery to Map Longleaf Pine Forest Characteristics in Georgia, USA. *Remote Sensing*, *11*(15), Article 15. https://doi.org/10.3390/rs11151803

Housman, I. W., Chastain, R. A., & Finco, M. V. (2018). An Evaluation of Forest Health Insect and Disease Survey Data and Satellite-Based Remote Sensing Forest Change Detection Methods: Case Studies in the United States. *Remote Sensing*, *10*(8), Article 8. https://doi.org/10.3390/rs10081184

Humagain, K., Portillo-Quintero, C., Cox, R. D., & Cain, J. W. (2017). Mapping Tree Density in Forests of the Southwestern USA Using Landsat 8 Data. *Forests*, *8*(8), Article 8. https://doi.org/10.3390/f8080287

Jemaa, H., Bouachir, W., Leblon, B., LaRocque, A., Haddadi, A., & Bouguila, N. (2023). UAV-Based Computer Vision System for Orchard Apple Tree Detection and Health Assessment. *Remote Sensing*, *15*(14), Article 14. https://doi.org/10.3390/rs15143558

Jolly, W. M., & Hadlow, A. M. (2012). A comparison of two methods for estimating conifer live foliar moisture content. *International Journal of Wildland Fire*, *21*(2), 180. https://doi.org/10.1071/WF11015

Joseph, J., Luster, J., Bottero, A., Buser, N., Baechli, L., Sever, K., & Gessler, A. (2021). Effects of drought on nitrogen uptake and carbon dynamics in trees. *Tree Physiology*, *41*(6), 927–943. https://doi.org/10.1093/treephys/tpaa146

Keyes, Christopher R. 2006. Foliar Moisture Contents of North American Conifers. In: Andrews, Patricia L.; Butler, Bret W., comps. 2006. Fuels Management-How to Measure Success: Conference Proceedings. 28-30 March 2006; Portland, OR. Proceedings RMRS-P-41. Fort Collins, CO: U.S. Department of Agriculture, Forest Service, Rocky Mountain Research Station. p. 395-399

Kreuzwieser, J., & Gessler, A. (2010). Global climate change and tree nutrition: Influence of water availability. *Tree Physiology*, *30*(9), 1221–1234. https://doi.org/10.1093/treephys/tpq055

Lad, L. E., Tinkham, W. T., Sparks, A. M., & Smith, A. M. S. (2023). Evaluating Predictive Models of Tree Foliar Moisture Content for Application to Multispectral UAS Data: A Laboratory Study. *Remote Sensing*, *15*(24), Article 24. https://doi.org/10.3390/rs15245703

Lentile, L. B., Holden, Z. A., Smith, A. M. S., Falkowski, M. J., Hudak, A. T., Morgan, P., Lewis, S. A., Gessler, P. E., & Benson, N. C. (2006). Remote sensing techniques to assess active fire characteristics and post-fire effects. *International Journal of Wildland Fire*, *15*(3), 319. https://doi.org/10.1071/WF05097

Littell, J. S., Peterson, D. L., Riley, K. L., Liu, Y., & Luce, C. H. (2016). A review of the relationships between drought and forest fire in the United States. *Global Change Biology*, *22*(7), 2353–2369. https://doi.org/10.1111/gcb.13275

Liu, J., Gao, L., Yuan, F., Guo, Y., & Xu, X. (2019). Climate Change Made Major Contributions to Soil Water Storage Decline in the Southwestern US during 2003–2014. *Water*, *11*(9), Article 9. https://doi.org/10.3390/w11091947

Marques, P., Pádua, L., Sousa, J., & Fernandes-Silva, A. (2023). Assessing the Water Status and Leaf Pigment Content of Olive Trees: Evaluating the Potential and Feasibility of Unmanned Aerial Vehicle Multispectral and Thermal Data for Estimation Purposes. *Remote Sensing*, *15*, 4777. https://doi.org/10.3390/rs15194777

Mast, J. N., Veblen, T. T., & Linhart, Y. B. (1998). Disturbance and climatic influences on age structure of ponderosa pine at the pine/grassland ecotone, Colorado Front Range. *Journal of Biogeography, 25*(4), 743–755. https://doi.org/10.1046/j.1365-2699.1998.2540743.x

Matthews, S. (2010). Effect of drying temperature on fuel moisture content measurements. *International Journal of Wildland Fire, 19*(6), 800. https://doi.org/10.1071/wf08188

Näsi, R., Honkavaara, E., Blomqvist, M., Lyytikäinen-Saarenmaa, P., Hakala, T., Viljanen, N., Kantola, T., & Holopainen, M. (2018). Remote sensing of bark beetle damage in urban forests at individual tree level using a novel hyperspectral camera from UAV and aircraft. *Urban Forestry & Urban Greening*, *30*, 72–83. https://doi.org/10.1016/j.ufug.2018.01.010

Nauslar, N. J., Hatchett, B. J., Brown, T. J., Kaplan, M. L., & Mejia, J. F. (2019). Impact of the North American monsoon on wildfire activity in the southwest United States. *International Journal of Climatology*, *39*(3), 1539–1554. https://doi.org/10.1002/joc.5899

North, M., Stine, P., O'Hara, K., Zielinski, W., & Stephens, S. (2009). An ecosystem management strategy for Sierran mixed-conifer forests. *Gen. Tech. Rep. PSW-GTR-220 (Second Printing, with Addendum). Albany, CA: U.S. Department of Agriculture, Forest Service, Pacific Southwest Research Station. 49 p*, *220*. https://doi.org/10.2737/PSW-GTR-220

Pádua, L., Marques, P., Martins, L., Sousa, A., Peres, E., & Sousa, J. J. (2020). Monitoring of Chestnut Trees Using Machine Learning Techniques Applied to UAV-Based Multispectral Data. *Remote Sensing*, *12*(18), Article 18. https://doi.org/10.3390/rs12183032

Park Williams, A., Allen, C. D., Macalady, A. K., Griffin, D., Woodhouse, C. A., Meko, D. M., Swetnam, T. W., Rauscher, S. A., Seager, R., Grissino-Mayer, H. D., Dean, J. S., Cook, E. R., Gangodagamage, C., Cai, M., & McDowell, N. G. (2013). Temperature as a potent driver of regional forest drought stress and tree mortality. *Nature Climate Change*, *3*(3), 292–297. https://doi.org/10.1038/nclimate1693

Philpot, C.W. (1965). Diurnal fluctuation in moisture content of ponderosa pine and whiteleaf manzanita leaves. USDA Forest Service Research Note PSW-RN-67. 7 p.

Philpot, C. W., Mutch, R.W. (1971). The seasonal trends in moisture content, ether extractives, and energy of ponderosa pine and Douglas-fir needles. Res. Pap. INT-RP-102. Ogden, UT: USDA Forest Service, Intermountain Forest and Range Experiment Station. 21 p.

Phiri, D., Simwanda, M., Salekin, S., Nyirenda, V. R., Murayama, Y., & Ranagalage, M. (2020). Sentinel-2 Data for Land Cover/Use Mapping: A Review. *Remote Sensing*, *12*(14), Article 14. https://doi.org/10.3390/rs12142291

Pebesma, E., 2018. Simple Features for R: Standardized Support for Spatial Vector Data. *The R Journal, 10*(1), 439-446. https://doi.org/10.32614/RJ-2018-009

Peltier, D. M. P., Fell, M., & Ogle, K. (2016). Legacy effects of drought in the southwestern United States: A multi-species synthesis. *Ecological Monographs*, *86*(3), 312–326. https://doi.org/10.1002/ecm.1219

Pérez-Rodríguez, L. A., Quintano, C., Marcos, E., Suarez-Seoane, S., Calvo, L., & Fernández-Manso, A. (2020). Evaluation of Prescribed Fires from Unmanned Aerial Vehicles (UAVs) Imagery and Machine Learning Algorithms. *Remote Sensing*, *12*(8), Article 8. https://doi.org/10.3390/rs12081295

Pierce, L. L., Running, S. W., & Riggs, G. A. (1990). Remote detection of canopy water stress in coniferous forests using the NS001 Thematic Mapper simulator and the thermal infrared multispectral scanner. *Photogrammetric Engineering and Remote Sensing*, *56*(5), 579–586.

Plowright A (2024). _ForestTools: Tools for Analyzing Remote Sensing Forest Data_. R package version 1.0.2, <https://CRAN.R-project.org/package=ForestTools>.

R Core Team (2023). R: A Language and Environment for Statistical Computing. R Foundation for Statistical Computing, Vienna, Austria. <https://www.R-project.org/>.

Rautiainen, M., Lukeš, P., Homolová, L., Hovi, A., Pisek, J., & Mõttus, M. (2018). Spectral Properties of Coniferous Forests: A Review of In Situ and Laboratory Measurements. *Remote Sensing*, *10*(2), Article 2. https://doi.org/10.3390/rs10020207

Rock, B. N., Williams, D. L., Moss, D. M., Lauten, G. N., & Kim, M. (1994). High-spectral resolution field and laboratory optical reflectance measurements of red spruce and eastern hemlock needles and branches. *Remote Sensing of Environment*, *47*(2), 176–189. https://doi.org/10.1016/0034-4257(94)90154-6

Rouse, J. W., Haas, R. H., Schell, J. A., & Deering, D. W. (1974). Monitoring vegetation systems in the Great Plains with ERTS. https://ntrs.nasa.gov/citations/19740022614

Roussel J (2024). lasR: Fast and Pipeable Airborne LiDAR Data Tools. R package version 0.5.6, https://github.com/r-lidar/lasR

Roussel, J.R., Auty, D., Coops, N. C., Tompalski, P., Goodbody, T. R. H., Sánchez Meador, A., Bourdon, J.F., De Boissieu, F., Achim, A. (2020). lidR: An R package for analysis of Airborne Laser Scanning (ALS) data. *Remote Sensing of Environment*, *251*, 112061. https://doi.org/10.1016/j.rse.2020.112061

Roussel, J. R., Auty, D. (2024). Airborne LiDAR Data Manipulation and Visualization for Forestry Applications. R package version 4.1.0. https://cran.r-project.org/package=lidR

Ruthrof, K. X., Fontaine, J. B., Matusick, G., Breshears, D. D., Law, D. J., Powell, S., & Hardy, G. (2016). How drought-induced forest die-off alters microclimate and increases fuel loadings and fire potentials. *International Journal of Wildland Fire*, *25*(8), 819–830. https://doi.org/10.1071/WF15028

Ryan, K. C., Knapp, E. E., & Varner, J. M. (2013). Prescribed fire in North American forests and woodlands: History, current practice, and challenges. *Frontiers in Ecology and the Environment*, *11*(s1), e15–e24. https://doi.org/10.1890/120329

Ryan, M. G. (2011). Tree responses to drought. *Tree Physiology*, *31*(3), 237–239. https://doi.org/10.1093/treephys/tpr022

Simonin, K., Kolb, T. E., Montes-Helu, M., & Koch, G. W. (2006). Restoration thinning and influence of tree size and leaf area to sapwood area ratio on water relations of Pinus ponderosa. *Tree Physiology*, *26*(4), 493–503. https://doi.org/10.1093/treephys/26.4.493

Sohn, J. A., Saha, S., & Bauhus, J. (2016). Potential of forest thinning to mitigate drought stress: A meta-analysis. *Forest Ecology and Management*, *380*, 261–273. https://doi.org/10.1016/j.foreco.2016.07.046

Sparks, A., Kolden, C., Talhelm, A., Smith, A., Apostol, K., Johnson, D., & Boschetti, L. (2016). Spectral Indices Accurately Quantify Changes in Seedling Physiology Following Fire: Towards Mechanistic Assessments of Post-Fire Carbon Cycling. *Remote Sensing, 8*(7), 572. https://doi.org/10.3390/rs8070572

Steckel, M., Moser, W. K., del Río, M., & Pretzsch, H. (2020). Implications of Reduced Stand Density on Tree Growth and Drought Susceptibility: A Study of Three Species under Varying Climate. *Forests, 11*(6), Article 6. https://doi.org/10.3390/f11060627

Stephens, S. L., Collins, B. M., Fettig, C. J., Finney, M. A., Hoffman, C. M., Knapp, E. E., North, M. P., Safford, H., & Wayman, R. B. (2018). Drought, Tree Mortality, and Wildfire in Forests Adapted to Frequent Fire. *BioScience*, *68*(2), 77–88. https://doi.org/10.1093/biosci/bix146

Stevens-Rumann, C. S., & Morgan, P. (2019). Tree regeneration following wildfires in the western US: A review. *Fire Ecology*, *15*(1), 15. https://doi.org/10.1186/s42408-019-0032-1

Stout, D. L., & Sala, A. (2003). Xylem vulnerability to cavitation in Pseudotsuga menziesii and Pinus ponderosa from contrasting habitats. *Tree Physiology*, *23*(1), 43–50. https://doi.org/10.1093/treephys/23.1.43

Swayze, N. C., Tinkham, W. T., Vogeler, J. C., & Hudak, A. T. (2021). Influence of flight parameters on UAS-based monitoring of tree height, diameter, and density. *Remote Sensing of Environment*, *263*, 112540. https://doi.org/10.1016/j.rse.2021.112540

Tinkham, W. T., & Swayze, N. C. (2021). Influence of Agisoft Metashape Parameters on UAS Structure from Motion Individual Tree Detection from Canopy Height Models. *Forests, 12*(2), Article 2. https://doi.org/10.3390/f12020250

Tinkham, W. T., Swayze, N. C., Hoffman, C. M., Lad, L. E., & Battaglia, M. A. (2022). Modeling the Missing DBHs: Influence of Model Form on UAV DBH Characterization. *Forests*, *13*(12), Article 12. https://doi.org/10.3390/f13122077

Tinkham, W.T., Woolsey, G.A. (2024). Influence of Structure for Motion Algorithm Parameters on Metrics of Individual Tree Detection Accuracy and Precision. *Remote Sensing*, *16*(20), 3844. https://doi.org/10.3390/rs16203844

User guide for micasense sensors – micasense knowledge base. (n.d.). https://support.micasense.com/hc/en-us/articles/360039671254-User-Guide-for-MicaSense-Sensors

Vogelmann, J. E., Tolk, B., & Zhu, Z. (2009). Monitoring forest changes in the southwestern United States using multitemporal Landsat data. *Remote Sensing of Environment*, *113*(8), 1739–1748. https://doi.org/10.1016/j.rse.2009.04.014

Wainwright, H. M., Steefel, C., Trutner, S. D., Henderson, A. N., Nikolopoulos, E. I., Wilmer, C. F., Chadwick, K. D., Falco, N., Schaettle, K. B., Brown, J. B., Steltzer, H., Williams, K. H., Hubbard, S. S., & Enquist, B. J. (2020). Satellite-derived foresummer drought sensitivity of plant productivity in Rocky Mountain headwater catchments: Spatial heterogeneity and geological-geomorphological control. *Environmental Research Letters*, *15*(8), 084018. https://doi.org/10.1088/1748-9326/ab8fd0

Williams, A. P., Cook, E. R., Smerdon, J. E., Cook, B. I., Abatzoglou, J. T., Bolles, K., Baek, S. H., Badger, A. M., & Livneh, B. (2020). Large contribution from anthropogenic warming to an

emerging North American megadrought. *Science*, *368*(6488), 314–318. https://doi.org/10.1126/science.aaz9600

Woolsey, G. (2024). *cloud2trees: Point Cloud Data to Forest Inventory Tree List*. R package version 0.1.0. Retrieved from https://CRAN.R-project.org/package=cloud2trees

Young, D. J. N., Estes, B. L., Gross, S., Wuenschel, A., Restaino, C., & Meyer, M. D. (2023). Effectiveness of forest density reduction treatments for increasing drought resistance of ponderosa pine growth. *Ecological Applications: A Publication of the Ecological Society of America*, *33*(4), e2854. https://doi.org/10.1002/eap.2854

Zarco-Tejada, P. J., González-Dugo, V., & Berni, J. A. J. (2012). Fluorescence, temperature and narrow-band indices acquired from a UAV platform for water stress detection using a micro-hyperspectral imager and a thermal camera. *Remote Sensing of Environment*, *117*, 322–337. https://doi.org/10.1016/j.rse.2011.10.007

Zhang, J., Finley, K. A., Johnson, N. G., & Ritchie, M. W. (2019). Lowering Stand Density Enhances Resiliency of Ponderosa Pine Forests to Disturbances and Climate Change. *Forest Science, 65*(4), 496–507. https://doi.org/10.1093/forsci/fxz006

CHAPTER 4 – MORTALITY IN PINUS MONTICOLA AND PSEUDOTSUGA MENZIESII SAPLINGS[2]

4.1 Introduction

Natural disturbances such as drought, fire, and insects are pivotal in shaping forest ecosystem composition, structure, and productivity by injuring and killing individual trees and altering forest succession (Paine et al. 1998; Turner 2010). The degree of disturbance-induced change largely depends on the intensity, frequency, and extent of the disturbance and can vary significantly between disturbance types (Dale et al. 2001). Compound disturbances, or disturbances occurring simultaneously or rapidly in sequence, can create greater ecosystem change than individual disturbance events alone, and can contribute to reduced forest resilience, or the time it takes a forest to recover to a pre-disturbance state (Kleinman et al. 2019; Millar and Stephenson 2015; Paine et al. 1998).

Compound disturbances represent a growing threat to western United States forests given projected increases in both drought and fire activity (Abatzoglou et al. 2021; Anderegg et al. 2022; Dai 2013), however, the extent and severity of this threat is largely unknown given that trees of differing species, sizes, and ages can have widely different physiological and mortality responses to drought and fire (Adams et al. 2017; Hood et al. 2018; McDowell et al. 2018). An improved understanding of the effects of simultaneous drought and fire stress is needed to inform natural resource managers on actions that could mitigate any amplified detrimental impacts.

[2] Chapter published as: Sparks, A. M., Blanco, A. S., Lad, L. E., Smith, A. M. S., Adams, H. D., & Tinkham, W. T. (2024). Prefire Drought Intensity Drives Postfire Recovery and Mortality in Pinus monticola and Pseudotsuga menziesii Saplings. *Forest Science*, fxae013. https://doi.org/10.1093/forsci/fxae013

The combined effects of drought and fire on tree physiology, recovery, and mortality are poorly understood (Kleinman et al. 2019; Millar and Stephenson 2015; Sturtevant and Fortin 2021). Drought can prompt trees to close stomata to limit water loss, which reduces carbon assimilation via photosynthesis and increases dependence on nonstructural carbohydrate (NSC) stores for cellular maintenance and repair (McDowell et al. 2011, 2022). Drought also depletes tree water content, increasing flammability (Ruffault et al. 2023; Weir and Scasta 2014), and if persistent, can result in xylem hydraulic dysfunction and eventual phloem transport failure (McDowell et al. 2022). Fires can exacerbate the stress of droughted trees by damaging critical tissues and organs necessary for NSC production and transport (Hood et al. 2018; Partelli-Feltrin et al. 2023). Depending on the fire intensity and presence or absences of fire-resistant tree traits (e.g., bark thickness, crown height above ground), and strategies (e.g., NSC storage belowground, serotiny), fire can damage sensitive foliage and buds in the crown (Michaletz and Johnson 2006; Smith et al. 2017; Sparks et al. 2023) and stem/branch phloem that are necessary for the translocation of NSC from the crown to the roots (Partelli-Feltrin et al. 2023). Because drought reduces the NSC stores that a tree needs for repairing fire-damaged tissues, drought is hypothesized to increase postfire tree mortality, especially for trees exposed to higher-intensity fires (figure 4.1) (Smith et al. 2017; Sparks et al. 2018; van Mantgem et al. 2018). Several studies have provided evidence in support of this hypothesis in *Pinus ponderosa* and *Larix occidentalis* saplings, where mortality generally increased with increasing drought and fire intensity (Partelli-Feltrin et al. 2020; Sparks et al. 2018). Similarly, others have shown that drought stress and associated reductions in tree vigor (e.g., reduced growth rate) in mature conifers increased vulnerability to fire-induced mortality (Slack et al. 2016; van Mantgem et al.

2013, 2018). Conversely, others have observed no or very low levels of mortality in resprouting *Quercus* spp. and *Pinus palustris* that were subjected to drought and surface fires (Chiatante et al. 2015; Di Iorio et al. 2011; Wilson et al. 2022). Although these studies have advanced our understanding of drought and fire effects, some are limited, as they did not have a drought-only treatment to isolate drought and combined drought and fire effects (Sparks et al. 2018). Others did not test severe drought intensities that could cause even nonburned trees to die (Partelli-Feltrin et al. 2020; Wilson et al. 2022) or did not quantify the fire intensity (Chiatante et al. 2015; Di Iorio et al. 2011; van Mantgem et al. 2013, 2018).

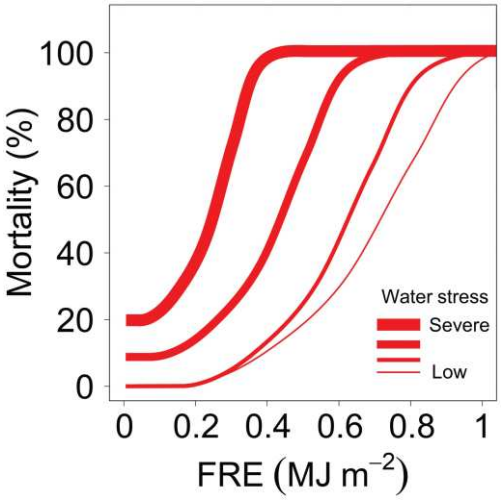

Figure 4.1: Hypothesized leftward shift of increased vulnerability in the relationship between fire intensity, reported here as fire radiative energy (FRE; units: MJ m^{-2}), and conifer sapling mortality as water stress increases (adapted from Sparks et al. 2018). At severe water stress levels, mortality will occur even in trees exposed to very low-intensity fires or no fire and is denoted by the upward shift of the FRE-mortality relationship. The "Low" water stress line represents the average mortality observed across FRE doses from 0 to 1 MJ m^{-2} for well watered conifer saplings of similar size and age to those in this study (Smith et al. 2017; Sparks et al. 2023; Steady et al. 2019).

Understanding how trees respond to drought and fire is important for tree mortality modeling and identifying early warning signs of tree mortality. Tree mortality models underlie software tools used in fire management planning (e.g., First Order Fire Effects Model, Lutes

2020; FFE-FVS, Rebain 2022), and thus their accuracy is of critical importance (Hood et al. 2018; Woolley et al. 2012). Few equations used within these models focus on smaller trees (Battaglia et al. 2009), which represents a considerable knowledge gap given that prescribed burning commonly includes objectives to purposefully kill, or reduce the mortality of, smaller trees (Hood et al. 2018). Furthermore, climate change is predicted to decrease the time between fires in the western United States (Abatzoglou et al. 2017; Bowman et al. 2017) and this region is also expected to need a higher frequency of prescribed fires to reduce wildfire hazard (Voelker et al. 2019), compounding to increase the occurrence of fires on younger cohorts of trees. Many models use prefire morphological attributes (e.g., bark thickness and crown base height) and postfire injury (e.g., crown scorch and stem charring) to predict postfire mortality (Ryan and Reinhardt 1988; Shearman et al. 2019; Stephens and Finney 2002), but it is not well understood whether using only prefire physiological and morphological characteristics and fire intensity can provide accurate mortality predictions. Prefire morphology could potentially improve mortality prediction given that prior observations have shown size dependent relationships, where smaller trees are killed at higher proportions than larger trees at a given fire intensity (McDowell et al. 2018; Stephens and Finney 2002). Inclusion of morphology may be advantageous, given that some metrics can be accurately quantified (e.g., total height, crown base height) or modeled (e.g., diameter) at the individual tree level across large spatial scales using airborne laser scanning (Hyyppa and Inkinen 1999; Popescu 2007; Popescu and Zhao 2008; Sparks et al. 2022), whereas estimates of crown scorch and stem char are difficult to collect at large scales, as they need to be assessed by ground observation personnel (Varner et al. 2021). Other studies have shown that prefire physiological condition, including minimal

water stress (Partelli-Feltrin et al. 2020; Sparks et al. 2018), greater photosynthetic efficiency (expressed as chlorophyll fluorescence) (Smith et al. 2017), and increased growth rate (van Mantgem et al. 2003) increase the probability of postfire tree survival. Remotely sensed observations of chlorophyll fluorescence, which provide information on the efficiency of leaf photochemistry (Maxwell and Johnson 2000; Murchie and Lawson 2013), could provide a mechanistic and scalable metric of postfire tree physiological condition. Chlorophyll fluorescence is highly sensitive to plant stress (e.g., water, cold, heat) (Ač et al. 2015; Guadagno et al. 2017), which suggests that it could provide an early warning sign and predictor variable in postfire mortality modeling, but limited research has assessed this potential (Smith et al. 2017; Sparks et al. 2023).

The objective of this study was to quantify the impact of variable-intensity drought and fire on *Pinus monticola* var. *minima* Lemmon and *Pseudotsuga menziesii* (Mirb.) Franco var. *glauca* (Beissn.) Franco sapling physiology and mortality. We specifically address the following questions:

(1) How does increasing drought stress and fire intensity affect sapling postfire recovery?
(2) How does increasing sapling drought stress affect the fire intensity-mortality dose-response relationship?
(3) Can we accurately model postfire sapling mortality using prefire physiological and morphological characteristics and fire intensity?

To answer these questions, we used a controlled dose-response approach (Smith et al. 2016; Sparks et al. 2023) where *P. monticola* and *P. menziesii* saplings were subjected to varying drought and surface fire intensities and monitored for up to 10 weeks postfire. Prefire sapling physiological condition and morphology observations were used as inputs in a random forest

classifier to assess the accuracy and relative importance of these attributes when predicting sapling mortality.

4.2 Materials and Methods

4.2.1 Pinus monticola and P. menziesii Saplings and Study Treatments

Pinus monticola and *P. menziesii* saplings (N = 64 per species) were acquired from the Franklin H. Pitkin Forest Nursery at the University of Idaho and were grown in 9.5 L pots through two-and-a-half growing seasons under natural light conditions in a climate-controlled greenhouse in Moscow, Idaho, USA (N 46.73° W 117.00°). During this period, saplings were watered to field capacity daily to minimize water stress. Prior to drought and fire treatments, the mean (±SE) diameter at root collar (DRC) was 1.7 ± 0.03 cm and 2.1 ± 0.05 cm and mean height was 0.82 ± 0.02 m and 1.0 ± 0.02 m for *P. monticola* and *P. menziesii*, respectively. The mean height to live crown was 13.6 ± 0.71 cm and 6.8 ± 0.53 cm and number of live branches was 17 ± 0.7 and 34 ± 0.9 for *P. monticola* and *P. menziesii*, respectively.

We conducted a pilot drought to determine the length of time and foliar moisture content (FMC) at which the saplings would start dying during drought. Three saplings of each species had water withheld until mortality was determined. Mortality was defined as the death of all foliage and the inability to regenerate shoots. A stem cambium scratch test was also used to confirm mortality, where living cambium is green and dead cambium is brown. Mature needles produced in the previous year were collected from each sapling every ~7 days and were used to calculate FMC. At each sampling date, ~5 g of needles were collected randomly throughout the top third of each sapling crown and had their fresh sample weight recorded (±

0.01 g). These foliar samples were then oven dried for 24 hours at 100°C and weighed again to acquire their dry weight. Foliar moisture content (FMC, %) was calculated on a dry weight basis. After 21 days without water, all trees were dead except one *P. monticola* sapling.

Following the pilot drought, *P. monticola* and *P. menziesii* saplings were randomly divided into one of four drought groups and one of three fire treatment groups (Table 1). The most severe drought treatment was slightly longer than the pilot drought to ensure some drought-induced mortality. Starting at 25 days prefire, the three drought groups had water withheld for progressively shorter intervals while the control was watered to field capacity daily. After the drought treatments were complete, the saplings in the drought and fire treatment groups were subjected to surface fires with a known fire intensity dose (Table 1), reported as fire radiative energy (FRE, in MJ m-2), or the total radiative heat flux. Surface fires were conducted at the Idaho Fire Initiative for Research and Education (IFIRE), a climatically controlled indoor combustion laboratory. We used FRE as the dose metric, given that prior studies have shown that pure fuel beds with the same mass and moisture content produce consistent and repeatable quantities of FRE (Smith et al. 2013, 2016; Wooster et al. 2021). We used FRE doses of 0 MJ m^{-2} (i.e., no fire), 0.4 MJ m^{-2}, and 0.6 MJ m^{-2}, as these doses are known to result in low-to-moderate mortality levels in saplings with minimal water stress (Sparks et al. 2023). The specific FRE doses were created by burning fuel beds of pure *P. monticola* needles at <1% moisture content. The relationship between fuel load and FRE reported in Smith et al. (2017) was used to calculate the necessary fuel load for each dose group, where the needle fuel load (kg) = 2.679 / FRE. Before burning each sapling, ~5 g of needles were collected randomly throughout the top third and bottom third of each sapling crown for FMC estimation. Saplings

in each dose group were burned individually and were inserted into a custom-cut concrete board so that the soil surface of the sapling pot was level with the board. The corresponding fuel load of dry needles was evenly distributed in a 1 m2 circular area surrounding each sapling and ignited on one side to produce a surface fire with a uniform flaming front (figure 4.2). After the fire treatments, all saplings, including those in unburned treatment groups, were watered to field capacity daily.

Table 4.1: Sample size for each treatment group for each species (N = 64 per species). FRE, fire radiative energy.

Drought treatment group (days without water)	**Number of saplings at each FRE dose**		
	0 (no fire)	**0.4 MJ m^{-2}**	**0.6 MJ m^{-2}**
0	4	6	6
14	4	6	6
19	4	6	6
25	4	6	6

4.2.2 Chlorophyll Fluorescence Measurements

Chlorophyll fluorescence is the re-emission of light absorbed by chlorophyll molecules associated with photosystem II (PSII). Fluorescence represents one of three fates of harvested light energy, including energy used to drive photosynthesis and energy dissipated as heat. Because fluorescence occurs in competition with these other processes, fluorescence can provide useful information on the efficiency of leaf photochemistry (Maxwell and Johnson 2000; Murchie and Lawson 2013). A commonly used chlorophyll fluorescence metric is the maximum quantum yield of PSII (F_v/F_m), calculated following Genty et al. (1989):

$$\frac{F_v}{F_m} = \frac{F_m - F_o}{F_m} \quad (1)$$

where F_v is the difference between the maximum fluorescence (F_m) and the minimum fluorescence (F_o). Subjecting a dark-adapted leaf to a saturating pulse of light energy induces

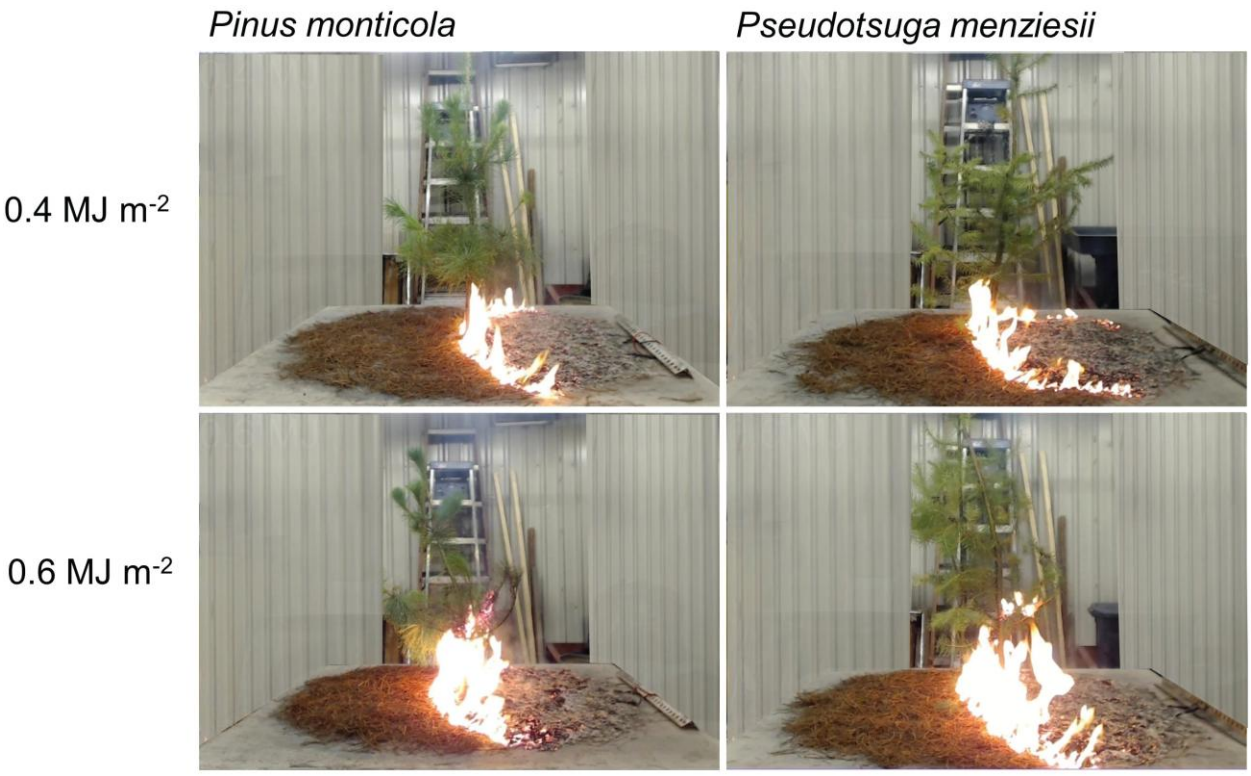

Figure 4.2: Experimental burn setup for representative *Pinus monticola* (left column) and *Pseudotsuga menziesii* (right column) saplings subjected to surface fires with fire radiative energy of 0.4 MJ m^{-2} (top row) and 0.6 MJ m^{-2} (bottom row).

maximum fluorescence, as there is assumed to be little to no heat dissipation (Murchie and Lawson 2013). Likewise, minimal fluorescence can be measured by subjecting a dark-adapted leaf to a weak pulse of light energy. Generally, stressed plants will have F_v/F_m values less than 0.8 (Maxwell and Johnson 2000). Water stress, in particular, impedes electron donation in PSII and is reflected in decreases in F_v (Downton et al. 1981).

Chlorophyll fluorescence measurements were acquired weekly on all study trees from 1 week prefire to 4 weeks postfire and then biweekly until 8 weeks postfire using an OS30p+ fluorometer (Opti-Sciences, Hudson, NH). Measurements were acquired at night, at least 1 hour after sunset, so that needles could dark adapt. Measurements were taken on needles with minimal visible damage or discoloration in the top one-third of each sapling crown. Minimal

fluorescence (F_o) was measured, and maximum fluorescence (F_m) was measured after a short saturation pulse (3500 µmol m^{-2} s^{-1}) of red light centered at 660 nm.

4.2.3 Morphological Measurements and Mortality Assessment

Total sapling height and DRC were measured at weekly intervals starting from 1 week prefire to 4 weeks postfire. The height to live crown and number of live branches were also measured for each sapling prior to the start of the drought treatments. Fire-induced crown scorch was not measured, as it was impossible to visually differentiate foliage killed by the fire and dying or killed foliage due to the prefire drought. Mortality was assessed at 1 day prefire and 10 weeks postfire.

4.2.4 Analysis and Mortality Modeling

Differences in prefire physiology and foliar moisture content among drought treatments were compared with ANOVA, and if significant ($\alpha = 0.05$), a Tukey's honest significant difference test. We quantified the effect of FMC and FRE dose on sapling mortality using logistic regression in R statistical software (R Core Team 2023). Logistic regression models were fit separately for each FRE dose group and were used to determine
the lethal threshold of FMC at which 50% of saplings died.

A random forest classification approach was used to model postfire mortality. Random forest is an ensemble learning algorithm that uses bootstrap samples of the training data to train each tree in an ensemble of n trees (Breiman 2001). Trees are assigned live or dead classification by a majority vote of the ensemble of trees and cross-validated against the data not included in the bootstrap samples, referred to as the "out-of-bag observations." Random

forest classification does not make distributional assumptions about the data and is insensitive to collinearity among predictor variables (Cutler et al. 2007). It has also been shown to be superior to other modeling approaches, such as logistic regression, when using unbalanced datasets such as tree mortality datasets (Shearman et al. 2019).

Random forest classification was conducted using the 'randomForest' (Liaw and Wiener 2002) R package in R statistical software (R Core Team 2023). The classifier was trained with n = 500 'trees', and the number of variables at each split was set to the square root of the total number of predictor variables. We split each species dataset into training and validation datasets using an 80:20 ratio. To avoid the large variability in classification accuracy that arises by doing a single split of data into training and validation datasets, we repeatedly split each dataset into training and validation sets using bootstrapping following Lyons et al. (2018). In total, one hundred different sets were generated, and a classification was performed using each set. Predictor variables included prefire F_v/F_m, FMC, FRE dose, height, DRC, number of live branches, and height to live crown. Predictor variable importance was calculated as the mean decrease in classification accuracy or the normalized difference in the misclassification rate between the original and modified classifications where values of the predictor variable of interest were randomly permuted in the out-of-bag observations.

Validation was performed for each classification iteration using confusion matrices calculated between the predicted live or dead classification and the reference observations. These confusion matrices were used to calculate average overall accuracy, omission and commission errors, and associated 95% confidence intervals (Story and Congalton 1986). The overall accuracy is the percentage of correctly classified saplings divided by the total

number of saplings. Commission error is calculated as 1 minus user's accuracy, where user's accuracy represents the proportion of saplings classified as class *i* that have reference class *i*. Omission error is calculated as 1 minus producer's accuracy, where producer's accuracy represents the proportion of saplings of reference class *j*, classified as class *j*.

4.3 Results

4.3.1 Drought Impacts on Prefire Sampling Physiology

The conifer saplings' FMC declined with lengthening drought treatments (figure 4.3). At the end of the drought period, *P. monticola* 0–19 day drought groups did not have significant differences in their FMC, whereas the 25 day drought group was significantly lower ($P < 0.001$) (figure 4.3). *Peudotsuga menziesii* drought groups were more variable, with progressively lower FMC ($P < .001$) in the 19–25 day drought groups than the 0–14 day drought groups. Although not significantly different, the lower crown FMC was 9% and 12% lower than upper crown FMC, on average, for *P. monticola* and *P. menziesii*, respectively.

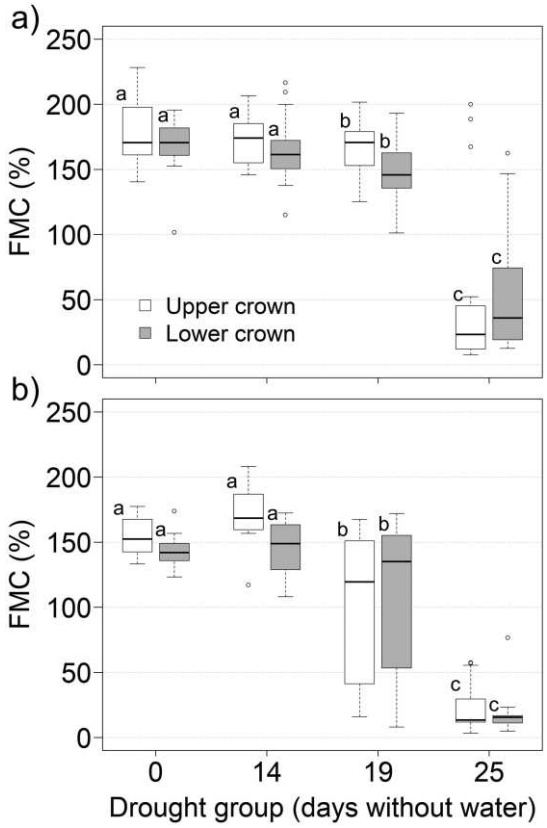

Figure 4.3: Foliar moisture content (FMC) for the upper and lower crown needles for (a) *Pinus monticola* and (b) *Pseudotsuga menziesii* prior to fire treatments. Mean values sharing the same letter are not significantly different ($P < 0.05$).

For both species, F_v/F_m followed the same pattern as FMC. At the end of the drought period, the average F_v/F_m for *P. monticola* in the 0–19 day drought groups were not significantly different, and the 25 day drought group was lower ($P < 0.001$) (figure 4). Although not significantly different, the average F_v/F_m for *P. monticola* in the 19 day drought group was 7.5% lower than in the 0–14 day drought groups. The average F_v/F_m for *P. menziesii* was progressively lower in the 19–25 day drought groups than in the 0–14 day drought groups ($P < 0.001$) (figure 4).

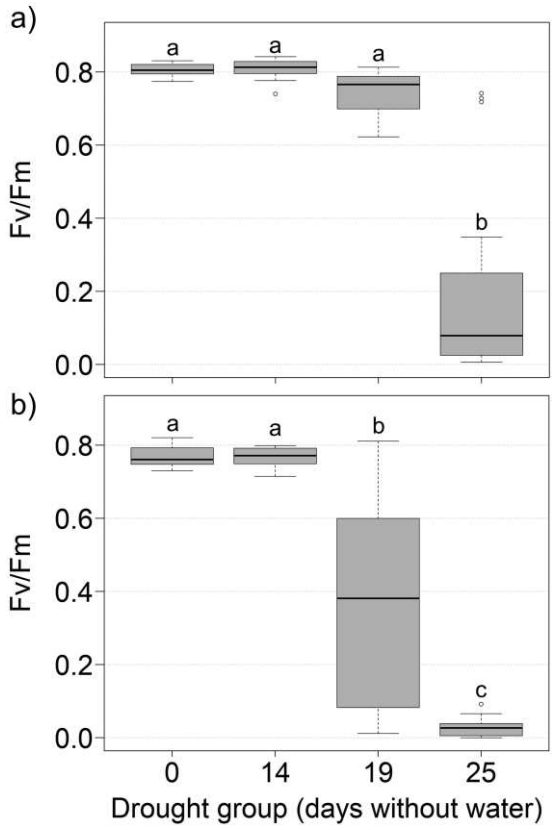

Figure 4.4: Chlorophyll fluorescence (F_v/F_m) across drought groups for (a) *Pinus monticola* and (b) *Pseudotsuga menziesii* saplings prior to fire treatments. Mean values sharing the same letter are not significantly different ($P < 0.05$).

4.3.2 Drought and Fire Impacts on Sampling Physiology and Mortality

F_v/F_m displayed differing temporal trajectories from 1 week prefire to 8 weeks postfire for saplings that lived versus those that died by 10 weeks postfire (figures 4.5 and 4.6). Generally, saplings alive at 10 weeks postfire maintained high F_v/F_m (>0.6) throughout the monitoring period. A majority of saplings (~82%) in the 0–14 day drought groups that were subjected to surface fires experienced an immediate 1 week postfire decline in F_v/F_m, followed by a slight increase 2–3 weeks postfire. The average magnitude of the F_v/F_m loss was greater for *P. menziesii* saplings in the 0- and 14-day drought groups subjected to 0.6 MJ m^{-2} fires (-41% and -35%, respectively) than those subjected to 0.4 MJ m^{-2} fires (-23% and -14%, respectively).

Conversely, there was no difference in the magnitude of the F_v/F_m loss for *P. monticola* saplings in the 0- and 14-day drought groups subjected to 0.4 MJ m^{-2} fires (-7% and -8%, respectively) and those subjected to 0.6 MJ m^{-2} fires (-7% and -8%, respectively). Saplings that lived were able to maintain F_v/F_m recovery (figures 4.5b and c and 4.6b and c), whereas saplings that died displayed decreasing F_v/F_m for the remainder of the monitoring period (figures 4.5e and f and 4.6e and f). Saplings that recovered their F_v/F_m to prefire levels were generally in less severe drought groups (≤14 days drought) and lower FRE groups (≤0.4 MJ m^{-2}).

For both species, there was a leftward shift in the dose response relationship between FRE and mortality for saplings in more severe drought groups (figure 4.7). In other words, more severely water-stressed saplings had higher mortality rates than less water-stressed saplings when exposed to the same FRE dose. For P. monticola, the FRE dose at which some mortality occurred decreased from 0.6 MJ m-2 for the 14 day drought group to 0.4 MJ m-2 for the 19 day drought group to 0 MJ m-2 for the 25 day drought group (figure 4.7a). Pinus monticola in the 0 day drought group exhibited 0% mortality across all FRE doses. For P. menziesii, the FRE dose at which some mortality occurred decreased from 0.6 MJ m-2 for the 0 and 14 day drought groups to 0.4 MJ m-2 for the 19 day drought group to 0 MJ m-2 for the 25 day drought group (figure 4.7b). Mortality in unburned saplings occurred in the 25 day drought group for both P. monticola (75% mortality, figure 4.7a) and P. menziesii (100% mortality, figure 4.7b).

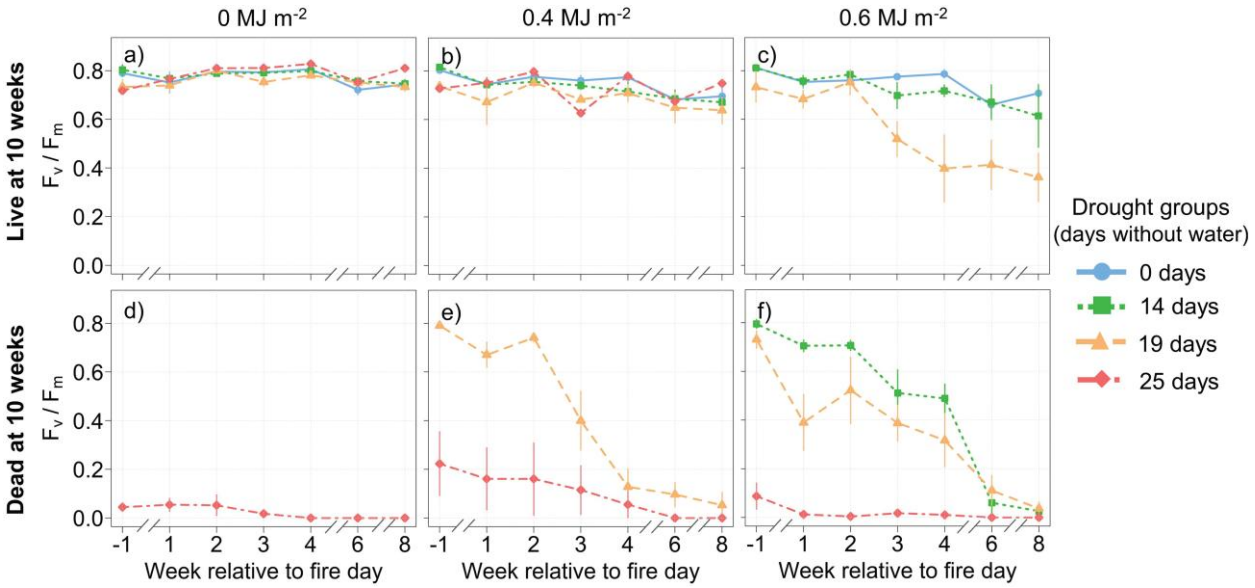

Figure 4.5: Temporal trajectories of average (±SE) *Pinus monticola* sapling chlorophyll fluorescence (Fv/Fm) from 1 week prefire to 8 weeks postfire for living (a–c) and dead (d–f) saplings at 10 weeks postfire. Panes show saplings in the 0 MJ m^{-2} (left), 0.4 MJ m^{-2} center), and 0.6 MJ m^{-2} (right) fire radiative energy (FRE) dose groups.

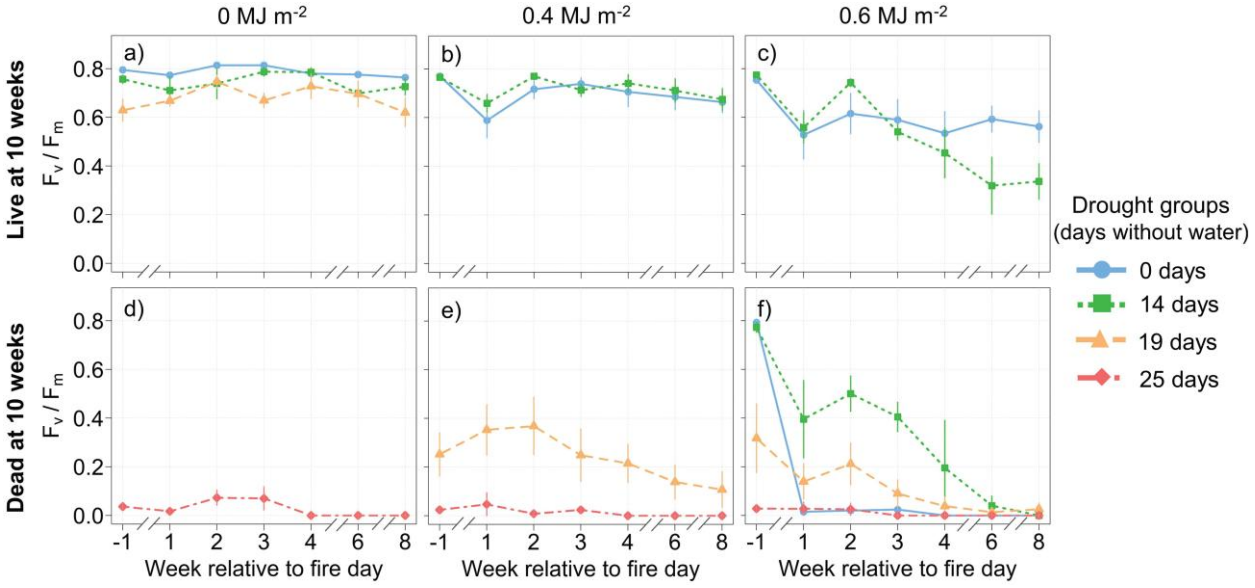

Figure 4.6: Temporal trajectories of average (±SE) *Pseudotsuga menziesii* sapling chlorophyll fluorescence (Fv/Fm) from 1 week prefire to 8 weeks postfire for living (a–c) and dead (d–f) saplings at 10 weeks postfire. Panes show saplings in the 0 MJ m^{-2} (left), 0.4 MJ m^{-2} center), and 0.6 MJ m^{-2} (right) fire radiative energy (FRE) dose groups.

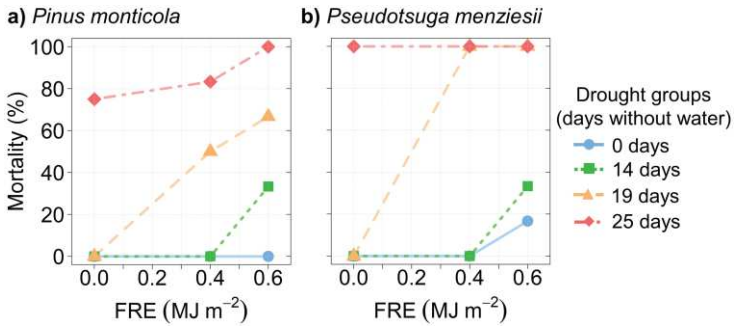

Figure 4.7: Dose-response relationships between fire radiative energy (FRE) and mortality at 10 weeks postfire for (a) *Pinus monticola* and (b) *Pseudotsuga menziesii* across the four drought groups.

The 50% lethal FMC (LD50) for both *P. monticola* and *P. menziesii* increased with greater FRE (figure 4.8). The LD50 for *P. monticola* increased from 88.2% for unburned saplings to 152.5% for saplings in the 0.6 MJ m^{-2} FRE dose group. Likewise, the LD50 for *P. menziesii* increased from 37.1% for unburned saplings to 136.5% for saplings in the 0.6 MJ m^{-2} FRE dose group. All unburned saplings that died had an FMC lower than 50%, whereas trees that died in

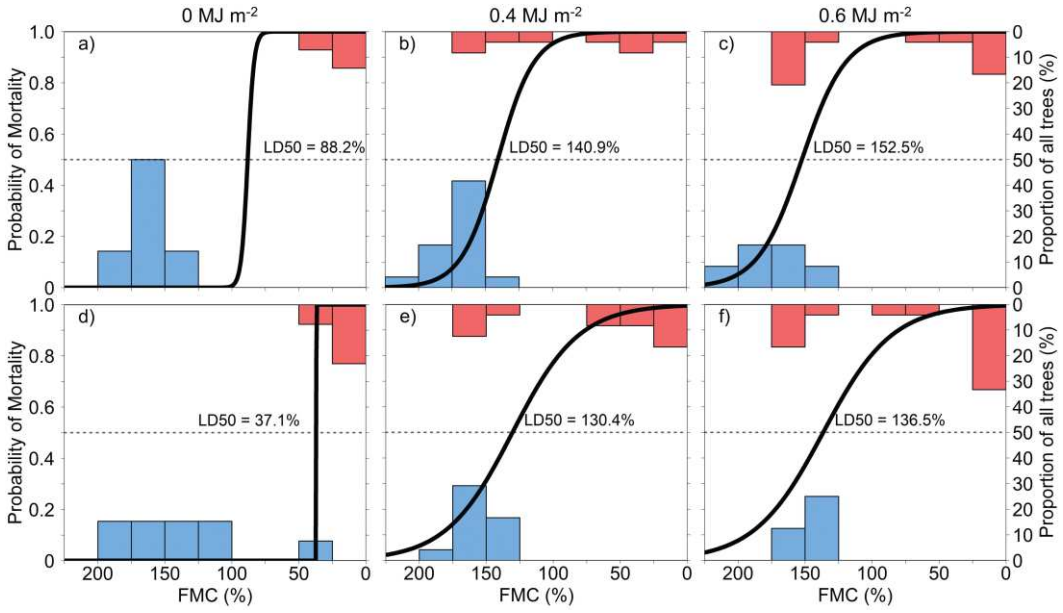

Figure 4.8: The 50% lethal foliar moisture content (FMC LD50, dashed line) increased for *Pinus monticola* (a–c) and *Pseudotsuga menziesii* (d–f) at 10 weeks postfire as fire radiative energy (FRE) increased from 0 MJ m^{-2} (left column) to 0.6 MJ m^{-2} (right column). Bars represent the proportion of living (blue) and dead (red) trees in each 25% FMC bin for each FRE dose group and the solid black line is the logistic regression fit.

the 0.4 and 0.6 MJ m^{-2} FRE dose groups had a wider range of FMC, with some mortality occurring in saplings with FMC greater than 150%.

4.3.3 Postfire Sampling Mortality Prediction

The overall accuracy for the random forest live or dead classification, averaged over the one hundred dataset iterations, was moderately high for both *P. monticola* (82.0%) and *P. menziesii* (78.5%) (Table 4.2). For both species, omission errors for dead sapling classification were higher than commission errors, and commission errors for live saplings were higher than omission errors. These patterns indicate that the classifier tended to misclassify dead saplings as live. Our assessment of predictor variable importance shows that for both species, prefire physiological condition (e.g., water stress and F_v/F_m) is more important than FRE dose for predicting mortality at 10 weeks postfire (figure 4.9). Morphological metrics were generally not as important for predicting tree mortality; however, height was the most important morphological variable for both species.

Table 4.2: Confusion matrix results showing live or dead classification accuracy for *Pinus monticola* and *Pseudotsuga menziesii*, averaged across the 100 classification iterations. Accuracy metrics report the mean (±95% confidence interval).

Classification	**Accuracy metric**	***P. monticola***	***P. menziesii***
Dead	Producer's accuracy	58.9 (5.3)	68.8 (4.0)
	Omission error	41.1 (5.3)	31.1 (4.0)
	User's accuracy	82.4 (4.9)	79.3 (3.6)
	Commission error	17.6 (4.9)	20.7 (3.6)
Live	Producer's accuracy	93.4 (1.7)	86.2 (2.3)
	Omission error	6.5 (1.7)	13.8 (2.3)
	User's accuracy	82.7 (2.2)	79.1 (2.8)
	Commission error	17.3 (2.2)	20.8 (2.8)
	Overall accuracy	82.0 (1.9)	78.5 (1.9)

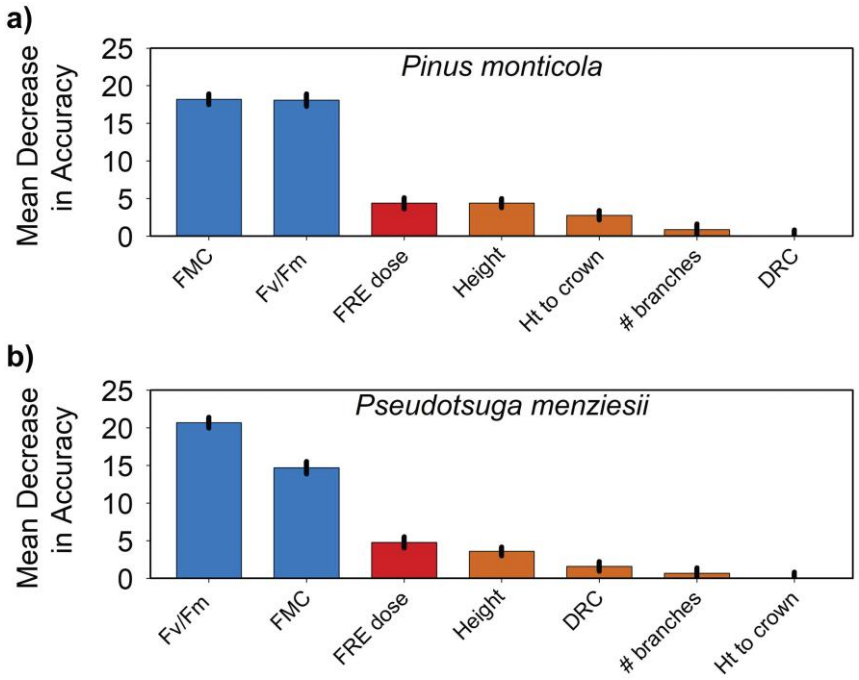

Figure 4.9: Predictor variable importance reported as the mean (±95% confidence interval) decrease in live or dead classification accuracy for (a) *Pinus monticola* and (b) *Pseudotsuga menziesii*. All physiological (blue) and morphological (brown) variables were measured prior to fire. Higher values indicate variables that are more important to the classification. FMC, foliar moisture content; Fv/Fm, chlorophyll fluorescence; FRE, fire radiative energy;height, total sapling height; Ht to crown, height to live crown; # branches, number of live branches; DRC, diameter-at-root-collar.

4.3.4 Discussion

This study used a toxicological dose-response approach to assess how compound disturbances, specifically drought and fire, affect tree physiology, recovery, and mortality. In general, we observed an amplified response, where *P. monticola* and *P. menziesii* saplings subjected to higher intensity drought and fire treatments showed reduced capacity to recover photosynthetic capacity after the treatments. Likewise, mortality also increased with greater drought and fire intensity. As hypothesized by Smith et al. (2017) and Sparks et al. (2018) (figure 4.1), the FRE-mortality dose-response relationship shifted leftward and upward (figure 4.7), and the most severe drought treatments were sufficient to cause mortality in the absence

of fire. Similarly, the LD50, the FMC at which it is more likely for trees to die than survive at each FRE dose, increased with increasing FRE (figure 4.8), demonstrating the shifting vulnerability of trees with varying compound disturbance intensity. Overall, *P. monticola* generally maintained higher FMC and F_v/F_m and had lower mortality than P. menziesii across most treatment intensities, indicating a higher drought-fire resistance. Mortality was accurately predicted in both species using prefire physiological status, morphological attributes, and surface fire intensity. Physiological status in terms of FMC and F_v/F_m and fire intensity were the most important predictor variables, and morphological variables were the least important (figure 4.9). It is important to note that these findings may not translate to older and larger trees that have more developed morphological features, such as thicker bark and a higher crown base height, that would increase their probability of survival. Numerous studies have observed that bark thickness, coupled with postfire injury observations such as crown scorch, can accurately predict tree mortality across a range of species (Cansler et al. 2020; Ryan and Reinhardt 1988; Stephens and Finney 2002). However, the findings of this study and others in mature trees (Furniss et al. 2018; Shearman et al. 2023), suggest that modeling systems reliant on deriving fire-induced tree mortality from tree morphological traits should explore including physiological traits and parameters associated with fire-resistant mechanisms to improve prediction accuracy when dealing with fire-drought scenarios.

There were some key similarities and differences in the physiological response of *P. monticola* and *P. menziesii* saplings to the drought and fire treatments. Prior to the fire treatments, FMC for both species was higher in the 0–14 day drought groups and lower in the 19–25 day drought groups (figure 4.3). The substantial reduction in FMC for saplings droughted

beyond 19 days for *P. monticola* and 14 days for *P. menziesii* is likely associated with increased water loss after loss of cell turgor pressure (Nolan et al. 2018, 2020; Tyree and Hammel 1972). *P. monticola* maintained higher FMC across all groups and had a longer drought length until a significant decrease in FMC (~19 days) compared with *P. menziesii* (14 days). This may be partially owing to the higher stomatal sensitivity of *P. monticola* during the onset of drought stress, as closing stomata reduces water loss due to evapotranspiration. For example, Lopushinsky and Klock (1974) observed a steeper decline in transpiration for Pinus spp. seedlings versus *P. menziesii* seedlings as water stress increased, indicating higher stomatal sensitivity in *Pinus* spp. seedlings. Differences in FMC during the course of our drought treatment may also have been driven by differences in minimum leaf conductance after stomatal closure (Duursma et al. 2019). Prefire F_v/F_m in both species mirrored FMC, where F_v/F_m was higher in the 0–14 day drought groups and lower in the 0–14 day drought groups (figure 4). As water limitation in plants impedes electron donation in PSII, resulting in lower F_v (Downton et al. 1981), it is consistent that F_v/F_m was lower in more severely droughted saplings.

Multitemporal observations of F_v/F_m provided useful information on the damage, repair, and recovery trajectory of PSII in both species. F_v/F_m in both species declined at 1 week postfire, followed by an increase at 2–3 weeks postfire, likely indicating damage to and subsequent repair of the photosynthetic apparatus. Although not statistically significant, *P. menziesii* saplings exposed to the highest FRE dose (0.6 MJ m^{-2}) generally had a greater F_v/F_m dip than those exposed to lower doses ($P = 0.26$). This damage-then-repair pattern has also been observed in non-water-stressed *P. monticola* saplings (Sparks et al. 2023) and *Pinus contorta* var. *latifolia* saplings (Smith et al. 2017) exposed to low intensity fires, where F_v/F_m recovered

within several weeks postfire and then declined until sapling death. Other studies have observed similar short term F_v/F_m dips after heat stress. For example, Marias et al. (2017) observed a significant decrease (~50% reduction) in F_v/F_m in 1 year old *Pinus ponderosa* and *Pseudotsuga menziesii* seedlings for 1–2 days after exposure to 45°C air temperature for 1 hour. Generally, saplings in the current experiment with a low prefire F_v/F_m (<0.5) or a decreasing F_v/F_m trajectory after 2 weeks postfire were observed to be dead at 10 weeks postfire (figures 4.5 and 4.6). These results suggest that repeated chlorophyll fluorescence observations could be used as an early warning sign of death in these species. For example, dying trees could potentially be identified as those with a negative postfire chlorophyll fluorescence trajectory.

Amplified mortality in drought-stressed saplings subjected to low intensity surface fires appears to be highly dependent on species. Our observations of greater mortality in *P. monticola* and *P. menziesii* saplings exposed to greater drought and surface fire intensity match some prior studies but not others. Similar to our observations, Partelli-Feltrin et al. (2020) observed greater mortality in water stressed ($\Psi_{predawn}$: -0.84 MPa) *P. ponderosa* saplings subjected to low intensity surface fire (FRE = 0.7 MJ m^{-2}) (100% mortality) than in well-watered saplings (~25% mortality). Likewise, Sparks et al. (2018) observed greater mortality (86%) in water-stressed ($\Psi_{predawn}$: -1 to -1.75 MPa) *Larix occidentalis* saplings subjected to low-intensity surface fires (0.4 MJ m^{-2}) compared with well-watered saplings (14% mortality). Notably, severely water-stressed ($\Psi_{predawn}$: -2 to -2.75 MPa) *L. occidentalis* saplings whose foliage senesced prior to the surface fires displayed lower mortality (14%) than saplings that did not senesce (86%). These mortality patterns are in stark contrast to observations of species that can resprout from insulated buds near or below the soil surface. Wilson et al. (2022) observed less

than 10% mortality in water stressed ($\Psi_{predawn}$: -2.4 MPa) *P. palustris* seedlings that were subjected to surface fires with a FRE of ~5 MJ m^{-2}. However, it should be noted that these seedlings were in their highly fire-resistant "grass stage," where seedlings only have a tuft of needles and a few centimeters of stem above the soil surface. Similarly, other studies have observed no mortality in water stressed Quercus spp. saplings that were top killed in surface fires (Chiatante et al. 2015; Di Iorio et al. 2011). Clearly, the observed variability in drought and fire responses among studies underscores the need to repeat similar experiments in more species and size classes.

The most important mortality predictor variables were prefire FMC, F_v/F_m, and FRE dose, and the least important were morphological attributes. Our finding that prefire physiological status plays a dominant role in postfire survival is perhaps unsurprising given its observation in prior studies (e.g., Partelli-Feltrin et al. 2020; Sparks et al. 2018; Wilson et al. 2022); however, we demonstrate that measures of prefire physiological status coupled with fire intensity can increase the accuracy of postfire mortality prediction. FMC and chlorophyll fluorescence can be accurately estimated using airborne and satellite-based sensors (Yebra et al. 2013; Ač et al. 2015; Lad et al. 2023) and could potentially be used to predict tree mortality after fire across large spatial scales. This is in contrast to postfire characteristics used for mortality modeling, such as crown scorch and stem charring, which provide accurate mortality predictions but are difficult to collect at large scales as they need to be assessed on the ground (Varner et al. 2021). However, conifer foliage water content has been accurately quantified using multispectral terrestrial laser scanning systems (Junttila et al. 2015, 2018). A similar airborne sensor could potentially be used to infer the proportion of the tree crown that was

scorched, as scorched foliage would likely have a lower FMC due to desiccation (Varner et al. 2021). Estimates of sapling FMC or F_v/F_m could be useful for informing prescribed fire practitioners of the sapling conditions and fire intensity needed to increase or reduce mortality in undesired or desired species, respectively (Smith et al. 2017; Steady et al. 2019). Beyond physiological condition and fire intensity, height was the most important morphological predictor variable. This finding is consistent with observed and theorized size-dependent fire-induced mortality where fire kills a higher proportion of smaller trees versus larger trees (McDowell et al. 2018; Stephens and Finney 2002). Generally, this mortality pattern occurs given fire-resistant traits such as thick bark, which protects sensitive cambium and phloem tissues, and high crowns, which protect sensitive foliage, are not fully developed in younger, smaller trees (Starker 1934; Vanderweide and Hartnett 2011). In our study, *P. monticola* that were alive at 10 weeks postfire had a higher average prefire height (83 cm) than those that died (80 cm). Likewise, living *P. menziesii* had a higher average prefire height (117 cm) than dead saplings (99 cm) at 10 weeks postfire. It is likely that shorter saplings had a higher proportion of crown scorch within a given FRE dose level given the relationship between fire intensity and crown scorch height (van Wagner 1973).

Although this study improves our understanding of compound disturbance effects on young conifers, several limitations should be explored in future research. This study watered saplings immediately after the fire treatments, which is unlikely to occur in natural ecosystems. Future research should examine the effects of pre- and postfire drought on tree injury and mortality to understand compounding effects more fully. Using potted saplings allows for highly controlled manipulation, including drought length and fire intensity; however, this approach

does have limitations. Namely, potted saplings have limited rooting volume and likely have higher water stress than saplings in natural settings that have unrestricted rooting volume (Poorter et al. 2012). It is possible that the FRE-mortality relationships for saplings in natural settings would change given that their unrestricted root growth would allow for access to deeper water sources. Additionally, saplings and mature trees in natural settings may have improved resilience to and recovery from fire from local mycorrhizal symbioses (Atala and Molina-Montenegro 2023). This study used a random forest classification approach to predict mortality, which does have some limitations. In general, random forest approaches are less interpretable (i.e., "black box") than other modeling approaches when it comes to understanding why certain outcomes were produced (Cutler et al. 2007). However, in terms of modeling tree mortality, accurate prediction may be more important than interpretability for forest management applications (Shearman et al. 2019). The modeling also highlights that further research is needed to assess predictive mortality relationships that address coupled fire and drought interactions in other species with the goal to provide a critical update to fire effects modeling systems. Equally, future studies should consider incorporating additional dimensions of enquiry, such as how such shifts of the fire-intensity-to mortality dose-response curves are affected by increases in tree age as well as other environmental, abiotic, and biotic factors such as nutrient availability, microclimatic conditions, topographic variables, among others.

4.5 Conclusions

The quantification of compound disturbance effects on trees is a forest management research need given projected increased frequency of drought and wildfire in the western

United States. This study advances our understanding of drought and fire effects through the use of a controlled dose-response approach, where saplings were subjected to varying drought and fire intensities and physiological condition and mortality were measured for several months postfire. Results show that droughted *P. monticola* and *P. menziesii* saplings exhibit diminished recovery in terms of photosynthetic efficiency and greater mortality after low intensity surface fires. The higher postfire photosynthetic efficiency and lower mortality of *P. monticola* compared with *P. menziesii* demonstrates the higher fire resistance of *P. monticola* at this life stage. For both species, repeated observations of postfire chlorophyll fluorescence, an indicator of photosynthetic efficiency and stress, suggest that the trajectory of postfire fluorescence could be used as an early warning sign of impending tree death and a predictor variable in tree mortality modeling. Postfire mortality modeling using prefire physiological and morphological attributes and fire intensity provided accurate mortality predictions and highlights the importance of prefire tree physiological condition and fire intensity for mortality prediction. However, this analysis should be repeated for more species and size classes with a larger variation in morphological attributes. The results of this study and others lay a foundational knowledge base for natural resource managers seeking to understand which prefire tree condition and fire intensity decreases or increases mortality of desired and undesired species. Additionally, the amplified drought and fire sapling responses observed in this study and others highlights the need to incorporate these relationships into tree mortality models used by natural resource managers.

4.6 References

Abatzoglou, John T, David S. Battisti, A. Park Williams, Winslow D. Hansen, Brian J. Harvey, and Crystal A. Kolden. 2021. "Projected Increases in Western US Forest Fire Despite Growing Fuel Constraints." Communications Earth & Environment 2 (1): 227.

Abatzoglou, John T, Crystal A. Kolden, A. Park Williams, James A. Lutz, and Alistair M.S Smith. 2017. "Climatic Influences on Interannual Variability in Regional Burn Severity Across Western US Forests." International Journal of Wildland Fire 26 (4): 269–275.

Ač, Alexander, Zbyněk Malenovský, Julie Olejníčková, Alexander Gallé, Uwe Rascher, and Gina Mohammed. 2015. "Meta-Analysis Assessing Potential of Steady-State Chlorophyll Fluorescence for Remote Sensing Detection of Plant Water, Temperature and Nitrogen Stress." Remote Sensing of Environment 168: 420–436.

Adams, Henry D, Melanie JB Zeppel, William RL Anderegg, Henrik Hartmann, Simon M. Landhäusser, David T. Tissue, Travis E. Huxman, et al. 2017. "A Multi-Species Synthesis of Physiological Mechanisms in Drought-Induced Tree Mortality." Nature Ecology & Evolution 1 (9): 1285–1291.

Anderegg, William RL, Oriana S. Chegwidden, Badgley Grayson, Anna T. Trugman, Danny Cullenward, John T. Abatzoglou, Jeffrey A. Hicke, et al. 2022. "Future Climate Risks From Stress, Insects and Fire Across US Forests." Ecology Letters 25 (6): 1510–1520.

Atala, Cristian, Sebastián A. Reyes, and Marco A. Molina-Montenegro. 2023. "Assessing the Importance of Native Mycorrhizal Fungi to Improve Tree Establishment After Wildfires." Journal of Fungi 9 (4): 421. https://doi.org/10.3390/jof9040421

Battaglia, Mike, Frederick W. Smith, Wayne D. Shepperd. 2009. "Predicting Mortality of Ponderosa Pine Regeneration after Prescribed Fire in the Black Hills, South Dakota, USA." International Journal of Wildland Fire 18 (2): 176–190. https://doi.org/10.1071/wf07163

Bowman, David M.J.S., Grant J. Williamson, John T. Abatzoglou, Crystal A. Kolden, Mark A. Cochrane, and Alistair M.S. Smith. 2017. "Human Exposure and Sensitivity to Globally Extreme Wildfire Events." Nature Ecology & Evolution 1 (3): 0058.

Breiman, L. 2001. "Random Forests." Machine Learning 45: 5–32.

Cansler, C. Alina, Sharon M. Hood, Phillip J. van Mantgem, and J. Morgan Varner. 2020. "A Large Database Supports the Use of Simple Models of Postfire Tree Mortality for Thick-Barked Conifers, with Less Support for Other Species." Fire Ecology 16 (1): 1–37.

Chiatante, D., R. Tognetti, G. S. Scippa, T. Congiu, B. Baesso, M. Terzaghi, and A. Montagnoli. 2015. "Interspecific Variation in Functional Traits of Oak Seedlings (Quercus ilex, Quercus trojana, Quercus virgiliana) Grown under Artificial Drought and Fire Conditions." Journal of Plant Research 128 (4): 595–611. https://doi.org/10.1007/s10265-015-0729-4

Cutler, D. Richard, Thomas C. Edwards Jr, Karen H. Beard, Adele Cutler, Kyle T. Hess, Jacob Gibson, and Joshua J. Lawler. 2007. "Random Forests for Classification in Ecology." Ecology 88 (11): 2783–2792. https://doi.org/10.1890/07-0539.1

Dai, Aiguo. 2013. "Increasing Drought under Global Warming in Observations and Models." Nature Climate Change 3 (1): 52–58. Dale, Virginia H, Linda A. Joyce, Steve McNulty, Ronald P. Neilson, Matthew P. Ayres, Michael D. Flannigan, Paul J. Hanson, et al. 2001. "Climate Change and Forest Disturbances: Climate Change Can Affect Forests by Altering the

Frequency, Intensity, Duration, and Timing of Fire, Drought, Introduced Species, Insect and Pathogen Outbreaks, Hurricanes, Windstorms, Ice Storms, or Landslides." BioScience 51 (9): 723–734.
Di Iorio, Antonino, Antonio Montagnoli, Gabriella Stefania Scippa, and Donato Chiatante. 2011. "Fine Root Growth of Quercus Pubescens Seedlings after Drought Stress and Fire Disturbance." Environmental and Experimental Botany 74: 272–279.
Downton, W. J. S., D. C. Fork, and P. A. Armond. 1981. "Chlorophyll A Fluorescence Transient as an Indicator of Water Potential of Leaves." Plant Science Letters 20 (3): 191–194.
Duursma, Remko A., Christopher J. Blackman, Rosana Lopéz, Nicolas K. Martin-StPaul, Hervé Cochard, and Belinda E. Medlyn. 2019. "On the minimum leaf conductance: its role in models of plant water use, and ecological and environmental controls." New Phytologist 221 (2): 693–705.
Furniss, Tucker J, Andrew J. Larson, Van R. Kane, and James A. Lutz. 2018. "Multi-scale Assessment of Postfire Tree Mortality Models." International Journal of Wildland Fire 28 (1): 46–61.
Genty, Bernard, Briantais Jean-Marie, and Neil R. Baker. 1989. "The Relationship between the Quantum Yield of Photosynthetic Electron Transport and Quenching of Chlorophyll Fluorescence." Biochimica et Biophysica Acta (BBA)-General Subjects 990 (1): 87–92.
Guadagno, Carmela R, Brent E. Ewers, Heather N. Speckman, Timothy Llewellyn Aston, Bridger J. Huhn, Stanley B. DeVore, Joshua T. Ladwig, et al. 2017. "Dead or Alive? Using Membrane Failure and Chlorophyll a Fluorescence to Predict Plant Mortality from Drought." Plant Physiology 175 (1): 223–234. https://doi.org/10.1104/pp.16.00581
Hood, Sharon M, J. Morgan Varner, Phillip Van Mantgem, and C. Alina Cansler. 2018. "Fire and Tree Death: Understanding and Improving Modeling of Fire-Induced Tree Mortality." Environmental Research Letters 13 (11): 113004.
Hyyppa, Juha, and Mikko Inkinen. 1999. "Detecting and Estimating Attributes for Single Trees Using Laser Scanner." The Photogrammetric Journal of Finland 16: 27–42.
Junttila, Samuli, Sanna Kaasalainen, Mikko Vastaranta, Teemu Hakala, Olli Nevalainen, and Markus Holopainen. 2015. "Investigating Bi-Temporal Hyperspectral LiDAR Measurements From Declined Trees—Experiences from Laboratory Test." Remote Sensing 7 (10): 13863–13877. https://doi.org/10.3390/rs71013863
Junttila, Samuli, Junko Sugano, Mikko Vastaranta, Riikka Linnakoski, Harri Kaartinen, Antero Kukko, Markus Holopainen, et al. 2018. "Can Leaf Water Content be Estimated Using Multispectral Terrestrial Laser Scanning? A Case Study with Norway Spruce Seedlings." Frontiers in Plant Science 9: 299. https://doi.org/10.3389/fpls.2018.00299
Kleinman, J. S., J. D. Goode, A. C. Fries, and J. L. Hart. 2019. "Ecological Consequences of Compound Disturbances in Forest Ecosystems: A Systematic Review." Ecosphere 10 (11): e02962.
Lad, Lauren E, Wade T. Tinkham, Aaron M. Sparks, and Alistair M.S. Smith. 2023. "Evaluating Predictive Models of Tree Foliar Moisture Content for Application to Multispectral UAS Data: A Laboratory Study." Remote Sensing 15: 5703.
Liaw, Andy, and Wiener Matthew. 2002. "Classification and Regression by randomforest." R News 2 (3): 18–22. https://CRAN.R-project.org/doc/Rnews/

Lopushinsky, W., and G. O. Klock. 1974. “Transpiration of Conifer Seedlings in Relation to Soil Water Potential.” Forest Science 20 (2): 181–186.
Lutes, Duncan. 2020. FOFEM 6.7 First Order Fire Effects Model User Guide, Fire and Aviation Management. Fort Collins: USDA Rocky Mountain Research Station Fire Modelling Institute. Updated September 20, 2023 https://www.firelab.org/document/fofem-files
Lyons, Mitchell B, David A. Keith, Stuart R. Phinn, Tanya J. Mason, and Jane Elith. 2018. “A Comparison of Resampling Methods for Remote Sensing Classification and Accuracy Assessment.” Remote Sensing of Environment 208: 145–153. https://doi.org/10.1016/j.rse.2018.02.026
Marias, Danielle E, Frederick C. Meinzer, David R. Woodruff, and Katherine A. McCulloh. 2017. “Thermotolerance and Heat Stress Responses of Douglas-Fir and Ponderosa Pine Seedling Populations from Contrasting Climates.” Tree Physiology 37 (3): 301–315. https://doi.org/10.1093/treephys/tpw117
Maxwell, Kate, and N. Johnson Giles. 2000. “Chlorophyll Fluorescence—A Practical Guide.” Journal of Experimental Botany 51 (345): 659–668.
McDowell, Nate G, David J. Beerling, David D. Breshears, Rosie A. Fisher, Kenneth F. Raffa, and Mark Stitt. 2011. “The Interdependence of Mechanisms Underlying Climate-Driven Vegetation Mortality.” Trends in Ecology & Evolution 26 (10): 523–532. https://doi.org/10.1016/j.tree.2011.06.003
McDowell, Nate G, Sean T. Michaletz, Katrina E. Bennett, Kurt C. Solander, Chonggang Xu, Reed M. Maxwell, and Richard S. Middleton. 2018. “Predicting Chronic Climate-Driven Disturbances and Their Mitigation.” Trends in Ecology & Evolution 33 (1): 15–27. https://doi.org/10.1016/j.tree.2017.10.002
McDowell, Nate G, Gerard Sapes, Alexandria Pivovaroff, Henry D. Adams, Craig D. Allen, William RL Anderegg, Matthias Arend, et al. 2022. “Mechanisms of Woody-Plant Mortality under Rising Drought, CO2 and Vapour Pressure Deficit.” Nature Reviews Earth & Environment 3 (5): 294–308.
Michaletz, S. T., and E. A. Johnson. 2006. “A Heat Transfer Model of Crown Scorch in Forest Fires.” Canadian Journal of Forest Research 36 (11): 2839–2851. https://doi.org/10.1139/x06-158
Millar, Constance I, and Nathan L Stephenson. 2015 “Temperate Forest Health in an Era of Emerging Megadisturbance.” Science 349 (6250): 823–826. https://doi.org/10.1126/science.aaa9933
Murchie, Erik H, and Tracy Lawson. 2013. “Chlorophyll Fluorescence Analysis: A Guide to Good Practice and Understanding Some New Applications.” Journal of Experimental Botany 64 (13): 3983–3998. https://doi.org/10.1093/jxb/ert208
Nolan, Rachael H, Chris J. Blackman, Víctor Resco de Dios, Brendan Choat, Belinda E. Medlyn, Ximeng Li, Ross A. Bradstock, et al. 2020. “Linking Forest Flammability and Plant Vulnerability to Drought.” Forests 11 (7): 779. https://doi.org/10.3390/f11070779
Nolan, Rachael H, Javier Hedo, Carles Arteaga, Tetsuto Sugai, and Víctor Resco de Dios. 2018. “Physiological Drought Responses Improve Predictions of Live Fuel Moisture Dynamics in a Mediterranean Forest.” Agricultural and Forest Meteorology 263: 417–427.
Paine, Robert T, Mia J. Tegner, and Edward A. Johnson. 1998. “Compounded perturbations yield ecological surprises.” Ecosystems 1 (6): 535–545. https://doi.org/10.1007/s100219900049

Partelli-Feltrin R, Johnson DM, Sparks AM, Adams HD, Kolden CA, Nelson, AS and Smith AM. 2020. “Drought Increases Vulnerability of Pinus Ponderosa Saplings to Fire-Induced Mortality.” Fire 3 (4): 56.

Partelli-Feltrin, Raquel, Alistair MS Smith, Henry D. Adams, R. Alex Thompson, Crystal A. Kolden, Kara M. Yedinak, and Daniel M. Johnson. 2023. “Death From Hunger or Thirst? Phloem Death, Rather than Xylem Hydraulic Failure, as a Driver of Fire-Induced Conifer Mortality.” New Phytologist 237 (4): 1154–1163.

Poorter, Hendrik, Jonas Bühler, Dagmar van Dusschoten, José Climent, and Johannes A. Postma. 2012. “Pot Size Matters: A Meta-Analysis of the Effects of Rooting Volume on Plant Growth.” Functional Plant Biology 39 (11): 839–850. https://doi.org/10.1071/fp12049

Popescu, Sorin C. 2007. “Estimating Biomass of Individual Pine Trees Using Airborne Lidar.” Biomass and Bioenergy 31 (9): 646–655. https://doi.org/10.1016/j.biombioe.2007.06.022

Popescu, Sorin C, and Kaiguang Zhao. 2008. “A Voxel-Based Lidar Method for Estimating Crown Base Height for Deciduous and Pine Trees.” Remote Sensing of Environment 112 (3): 767–781. https://doi.org/10.1016/j.rse.2007.06.011

R Core Team 2023. R: A Language and Environment for Statistical Computing. Vienna, Austria: R Foundation for Statistical Computing.

Rebain, Stephanie A. 2022. The Fire and Fuels Extension to the Forest Vegetation Simulator: Updated Model Documentation; Internal Report. Fort Collins, CO: USDA Forest Service, Forest Management Service Center.

Ruffault, Julien, Limousin Jean-Marc, Pimont François, Dupuy Jean-Luc, Miquel De Càceres, Hervé Cochard, Florent Mouillot, et al. 2023. “Plant Hydraulic Modelling of Leaf and Canopy Fuel Moisture Content Reveals Increasing Vulnerability of a Mediterranean Forest to Wildfires under Extreme Drought.” New Phytologist 237 (4): 1256–1269.

Ryan, Kevin C, and Elizabeth D Reinhardt. 1988. “Predicting Postfire Mortality of Seven Western Conifers” Canadian Journal of Forest Research 18 (10): 1291–1297. https://doi.org/10.1139/x88-199

Shearman, Timothy M, J. Morgan Varner, Sharon M. Hood, C. Alina Cansler, and J. Kevin Hiers. 2019. “Modelling Postfire Tree Mortality: Can Random Forest Improve Discrimination of Imbalanced Data?.” Ecological Modelling 414: 108855.

Shearman, Timothy M, J. Morgan Varner, Sharon M. Hood, Phillip J. van Mantgem, C. Alina Cansler, and Micah Wright. 2023. “Predictive Accuracy of Post-Fire Conifer Death Declines Over Time in Models Based on Crown and Bole Injury.” Ecological Applications 33 (2): e2760.

Slack, Andrew W, Nickolas E. Zeibig-Kichas, Jeffrey M. Kane, and J. Morgan Varner. 2016. “Contingent Resistance in Longleaf Pine (Pinus palustris) Growth and Defense 10 Years Following Smoldering Fires.” Forest Ecology and Management 364: 130–138. https://doi.org/10.1016/j.foreco.2016.01.014

Smith, Alistair MS, Aaron M. Sparks, Crystal A. Kolden, John T. Abatzoglou, Alan F. Talhelm, Daniel M. Johnson, Luigi Boschetti, et al. 2016. “Towards a New Paradigm in Fire Severity Research Using Dose-Response Experiments.” International Journal of Wildland Fire 25 (2): 158–166.

Smith, Alistair MS, Alan F. Talhelm, Daniel M. Johnson, Aaron M. Sparks, Crystal A. Kolden, Kara M. Yedinak, Kent G. Apostol, et al. 2017. “Effects of Fire Radiative Energy Density Dose on

Pinus Contorta and Larix occidentalis Seedling Physiology and Mortality." International Journal of Wildland Fire 26 (1): 82–94.
Smith, Alistair MS, Wade T. Tinkham, David P. Roy, Luigi Boschetti, Robert L. Kremens, Sanath S. Kumar, Aaron M. Sparks, Michael J. Falkowski. 2013. "Quantification of Fuel Moisture Effects on Biomass Consumed Derived from Fire Radiative Energy Retrievals." Geophysical Research Letters 40 (23): 6298–6302.
Sparks, Aaron M, Alexander S. Blanco, David R. Wilson, Dylan W. Schwilk, Daniel M. Johnson, Henry D. Adams, David MJS Bowman, et al. 2023. "Fire Intensity Impacts on Physiological Performance and Mortality in Pinus monticola and Pseudotsuga menziesii Saplings: A Dose-Response Analysis." Tree Physiology 43(8): tpad051.
Sparks, Aaron M, Mark V. Corrao, and Alistair MS Smith. 2022. "Cross-Comparison of Individual Tree Detection Methods Using Low and High Pulse Density Airborne Laser Scanning Data." Remote Sensing 14 (14): 3480.
Sparks, Aaron M, Alan F. Talhelm, Raquel Partelli Feltrin, Alistair MS Smith, Daniel M. Johnson, Crystal A. Kolden, and Luigi Boschetti. 2018. "An Experimental Assessment of the Impact of Drought and Fire on Western Larch Injury, Mortality and Recovery." International Journal of Wildland Fire 27 (7): 490–497.
Starker, T. J. 1934. "Fire Resistance in the Forest." Journal of Forestry 32 (4): 462–467.
Steady, Wade D., Raquel Partelli Feltrin, Daniel M. Johnson, Aaron M. Sparks, Crystal A. Kolden, Alan F. Talhelm, James A. Lutz, et al. 2019. "The Survival of Pinus ponderosa Saplings Subjected to Increasing Levels of Fire Behavior and Impacts on Postfire Growth." Fire 223 (2): 1–13.
Stephens, Scott L., and Mark A. Finney. 2002. "Prescribed Fire Mortality of Sierra Nevada Mixed Conifer Tree Species: Effects of Crown Damage and Forest Floor Combustion." Forest Ecology and Management 162 (2-3): 261–271. https://doi.org/10.1016/s0378-1127(01)00521-7
Story, Michael, and Russel G. Congaltonl. 1986. "Accuracy Assessment: A User's Perspective." Photogrammetric Engineering and Remote Sensing 52 (3): 397–399.
Sturtevant, B.R., and M.J Fortin. 2021. "Understanding and Modeling Forest Disturbance Interactions at the Landscape Level." Frontiers in Ecology and Evolution 9: 653647.
Turner, Monica G. 2010. "Disturbance and Landscape Dynamics in A Changing World." Ecology 91 (10): 2833–2849. https://doi.org/10.1890/10-0097.1
Tyree, Melvin T, and Harold T. Hammel. 1972. "The Measurement of the Turgor Pressure and the Water Relations of Plants by the Pressure-Bomb Technique." Journal of Experimental Botany 23 (1): 267–282. https://doi.org/10.1093/jxb/23.1.267
van Mantgem, Phillip J., Donald A. Falk, Emma C. Williams, Adrian J. Das, and Nathan L. Stephenson. 2018. "Pre-Fire Drought and Competition Mediate Post-Fire Conifer Mortality in Western US National Parks." Ecological Applications 28 (7): 1730–1739. https://doi.org/10.1002/eap.1778
van Mantgem, Phillip J., Jonathan CB Nesmith, Mary Beth Keifer, Eric E. Knapp, Alan Flint, Flint Lorriane. 2013. "Climatic Stress Increases Forest Fire Severity across the Western United States." Ecology Letters 16 (9): 1151–1156. https://doi.org/10.1111/ele.12151
van Mantgem, Phillip J., Nathan L. Stephenson, Linda S. Mutch, Veronica G. Johnson, Annie M. Esperanza, and David J. Parsons. 2003. "Growth Rate Predicts Mortality of Abies concolor in

Both Burned and Unburned Stands." Canadian Journal of Forest Research 33 (6): 1029–1038.
van Wagner, CE. 1973. "Height of Crown Scorch in Forest Fires." Canadian Journal of Forest Research 3 (3): 373–378.
VanderWeide, Benjamin L, and David C. Hartnett. 2011. "Fire Resistance of Tree Species Explains Historical Gallery Forest Community Composition." Forest Ecology and Management 261 (9): 1530–1538. https://doi.org/10.1016/j.foreco.2011.01.044
Varner, J. Morgan, Sharon M. Hood, Doug P. Aubrey, Yedinak Kara, J. Kevin Hiers, W. Matthew Jolly, Timothy M. Shearman, et al. 2021. "Tree Crown Injury from Wildland Fires: Causes, Measurement and Ecological and Physiological Consequences." New Phytologist 231 (5): 1676–1685.
Voelker, Steven L, Andrew G. Merschel, Frederick C. Meinzer, Danielle E.M. Ulrich, Thomas A. Spies, and Christopher J. Still. 2019. "Fire Deficits have Increased Drought Sensitivity in Dry Conifer Forests: Fire Frequency and Tree-Ring Carbon Isotope Evidence from Central Oregon." Global Change Biology 25 (4): 1247–1262.
Weir, John R, and J. Derek Scasta. 2014. "Ignition and Fire Behaviour of Juniperus virginiana in Response to Live Fuel Moisture and Fire Temperature in the Southern Great Plains." International Journal of Wildland Fire 23 (6): 839–844. https://doi.org/10.1071/wf13147
Wilson, Luke A., Robert N. Spencer, Doug P. Aubrey, Joseph J. O'Brien, Alistair M.S. Smith, Ream W. Thomas, and Daniel M. Johnson. 2022. "Longleaf Pine Seedlings are Extremely Resilient to the Combined Effects of Experimental Fire and Drought." Fire 5 (5): 128.
Woolley, Travis, David C. Shaw, Lisa M. Ganio, and Stephen Fitzgerald. 2012. "A Review of Logistic Regression Models Used to Predict Postfire Tree Mortality of Western North American Conifers." International Journal of Wildland Fire 21 (1): 1–35. https://doi.org/10.1071/wf09039
Wooster, Martin J, J. Roberts Gareth, Giglio Louis, P. Roy David, H. Freeborn Patrick, Boschetti Luigi, Justice Chris, et al. 2021. "Satellite Remote Sensing of Active Fires: History and Current Status, Applications and Future Requirements." Remote Sensing of Environment 267: 94.
Yebra, Marta, Philip E. Dennison, Emilio Chuvieco, David Riaño, Philip Zylstra, E. Raymond Hunt Jr, F. Mark Danson, Yi Qi, and Sara Jurdao. 2013. "A Global Review of Remote Sensing of Live Fuel Moisture Content for Fire Danger Assessment: Moving Towards Operational Products." Remote Sensing of Environment 136: 455-468.

CHAPTER 5 – EVALUATING THE UTILITY OF PRE-FIRE DATA FOR FINE-SCALE REMOTE SENSING OF CROWN SCORCH

5.1 Introduction

Fire plays a pivotal role in terrestrial ecosystems around the world by influencing species composition and diversity (Thonicke et al., 2001), supporting nutrient cycling (Pausas & Bond, 2020), modifying vegetation fuel loads (Stephens et al., 2009), and maintaining resilience to biotic and abiotic disturbances (Johnstone et al., 2016; Santos et al., 2023). Across global forest systems, fire serves as both a maintaining and transitionary force, depending on the system. However, decades of global fire suppression in fire-dependent forests have increased live fuel connectivity, vegetation density, and dead fuel loading, increasing fire intensity and severity (Moreira et al., 2020). Additionally, these changes in fuel complexity and loading are compounded by decreased fuel moisture due to increased temperatures and greater precipitation variability resulting from climate change (Abatzoglou et al., 2018). These changes in fuel complexity have caused wildfires to depart from historical fire behavior by increasing fire residence time, fireline intensity, and ultimately fire-induced mortality (Littell et al., 2016). However, in forest systems adapted to low-severity fire, the use of beneficial fire (i.e., controlled fires that mimic historic fire conditions) is essential for improving resilience and resistance to future fire and other disturbances. Low-severity beneficial fires help maintain ecosystem conditions and can reduce or reverse conversion to alternative vegetation types (Ryan et al. 2013; Walker et al., 2018). Across the globe, humans have long used controlled fire

to maintain ecosystem function and composition to sustain economic, societal, and cultural resources (Lake et al., 2017). Thus, prescribed fire can enhance and extend the footprint of forest management treatments in a cost-effective approach that improves ecosystem resilience to subsequent disturbances (Ryan et al., 2013; Westlind and Kerns, 2021).

Fire research and management have long utilized remote sensing to study both wildfires and prescribed fires. Satellite-based remote sensing is used for global assessments of burned area (Chuvieco et al., 2016), fire severity (Alonso-González and Fernández-García, 2021), and fire risk (Jaiswal et al., 2002). In pre-fire environments, remote sensing indices have been used to describe conditions such as foliar moisture, vegetation vigor, forest species composition and structure, and to estimate surface fuels (Sader and Winne, 1991; White et al., 1996; Ravan and Roy, 1997; Chuvieco et al., 1999). In post-fire environments, remote sensing indices have been used to describe conditions such as burn severity, including vegetation consumption, short- and long-term vegetation mortality, and changes to soil properties (White et al., 1996; Lentile et al., 2006). Differencing pre- and post-fire indices is commonly used to describe the ecological change resulting from fires at broader spatial scales than those that rely on field methods alone (Escuin et al., 2007). However, landscape-scale studies of fire are often limited in their application to forest-specific adaptive management as they lack the spatial resolution necessary for describing sub-plot level (i.e., at a tree or plant scale) fire effects (Lentile et al., 2006).

Uncrewed aerial systems (UAS) have emerged as a high spatial resolution remote sensing tool, that allows users to control the timing of data collection and providing individual tree-level information on structure and health attributes (Fernández-Guisuraga et al., 2018; Carvajal-Ramirez et al., 2019). In forests with a short fire-return interval, UAS have successfully

extracted individual tree structure (Swayze et al., 2021) and health metrics (Fraser and Congalton, 2023), which can then be used as a baseline for post-fire comparisons (Fernández-Guisuraga et al., 2018; Carvajal-Ramirez et al., 2019). Specifically, UAS data have been used to extract individual tree height, diameter at breast height, and crown extent and area (Tinkham et al., 2022; Creasy et al., 2021), classify tree species (Abdollahnejad and Panagiotidis, 2020), and identify tree health and stress (Fraser and Congalton, 2023; Lad et al., 2023). Further, these methods can be applied at multiple dates to examine changes to tree structure and health, thus providing a high-resolution long-term forest monitoring tool (Zhang et al., 2015). While UAS methods do not provide a perfect extraction of individual trees, for instance omission is often elevated for understory trees, the near-census inventory of tree approximate objects can reliably represent most forest structures in low to moderate canopy closure forests (<60% canopy cover; Hanna et al., 2024). Early testing shows potential for UAS to examine fire-induced impacts on vegetation as the temporal resolution can be controlled by users, allowing managers to examine forest structure and condition at relevant time points and spatial scales (Tang and Shao, 2015).

As the emphasis on prescribed fire use for managing fire hazard increases, reliable data sources for evaluating prescription effectiveness and informing adaptive management are pivotal. Past field-based research efforts have been used to inform plant community composition changes (Knapp et al., 2015) and alterations to fuel loading (Parresol et al., 2021), conduct fire behavior analyses (Hollingsworth et al., 2012), and understand ecosystem-specific fire-induced changes to individual tree health using UAS (Carvajal-Ramirez et al., 2019). An important metric for assessing the impacts and management objective success of prescribed

fire on forests is crown scorch (Varner et al., 2021). Crown scorch, or crown volume scorch (CVS), is a post-fire crown injury that denotes the visual change in foliage color from green to red, as well as the underlying physiological damage, and results from heat-induced tissue damage (Hood et al., 2018; Varner et al., 2021). While previous studies have demonstrated success in estimating CVS in the field (Sayer et al., 2020) and at broad scales using airborne thermal imaging (Hudak et al., 2018), these methods lack the temporal and spatial resolutions necessary for rapid assessment of tree-level fire effects across prescribed burns. Two recent studies used UAS to estimate post-burn CVS in conifer forests in Montana, United States, and British Columbia, Canada (Moran et al., 2022; Arkin et al., 2023). Both studies demonstrated that ultra-high-resolution multispectral imagery can identify scorched crowns. However, these studies either used a labor-intensive manual process that would be expensive to operationalize for managers (Moran et al., 2022) or lacked variability in scorch to allow for comprehensive testing of model predictions for moderate levels of CVS (Arkin et al., 2023). Further research that combines both temporal (i.e., at multiple times since fire) and spectral change is an important research gap that will improve our knowledge of fire's impact on ecosystem structure and function through time.

Operationalizing UAS tree-level fire effects monitoring to inform adaptive management will require testing the utility of multitemporal data in assessing tree health and condition at spatial scales relevant to managers. However, no studies that we are aware of have compared the use of post-fire only versus differenced pre- and post-fire UAS data to identify CVS. Additionally, the timing of post-fire data collection nor the comparison of RGB and multispectral sensors for CVS assessment has been made. Consequently, this study evaluates

how the timing of imagery collection and availability of post-fire versus pre- and post-fire imagery impacts the evaluation of CVS with time since fire. We examined 1) How does spectral approach (i.e., the use of multispectral data versus red-green-blue-Near Infrared (RGB-NIR) versus RGB data) affect model accuracy in predicting CVS, and 2) Does the inclusion of pre-fire data improve models of CVS compared to the use of post-fire data alone. By comparing the use of post-fire versus differenced imagery and RGB versus multispectral imagery we can evaluate tradeoffs between data collection investment, sensor cost, and technical requirements for processing. The study's results will provide a step towards optimizing UAS monitoring of fire effects in fire frequent forests and provide a feedback mechanism for managers to adapt burn plans to optimally achieve management objectives.

5.2 Methods

5.2.1 Study Area

This study was conducted in the Escambia Experimental Forest located in Escambia County, Alabama, United States. This area has a 30-year normal mean temperature between 18-20°C and mean annual precipitation between 1520-1780 mm. The burn covered a 17-ha unit in 2022 with data collection focusing on 6-ha on the northwestern edge of the unit (Figure 5.1). The study area was dominated by longleaf pine (*Pinus palustris* Mill.) with some shortleaf pine (*Pinus echinata* Mill.) and the site's soil is dominated by Lucy loamy sand with some sections of Troup fine sand and Orangeburg fine sandy loam. The site was last burned in 2016 resulting in scattered shrub fuels and young longleaf pine seedlings and saplings.

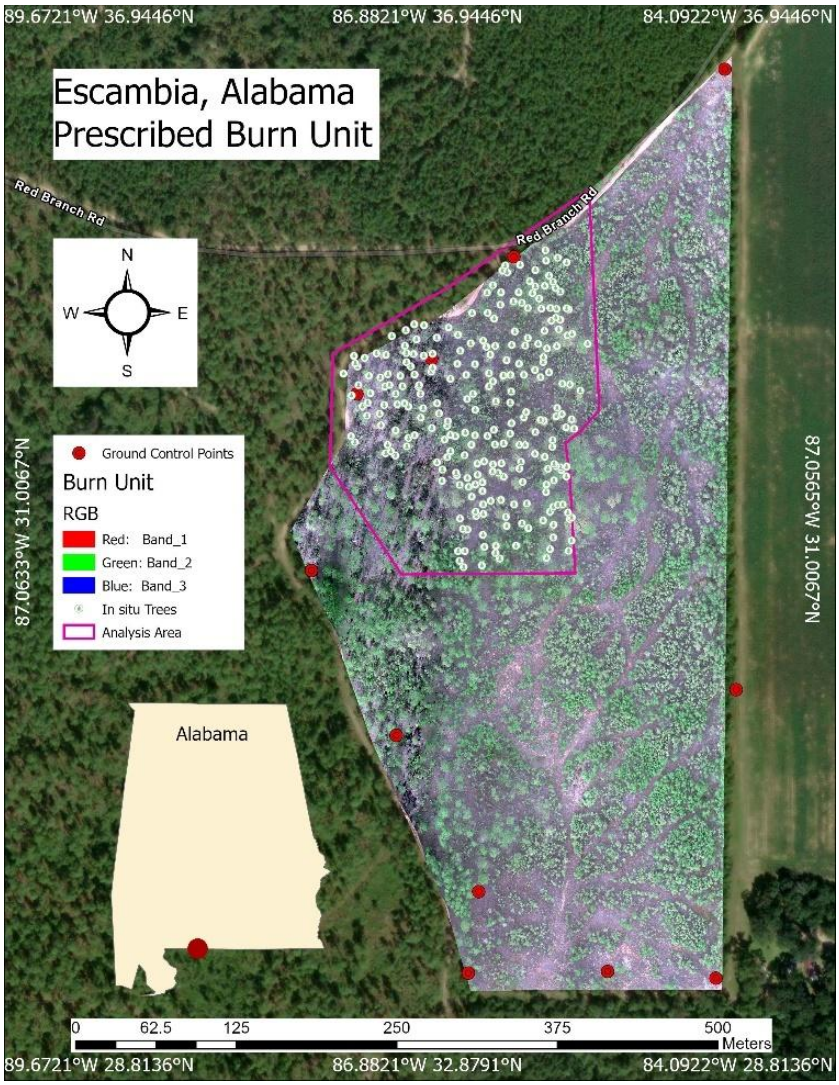

Figure 5.5. Study area map of the burn unit and in situ data collection points. The map shows a red-green-blue orthomosaic over an ESRI basemap. The orthomosaic was derived from UAS images taken 1-day post-fire and displays the *in situ* data collection area and the ground control points used for image georeferencing.

5.2.2 Prescribed Fire Details

The prescribed fire was conducted in the 17-ha site on 11 February 2022. The site was ignited at 1330 local time using strip head fires ignited from 20 m to 100 m apart, originating at the north and progressing south through the unit. Flame lengths ranged from 2 m to 8 m, with isolated torching of small pines (< 10 cm DBH); spot grid ignition was employed in portions of the southern mapped area (inset in Figure 4.1) to moderate intensity. Winds during the burn

were southerly (SW to S), ranging from 12 to 20 k hr^{-1}, with minor gusts. Air temperatures during the burn decreased from a high of 12° C to 11° C. Relative humidity ranged from 21 to 23% during the burn.

5.2.3 In Situ Data Collection

We surveyed scorched trees on the northwestern 6-ha of the burn unit. This 6-ha area was selected for its high level of variation in surface fuels and crown structure, which was anticipated to result in a wide range of crown scorch levels. We surveyed 300 overstory pines and mapped their location, recorded their species, and measured their total height, crown base height (CBH), and diameter at breast height (1.37 m; DBH). Between 10-days post-fire (when crown foliage was fully browned) and 35-days (when leaves were actively shedding), we measured tree bole char height (nearest 0.1 m in four cardinal directions), crown scorch height (to the nearest 0.1 m), and ocularly estimated crown volume scorched (%) for each tree (as in Peterson and Arbaugh, 1986). Within our main plot, we selected all pines > 20 cm DBH so that we could ensure accurate individual tree extraction. Trees were located using a Trimble Geo 7X GPS receiver with an attached external antenna and TerraSync software (Trimble Navigation Ltd., Sunnyvale, Calif.) achieving sub-meter horizontal and vertical accuracy.

A series of five UAS acquisitions were conducted across the 17-ha burn unit, including 1-day pre-fire and 1-, 3-, 10-, and 35-days post-fire. We used a DJI Matrice 210V2 (DJI, Shenzhen, China) UAS with a Micasense 10-band Dual-Camera system attached (Micasense, Seattle, WA, USA). Prior to and immediately after each UAS takeoff and landing, photos were taken of the Micasense reflectance panels to calibrate 100% spectral reflectance in field lighting conditions. The drone was flown in a serpentine pattern with 85% forward and 80% cross-track overlap at

90 m above ground level with a speed of 6 m sec^{-1}. The Micasense system acquired 10-band multispectral imagery at 6.3 cm pixel resolution (Table 5.1). To ensure spatial accuracy, 11 ground control points (GCPs) were placed across the burn unit and located with an Emlid Reach-RS2 real-time kinetic GPS. The placement of these GCPs was chosen based on visibility from the sky and dispersion across the flight area. The GCPs had a reported average horizontal and vertical root mean square error of 0.007 m and 0.010 m, respectively. Details on the weather and flight conditions during each acquisition can be found in Table 5.2. The time of flight was aimed at minimizing shadows while balancing weather variation and site access.

Table 5.5. List of bands available on the Micasense Dual-Camera System and the wavelengths covered compared to the bands available on Landsat 8 Operational Land Imager (OLI) and Sentinel 2 MultiSpectral Instrument (MSI). The bands are named in accordance with the Micasense suggestions and as such are not necessarily in numerical order of the wavelengths covered.

MicaSense Band	MicaSense λ	Landsat 8 OLI	Sentinel 2A MSI
Blue	430-458 nm	Band 1 – 433-453 nm	Band 1 – 433-453 nm
Blue 2	465-485 nm	Band 2 – 450-515 nm	Band 2 – 460-525 nm
Green	550-570 nm	Band 3 – 525-600 nm	Band 3 – 542-577 nm
Green 2	524-538 nm	Band 3 – 525-600 nm	Band 3 – 542-577 nm
Red	663-673 nm	Band 4 – 630-680 nm	Band 4 – 650-680 nm
Red 2	642-658 nm	Band 4 – 630-680 nm	Band 4 – 650-680 nm
Red Edge 1	712-722 nm	NA	NA
Red Edge 2	700-710 nm	NA	Band 5 – 697-711 nm
Red Edge 3	731-749 nm	NA	NA
Near Infrared	820-860 nm	Band 5 – 845-885 nm	Band 8 – 780-885 nm

Table 5.6. Description of flight timing and weather during UAS acquisitions.

Days From Fire	Flight Time	Weather Notes
1 Day Pre	11:30-12:45	Scattered cloud cover during the last 30 minutes
1 Day Post	12:45-13:50	Mixed cloud cover throughout the flight
3 Days Post	12:00-13:00	Cloud free with slight wind
10 Days Post	12:20-13:30	Consistent cloud cover with slight wind
35 Days Post	14:15-15:00	Scattered cloud cover and wind gusting up to 15mph

5.2.4 UAS Image Processing

UAS photos were processed in the Agisoft Metashape version 1.6.4 (Agisoft LLC., St. Petersburg, Russia) Structure from Motion algorithm set to High Quality and Mild Depth Map Filtering generation parameters for each flight date. These parameters have been found to maximize tree extraction and height accuracy in conifer forests of similar crown architecture (Tinkham and Woolsey, 2024). Photos of the reflectance panels taken pre- and post-flight were used to calibrate image spectral reflectance and correct for lighting inconsistencies. The GCP locations were imported to Metashape and iteratively georeferenced using a minimum of 10 photos per collection, resulting in a median error of 0.008 m across all collections. Once GCPs were georeferenced, UAS photos were aligned to produce 10-24 million tie points per acquisition as well as an orthomosaic and dense point cloud with information for the 10 spectral bands attached. The difference in the number of tie points for each collection can be attributed to some flights having additional spatial coverage outside the study area. The orthomosaics had a final pixel resolution of 6.3 cm. Prior to export, pixel and point values were converted to reflectance by dividing each band value by 32,768 following the recommendation of the camera manufacturer (MicaSense Seattle, WA, USA). Then, orthomosaics and point clouds were exported as GeoTiffs and LAS files, respectively, for each flight date in the North American Datum 1983 UTM zone 16 (NAD83, UTM 16) projected coordinate system. Image processing was completed for the entire 17-ha burn unit, while analysis focused on the northwestern 6-ha study area.

5.2.5 UAS Tree Extraction

Point clouds and orthomosaics were processed in RStudio version 4.3.2 (R Core Team, 2022) to extract individual trees and tree crowns. Point clouds were processed following steps from Tinkham & Woolsey (2024) using the cloud2trees package (Woolsey, 2024). This package uses functions from both the lasR (Roussel, 2024) and lidR (Roussel et al., 2020; Roussel & Auty, 2024) packages. First, we removed noise from raw point clouds by classifying and removing isolated and duplicate points. Next, we classified ground points to generate a digital terrain model (DTM) at 1.0 m resolution using Delaunay triangulation and pit fill, allowing us to height normalize the point cloud and generate a canopy height model (CHM) at 0.10 m resolution. We used a variable window function [Equation 1], as proposed by Creasy et al. (2021), to locate individual trees at least 4 meters tall, with the data visually inspected to minimize omission and commission errors. Next, tree crown were delineated using the marker-controlled watershed approach from the ForestTools package (Plowright, 2024). These steps resulted in a DTM and CHM raster, individual tree crown polygons, and tree top points with estimated height.

$$Variable\ Window\ Radius = 0.47 + CHM\ Value * 0.2 \quad [1]$$

The above process was repeated on all collection dates. For our differenced analysis (i.e., integrating pre- and post-fire imagery) we used the pre-fire extracted trees as the structure to be applied at post-fire dates. These extracted trees were spatially matched to post-fire spectral-rasters to extract within tree values at those locations at each time point. To analyze the use of only post-fire information for estimating scorch, we extracted individual trees at each respective post-fire date to examine individual tree extraction effectiveness when pre-fire tree data are not available. For both data strategies, we used the exact_extract function

from the exactextractr package (Baston, 2024) to derive all raster values from within the individual tree crown polygons, providing us with the 10-band spectral data clipped to these individual trees. These values were normalized to the reflectance scale by dividing each cell value for a given band by the global maximum of that respective band (Micasense). These normalized band values were used to calculate spectral indices (Table 5.3). We further summarized the crown-level spectral values as the mean, median, 10th, 20th, 25th, 30th, 40th, 60th, 70th, 75th, 80th, and 90th percentile band and index values for each tree, at each date. These band and index values were appended to the respective date's field tree list to be used as predictor variables of CVS. For the differenced analysis, pre-fire summarized values were subtracted from post-fire values to produce a delta value for each summarization approach, each band and index, and at each date. These differenced values are referred to as Δdate through the rest of the analysis.

Table 5.3. Equations for the 10 spectral indices tested for model utility.

Spectral Index	Index Name	Equation	Spectral Approach
NDVI	Normalized Difference Vegetation Index	$\frac{NIR - Red}{NIR + Red}$	Multispectral & RGB-NIR
NDVI2	Normalized Difference Vegetation Index 2	$\frac{NIR - Red_2}{NIR + Red_2}$	Multispectral
GNDVI	Green Normalized Difference Vegetation Index	$\frac{NIR - Green}{NIR + Green}$	Multispectral & RGB-NIR
GNDVI2	Green Normalized Difference Vegetation Index 2	$\frac{NIR - Green_2}{NIR + Green_2}$	Multispectral
GRVI	Green Ratio Vegetation Index	$\frac{NIR}{Green}$	RGB-NIR
PRI	Photochemical Reflectance Index	$\frac{Green_2 - Green}{Green_2 + Green}$	Multispectral
NDWI	Normalized Difference Water Index	$\frac{Green - NIR}{Green + NIR}$	Multispectral & RGB-NIR
FMCI	Foliar Moisture Content Index	$\frac{Red\ Edge_3 - NIR}{Red\ Edge_3 + NIR}$	Multispectral
NDRE	Normalized Difference Red Edge	$\frac{NIR - Red\ Edge_1}{NIR + Red\ Edge_1}$	Multispectral

NGRDI	Normalized Green Red Difference Index	$\frac{Green_1 - Red_1}{Green_1 + Red_1}$	Multispectral, RGB-NIR, RGB

Tree point locations, extracted from each date, were spatially matched to field collected tree locations following the methods of Tinkham et al. (2022). This spatial matching process used a maximum search distance of 10 m and maximum height error of 4 m to identify the UAS tree nearest to each field tree using the sf package (Pebesma, 2018). We then matched the UAS tree with the smallest height error to the field tree. Each collection resulted in a different number of matches due to differences in point cloud registration, tie point generation issues from tree movement due to wind, and GPS error (Table 5.4; Arkin et al., 2023). The pre-fire flight was interrupted mid-flight, resulting in a data gap and a reduction in sample size. These matches were inputs in the st_intesects function from the sf package and used to extract the nearest individual tree crown polygon.

Table 5.4: Final number of in situ trees at each date. The pre-fire trees were used for the differenced analysis.

Collection	**Number of Matched Trees (%)**
Pre-Fire	218 (72.67)
1-Day Post-Fire	245 (81.67)
3-Days Post-Fire	253 (84.33)
10-Days Post-Fire	248 (82.33)
35-Days Post-Fire	242 (80.67)

5.2.6 Modeling of Crown Volume Scorch

To examine our ability to predict CVS from UAS multispectral imagery, we conducted a multi-step modeling process involving 1) selection of the best summarization approach, 2) evaluation of predictor variable collinearity, and 3) stepwise fitting of logistic and beta regression models. In total, we fit 48 models, each corresponding to a unique combination of

post-fire vs differenced indices (2 levels), spectral predictor inputs (3 levels), post-fire date (4 levels), and model types (2 levels; Full structure: date/Δdate 2 x post-fire data 4 x spectral inputs 3 x logistic/beta model 2 = 48).

First, to identify the most appropriate crown summarization approach, for each of the 24 datasets (spectral input, data/Δdate, and post-fire date) we fit Random Forest models to each of the twelve sets of summarization metrics (e.g., 10th, 20th, 30th percentile etc.) using the RandomForest R package (Liaw & Wiener, 2002). These models were trained with 199 trees, using the default regression settings where each tree was fully grown with a minimum terminal node size of 5, and the number of predictors randomly sampled at each split was set to one-third of the total predictors. The models included the tree-level summary metrics for the ten spectral bands and ten spectral indices. The best summarization approach was identified as the model with the greatest variance explained by the Random Forest regression model.

After identifying the optimal summarization approach for each date and Δdate, we examined Pearson correlation between potential predictor variables (i.e., 20 for the multispectral model) and reduced the list of potential predictors by removing variables with greater than 70% correlation (Figure 5.2). We chose our initial variables to compare correlations against based on previous studies of CVS that found NDVI and greenness-based indices to be useful predictors of CVS (Moran et al., 2022; Arkin et al., 2023). This reduced list of predictors was used in the subsequent logistic and beta regression modeling. We used logistic regression to test the accuracy of a classification approach for grouping trees based on spectral data, aiding threshold-based management decisions. Beta regression, by modeling a continuous response, captured the full range of tree condition while accounting for proportional data.

Comparing these methods allowed us to assess both categorical and continuous representations of CVS.

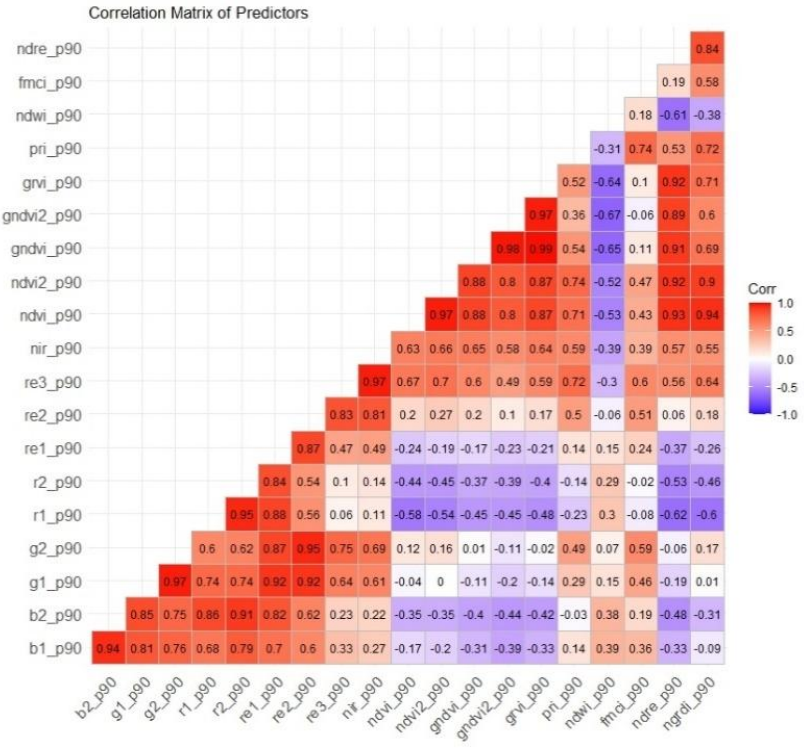

Figure 5.2. Correlation matrix between all potential predictor variables. This list of 20 variables was reduced based on correlation values of greater than 70%.

5.2.6.1 Logistic Regression

For the logistic regression models, we created a binary threshold of 90% CVS to separate the *in situ* trees into binary classes of likely-to-recover (<90% CVS) and potential-mortality (≥90% CVS). There are no established thresholds of CVS that are likely to result in morality for longleaf pine, due to its ability to recover from fire-induced needle damage at high percentages of CVS (Wilson et al., 2022). Thus, we used 90% as a threshold as trees with the highest likelihood of mortality. We selected this threshold after considering its practical implications in

this forest system, though alternative thresholds (e.g., 85%, 95%) did not substantially alter model performance.

For each of the 24 datasets that had been reduced using the random forest and collinearity variable reduction process, we fit logistic responses using generalized linear models with a binomial distribution using the reduced set of six non-colinear predictors which included NDVI, NDWI, FMCI, Green1, RedEdge3, and NIR. Next, we used forward-backward stepwise Akaike Information Criteria (AIC) to reduce to a final set of predictor variables using the glm function and step functions from base R. The stepwise selection process concluded when the addition or removal of predictors no longer reduced AIC. We exclusively considered main effects and did not test interactions or non-linear terms. For the final model, multicollinearity among predictors was assessed using Variance Inflation Factors (VIF) from the car package (Fox and Weisburg, 2019), ensuring all included variables had VIFs below 5 (O'Brien, 2007). To ensure stability of the model coefficients and evaluate model performance, we used a 10-fold cross-validation approach to test the final model. Each fold represented a random 10% of the available data, meaning that for each model fit, a nine-tenths training dataset was used to fit the model while the withheld data was used for validation. Within the 10-fold process, we evaluated model performance by comparing model accuracy in predicting CVS on the test data and the Area Under the Receiver Operating Characteristic Curve (AUC ROC) from the pROC package (Robin et al., 2011).

5.2.6.2 Bounded Response Beta Regression

For the beta regression modeling, all CVS field values were divided by 100 so their values were between 0 and 1, with 0s and 1s being converted to 0.0001 and 0.9999,

respectively. This was necessary to account for the truncated distribution assumptions of beta regression not including 0s and 1s. For each of the 24 datasets, we used the glmmTMB package in R (Brooks et al., 2017) to fit full models with the random forest and collinearity-reduced set of potential predictors. Next, we applied the stepGAIC function to perform forward-backward AIC stepwise selection, reducing the variable list iteratively by adding or removing predictors to minimize AIC. With multicollinearity addressed in the final model by calculating VIF of the stepwise-selected variables and removing any predictors with a VIF greater than 5, as high multicollinearity can distort regression coefficients and affect model performance.

Stability and performance of the final model for each dataset was assessed using a 10-fold cross-validation approach. During this process, a nine-tenths training dataset was used to fit the model while the withheld data was used for validation. Beta regression models were evaluated using mean and standard error of R^2, root-mean-square error (RMSE), and mean absolute error (MAE) across the folds.

5.3 Results

5.3.1 Field and Spectral Variability

The *in situ* sample trees had a mean height and canopy base height of 24.5 m and 12.7 m, respectively. The burn resulted in CVS being bimodally distributed with many values near 0% and 100%, with a mean CVS of 49.9% and a median CVS of 55.5% (Figure 5.3). CVS was first visually apparent at 3-days post-fire and scorched needles continued to transition from green to brown until needle drop (Figure 5.4). After this point, the study site was affected by high winds that increased the rate of needle drop from trees, resulting in only green unscorched

needles on less damaged crowns and bare crowns for the 100% scorched trees at 35-days post-fire.

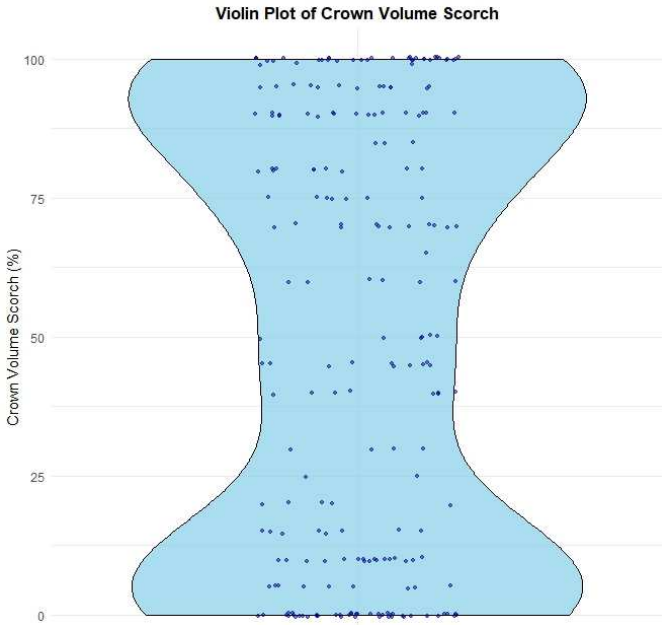

Figure 5.3: Violin plot showing the distribution of in situ crown volume scorch.

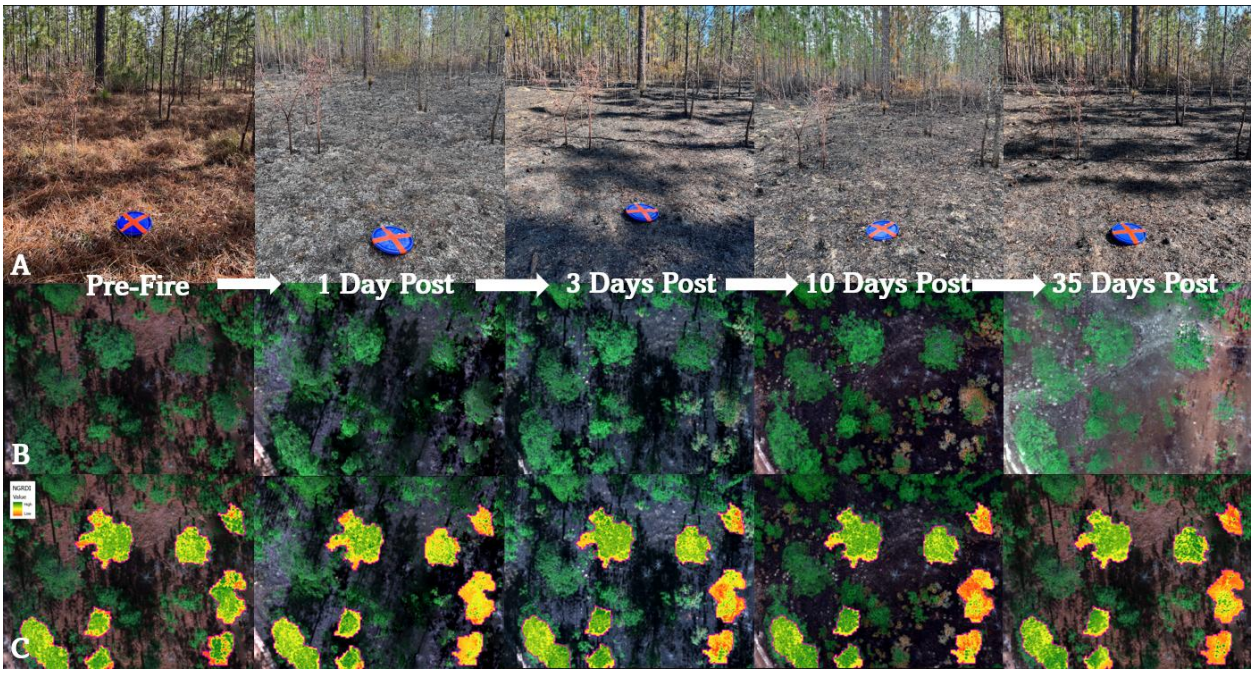

Figure 5.4: Progression images from pre-fire to 35-days post-fire at a ground control point (GCP) (row A), from the UAS orthomosaics (row B), and showing the Normalized Green Red Difference Index (NGRDI) within tree crown variation (row C).

The optimal summarization approach varied by collection date, whether the data was differenced, and the spectral bands and indices tested (Table 5.5). At least one post-fire collection for each spectral group had greater than 50% variance explained from the Random Forest model. The optimal summarization approach for the post-fire and differenced datasets were within However, the differenced collections, all had below 30% variance explained.

Table 5.5: Optimal summarization percentiles identified for each spectral range and collection date and the corresponding Random Forest percent variance explained. The optimal summarization approach was used for both the logistic and beta regression models.

Spectra Tested	Collection	Summarization	% Variance Explained
Multispectral	1-day post-fire	90th percentile	64.40
	3-days post-fire	50th percentile	60.84
	10-days post-fire	70th percentile	58.76
	35-days post-fire	20th percentile	53.47
	Δ 1-day post-fire	75th percentile	62.69
	Δ 3-days post-fire	Median	62.99
	Δ 10-days post-fire	90th percentile	62.67
	Δ 35-days post-fire	80th percentile	48.67
RGB-NIR	1-day post-fire	80th percentile	62.18
	3-days post-fire	50th percentile	58.47
	10-days post-fire	70th percentile	56.66
	35-days post-fire	70th percentile	48.27
	Δ 1-day post-fire	70th percentile	63.37
	Δ 3-days post-fire	75th percentile	65.79
	Δ 10-days post-fire	90th percentile	64.02
	Δ 35-days post-fire	60th percentile	51.21
RGB	1-day post-fire	30th percentile	60.66
	3-days post-fire	80th percentile	59.72
	10-days post-fire	90th percentile	55.97
	35-days post-fire	90th percentile	46.57
	Δ 1-day post-fire	80th percentile	63.29
	Δ 3-days post-fire	75th percentile	59.53
	Δ 10-days post-fire	90th percentile	63.74
	Δ 35-days post-fire	Mean	49.70

For multispectral data, high correlation between variables reduced our list of potential predictors to six, including NDVI, NDWI, FMCI, Green1, RedEdge3, and NIR. For the RGB-NIR

models, there were four potential bands (i.e., Red, Green, Blue, NIR) and five potential indices (i.e., NDVI, GNDVI, GRVI, NDWI, and NGRDI), which were reduced to NDVI, NDWI, Green1, and NIR following correlation analysis. For the RGB models, there were three potential bands (i.e., Red, Green, and Blue) and one potential index (i.e., NGRDI), however, correlation analysis reduced this list to NGRDI.

5.3.2 Logistic Regression

For the multispectral models, mean accuracy across the folds for the logistic regression (predicting >90% and <90% CVS) was highest at 10-days post-fire (86.93%, AUC=0.93) and at Δ 10-days post-fire (85.9%, AUC=0.91) (Table 5.6). Post-fire model accuracy generally increased as time since fire increased, peaking at 10-days post-fire, before dropping at 35-days post-fire. The Δ multispectral models achieved similar accuracies (~80%) for all dates except 10 days post-fire, which had slightly higher accuracy. Across all time points, Δ multispectral models were 1% to 8% less accurate than the corresponding post-fire models (Table 5.6).

For the RGB-NIR models, the highest mean accuracy was achieved at 35-days post-fire using just NDVI (85.74%, AUC=0.91) and at Δ10-days post-fire (84.0, AUC=0.91) using Green 1, NDVI, and NIR (Table 5.6). These dates had the lowest mean omission error in this spectral category, indicating a better ability to distinguish between the trees with the highest and lowest CVS compared to the other RGB-NIR models. Mean model accuracy fluctuated across post-fire dates, with moderately high accuracy at 1-day post-fire (83.21%), decreasing at 3-days post-fire (78.96%) before increasing at 10-days post-fire (80.80%) and peaking at 35-days post-fire (85.74%). Again, the post-fire models had greater accuracies by 2% to 7% compared to their Δ RGB-NIR counterparts for the same time points.

Table 5.6: Results of the logistic regression model runs with 10-fold cross-validation. The highest accuracy post-fire and Δ date models are bolded for each spectral group.

Spectra Tested	Collection	Summary %	Predictors	Mean Accuracy (%, SE)	Mean AUC (SE)	Mean Commission Error (%)	Mean Omission Error (%)
Multispectral	1-day	90th percentile	NDVI, NIR, RedEdge3	83.63 (0.003)	0.93 (0.002)	12.38	25.00
	3-days	50th percentile	NDVI, NIR, RedEdge3	85.35 (0.002)	0.90 (0.004)	14.29	15.00
	10-days	**70th percentile**	**Green 1, NDVI, RedEdge3, FMCI**	**86.93 (0.003)**	**0.93 (0.003)**	**9.90**	**19.72**
	35-days	20th percentile	Green 1, NDVI, NDWI, NIR, FMCI	81.92 (0.004)	0.92 (0.003)	15.21	23.19
	Δ 1-day	75th percentile	NDVI, NDWI	79.99 (0.009)	0.88 (0.007)	17.12	25.00
	Δ 3-days	Median	Green 1, NDVI, FMCI, NIR	82.69 (0.004)	0.90 (0.007)	16.15	19.82
	Δ 10-days	**90th percentile**	**Green 1, NDVI, RedEdge3**	**85.93 (0.007)**	**0.91 (0.004)**	**10.00**	**21.07**
	Δ 35-days	80th percentile	NDVI, NDWI, RedEdge3	80.66 (0.007)	0.89 (0.006)	15.83	25.35
RGB-NIR	1-day	80th percentile	Green 1, NDVI, NDWI, NIR	83.21 (0.003)	0.92 (0.005)	13.67	23.57
	3-days	50th percentile	Green 1, NDVI, NDWI, NIR	78.96 (0.006)	0.88 (0.003)	15.54	33.57
	10-days	70th percentile	Green 1, NDVI, NDWI	80.80 (0.005)	0.91 (0.003)	16.65	24.44
	35-days	**70th percentile**	**NDVI**	**85.74 (0.005)**	**0.91 (0.003)**	**15.21**	**12.22**
	Δ 1-day	70th percentile	NDVI, NDWI	81.01 (0.008)	0.88 (0.008)	17.88	20.71
	Δ 3-days	75th percentile	Green 1, NDVI, NIR	82.71 (0.006)	0.89 (0.007)	16.15	19.82
	Δ 10-days	**90th percentile**	**Green 1, NDVI, NIR**	**84.02 (0.007)**	**0.91 (0.005)**	**11.48**	**23.75**
	Δ 35-days	60th percentile	NDVI, NIR, NDWI	80.67 (0.008)	0.90 (0.006)	15.00	26.79
RGB	**1-day**	**30th percentile**	**NGRDI**	**85.03 (0.004)**	**0.92 (0.003)**	**12.38**	**20.54**
	3-days	80th percentile	NGRDI	84.94 (0.003)	0.89 (0.004)	14.29	16.43
	10-days	90th percentile	NGRDI	82.80 (0.006)	0.90 (0.004)	18.57	14.58
	35-days	90th percentile	NGRDI	84.47 (0.005)	0.9 2 (0.004)	14.58	17.08
	Δ 1-day	80th percentile	NGRDI	81.54 (0.006)	0.87 (0.007)	14.74	24.82
	Δ 3-days	**75th percentile**	**NGRDI**	**82.67 (0.006)**	**0.88 (0.007)**	**16.16**	**19.46**
	Δ 10-days	90th percentile	NGRDI	82.62 (0.005)	0.87 (0.005)	16.76	18.21
	Δ 35-days	Mean	NGRDI	77.03 (0.009)	0.83 (0.01)	20.00	28.03

For the RGB models, the highest mean accuracies were at 1-day post-fire (85.03%, AUC=0.92) and Δ 3-day post-fire (82.7, AUC=0.88) with both models using NGRDI as the predictor variable (Table 5.6). Model accuracy in this spectral category was highest at 1-day post-fire and decreased until 10-days post-fire before increasing at 35-days post-fire. For the post-fire models, commission errors remained relatively stable across post-fire models (ranging

from 12.38% to 18.57%), but omission errors were variable and peaked at 1-day post-fire at 20.54%. The Δ models exhibited higher omission errors than the post-fire models by 3% to 11%. Despite the increased omission errors for the Δ models, NGRDI demonstrated a strong ability to categorize scorch at multiple dates post-fire.

The best overall model achieved a mean accuracy across the 10-folds of 86.93% at 10-days post-fire using the 70th percentile of Green 1, NDVI, RedEdge3, and FMCI values (Table 5.6). Across the multispectral and RGB-NIR models, NDVI was a consistent predictor in all models, with Green 1 and NIR bands being significant in most models, both exclusively post-fire and differenced. The significance of NDVI and Green 1 in most models demonstrates their sensitivity to changes in canopy color and CVS. Omission error was generally higher than commission error for most models, with the highest omission errors occurring in the Δ models. High omission errors indicate that models were more likely to underpredict the presence of stressed trees, particularly with the inclusion of pre-fire data. Overall, post-fire models outperformed Δ models in both mean overall accuracy and in commission and omission errors. Further, all spectral model categories performed well, with the lowest mean accuracy being 77.03% at Δ 35-days post-fire using NGRDI, demonstrating the utility of UAS data in predicting CVS category, regardless of the spectral bands available for model training.

5.3.3 Bounded Response Beta Regression

For the multispectral post-fire models, the highest mean R^2 (0.614) and lowest RMSE (24.97) were observed at 1-day post-fire using the 90th percentile values of NDVI, NDWI, FMCI, and RedEdge3 (Table 5.7). As time since fire increased, R^2 values decreased, indicating decreased model performance.

Table 5.7. Results of the beta regression. The highest accuracy post-fire and Δ date models are bolded for each spectral group.

Spectra Tested	Spectra Tested	Summary %	Predictors	R^2	RMSE (% CVS)	MAE
Multispectral	**1-day post-fire**	**90th percentile**	**NDVI, NDWI, FMCI, RedEdge3**	**0.614**	**24.97**	**18.50**
	3-days post-fire	50th percentile	NDVI, NDWI, FMCI	0.604	24.88	18.02
	10-days post-fire	70th percentile	NDVI, FMCI, RedEdge3	0.586	26.07	18.65
	35-days post-fire	20th percentile	NDVI, NDWI	0.372	32.28	27.51
	Δ 1-day post-fire	75th percentile	NDVI	0.578	25.77	20.26
	Δ 3-days post-fire	**Median**	**NDVI**	**0.634**	**24.06**	**17.94**
	Δ 10-days post-fire	90th percentile	NDVI	0.562	26.55	20.88
	Δ 35-days post-fire	80th percentile	NDVI	0.572	25.97	20.41
RGB-NIR	**1-day post-fire**	**80th percentile**	**NDVI, Green1, NIR**	**0.626**	**24.57**	**18.39**
	3-days post-fire	50th percentile	NDVI, NDWI, Green1	0.528	27.10	19.80
	10-days post-fire	70th percentile	NDVI	0.554	27.05	20.63
	35-days post-fire	70th percentile	NDVI, NIR	0.531	27.89	22.25
	Δ 1-day post-fire	70th percentile	NDVI	0.583	25.63	20.17
	Δ 3-days post-fire	**75th percentile**	**NDVI**	**0.595**	**25.29**	**19.11**
	Δ 10-days post-fire	90th percentile	NDVI	0.562	26.55	20.88
	Δ 35-days post-fire	60th percentile	NDVI	0.578	25.78	20.37
RGB	**1-day post-fire**	**30th percentile**	**NGRDI**	**0.653**	**23.67**	**18.41**
	3-days post-fire	80th percentile	NGRDI	0.597	25.18	18.86
	10-days post-fire	90th percentile	NGRDI	0.565	26.74	20.45
	35-days post-fire	90th percentile	NGRDI	0.516	28.34	23.62
	Δ 1-day post-fire	80th percentile	NGRDI	0.540	26.87	20.93
	Δ 3-days post-fire	**75th percentile**	**NGRDI**	**0.574**	**25.95**	**20.09**
	Δ 10-days post-fire	90th percentile	NGRDI	0.549	26.94	21.12
	Δ 35-days post-fire	Mean	NGRDI	0.483	28.51	22.85

The Δ multispectral models performed similarly to those in the multispectral group, with the Δ3-days post-fire achieving an R^2 of 0.634 and RMSE of 24.06. For the RGB-NIR post-fire models, the best performing model also used 1-day post-fire data to achieve an R^2 of 0.626 and RMSE of 24.57 using the 80th percentile values of NDVI, Green 1, and NIR (Table 5.7). The Δ RGB-NIR models also performed similarly to the post-fire models at the same time-since-fire with all models achieving an R^2 between 0.562 (Δ 10-days post-fire) and 0.595 (Δ 3-days post-fire). The RGB models produced both the best and worst performances in terms of R^2 and RMSE (Table 5.7), with the strongest gradient of model decline from 1- to 35-days post-fire. The best

performing model was achieved at 1-day post-fire using the 30th percentile values of NGRDI to achieve an R^2 of 0.653 and RMSE of 23.67. Overall, 1-day post-fire models consistently demonstrated the best predictive performance for the post-fire models, while Δ 3-days post-fire consistently demonstrated the best predictive performance across all spectral groups for the differenced models. Across all beta regression models, prediction accuracy seems to be optimized for the least and most crown scorched trees, with approximately double the variability for intermediate scorch levels (Figure 5.5).

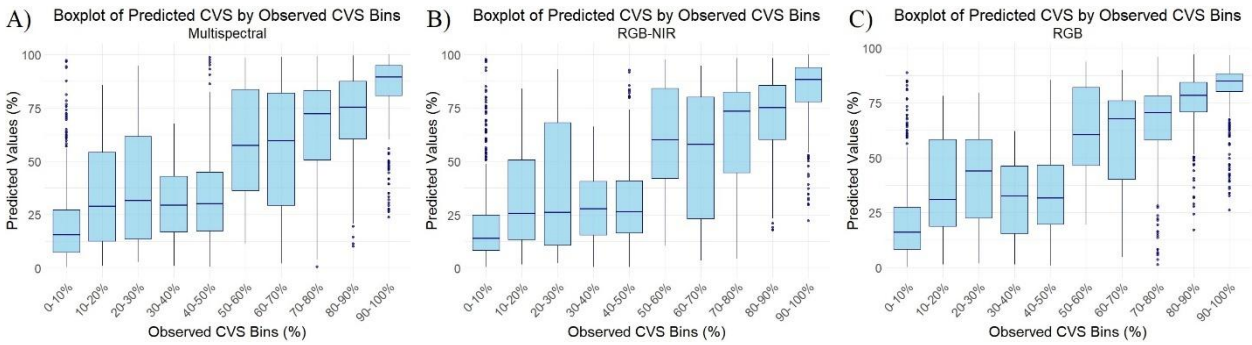

Figure 5.5. Predicted versus observed graphs from the 1-day post-fire beta regression models across 10-folds. Panel (A) is the multispectral model, (B) is the RGB-NIR model, and (C) is the RGB model.

5.4 Discussion

5.4.1 CVS Model Performance

The best logistic regression model successfully predicted CVS categories at 10-days post-fire with 86.93% accuracy using multispectral data, with similarly high accuracies as soon as 1-day post-fire (85.03%) using just RGB data. Model accuracy fluctuated with time-since-fire and spectra used, but all logistic models regardless of timing and spectra used had mean accuracies of at least 77%, indicating a strong ability to distinguish the trees with the greatest CVS at multiple dates and using a variety of spectra. The beta regression models did not achieve as

high of accuracies, but at 1-day post-fire our models predicted CVS to achieve an R^2 of 61.4 to 65.3 depending on spectra used. Overall, model results demonstrate a reasonable ability to predict CVS of longleaf pine at multiple dates post-fire, using either multispectral or RGB imagery. The multispectral indices NDVI, NDWI, and FMCI performed well, and RGB-based index NGRDI provided comparable results at most collection dates.

For the beta regression models, the inclusion of pre-fire data yielded similar model performance as the use of post-fire data. The Δ multispectral and RGB-NIR models all reduced to only use NDVI as their predictor variable, but differed in their summarization approach, resulting in differences in resultant R^2 of up to 0.04, highlighting the importance of selecting the appropriate summarization approach. The use of only post-fire vs differenced imagery caused R^2 to fluctuate by 0.01 to 0.11, with the better model varying by spectra and post-fire date. Although, difference imagery has been important for satellite-based predictions of fire-effects (Lentile et al., 2006; Escuin et al., 2007), these results suggests that these benefits might not scale to where pixels are smaller than the object being described.

Our findings align with previous research conducted by Moran et al. (2022) and Arkin et al. (2023) while expanding their work into a new forest type and testing the utility of multitemporal and multispectral data. Moran et al., (2022) used a UAS equipped with four spectral bands (RGB-NIR camera) following a prescribed burn in ponderosa pine forests in Montana and demonstrated that very-high-resolution imagery can be used to distinguish scorched crowns from uninjured crowns. However, this study used a labor-intensive manual processing method that would be unrealistic for assessing scorch across 1,000s of trees. Arkin et al. (2023) advanced these techniques by using a combination of orthomosaics and point

clouds to classify trees as burned/unburned and to estimate the height and volume of crown scorch, respectively in British Columbia, Canada. Their point cloud estimated CVS approach was within ±10% of field estimates for 83.3% of trees, demonstrating strong potential for using UAS to estimate scorch structurally (Arkin et al., 2023). By comparison, the present study had 33.3% of trees within 10% CVS error for the RGB beta regression model (Figure 5.6), with 65% within a 20% CVS error. Two things could contribute to our study's lower model accuracy. Arkin et al. (2023) validation dataset was dominated by trees with near 0% or 100% CVS, which theoretically should be easier to reliably predict compared to the more continuously distributed data available for the current study. Additionally, this could indicate a loss in predictive power using a two-dimensional spectral approach compared to the point-cloud approach of Arkin et al. (2023).

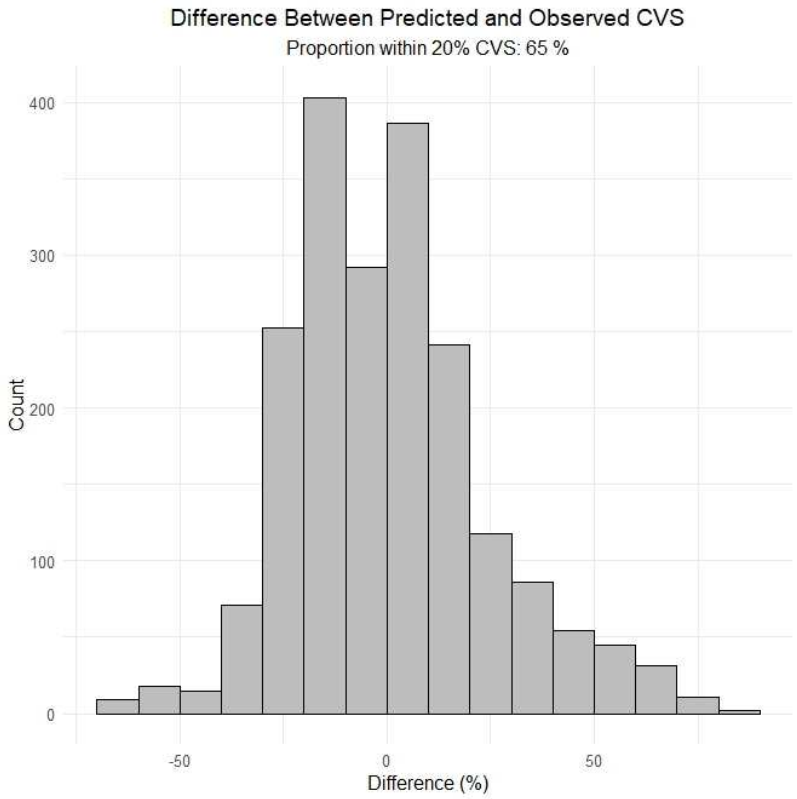

Figure 5.6. Differences between the predicted and observed values of crown volume scorch from the 1-day post-fire multispectral beta regression model across the 10-folds.

Our logistic regression models performed well in classifying CVS when using a threshold of 90% CVS. This threshold was defined by literature relevant to longleaf pine forests and should be adjusted if developing and applying similar models in different forest system, as different systems have different fire adaptations and species may be more vulnerable to mortality at lower thresholds. For ponderosa pine, a threshold of 88% is associated with high mortality (Fowler et al., 2010), while in Douglas-fir, this threshold can be as low as 20% (Engber & Varner, 2012). Further, our beta regression models trained on 2-dimensional data did not improve performance compared to previous studies that used 3-dimensional data (Arkin et al., 2023). Future work should examine the use of 3-dimensional voxel-based approaches that can

integrate the spectral signature across the 3-dimensional crown, particularly for trees with uneven scorch distribution.

The failure of the differenced datasets to consistently improve model predictions could be attributed to a combination of data alignment and spectral calibration. The potential for small shifts in the data to cause differencing issues could be the result of alignment issues as the GCPs had a horizontal RMSE of 7 cm, slightly larger than 1 pixel. In some of the sparser tree crowns, a one-pixel shift per date could result in the pre-fire crowns extracting background or lower canopy pixel values, particularly at the edges of tree crowns. The prescribed burn resulted in consumption of most understory fuels, so pre-fire data would have captured healthy vegetation, even in background pixels, while post-fire data had background pixels with primarily dead/charred vegetation. Further, alignment issues could be the result of wind differences between collection dates that resulted in incomplete crown reconstruction of some trees in the post-fire point clouds. This incomplete crown reconstruction effect also accounts for the small difference in tree extraction in the post-fire collections. Weather differences could also drive normalization issues across time as each date had different levels of cloud cover, with cloud cover also shifting during some individual collections. While reflectance calibration panels should overcome most of these differences, illumination can vary during the flight and those differences might not be perfectly captured in the pre- and post-flight panel photos (Stow et al., 2019). Further research should explore the influences of cloud cover, wind, and spatial alignment on multi-temporal imagery comparisons.

5.4.2 Implications for Prescribed Fire Management

In longleaf pine forests, scorch is first visually apparent around 3- to 5-days post-fire, and needle color will continue to transition over 30- to 50-days post-fire before abscising from the tree, with variation depending on weather and the seasonality of fire (Wilson et al., 2022). CVS is typically quantified ocularly as a percentage of the crown displaying red compared to green foliage (Alexander et al., 2019). The difference between red and green needles was captured well using NGRDI as soon as 1-day post-fire, representing a 20-day improvement in the timing of post-fire effects observations compared to our field-assessment timeline. Field estimates of CVS are often most accurate on trees with either very little or complete scorch and are prone to increased error when examining trees with intermediate scorch levels (Varner et al., 2021). The narrowing of the boxplot ranges at the tails of the CVS range in Figure 5.5 supports this finding and suggests that a large amount of training data for model fitting might be needed to average out observer errors. However, when collected reliably, CVS is a stronger indicator of post-fire mortality than scorch height alone, for both long- and short-needle conifer species (Peterson, 1985; Peterson and Arbaugh, 1986; Cansler et al., 2020). Post-fire mortality prediction is essential for informing management objective success and for planning future burns, thus many studies focus specifically on CVS as their metric of fire severity and eventual mortality (Hood et al., 2018; Cansler et al., 2020). This study demonstrates an approach that managers and researchers can use to model CVS to improve their understanding of prescribed fire effects and inform future prescriptions.

The application of our models will provide useful insights into prescribed burning practices. For example, managers could conduct a burn, collect UAS data, apply a model similar

to ours, and use the results to evaluate ignition patterns, time of burning, and burn frequency for planning subsequent fires. Our results suggest that UAS monitoring could be conducted as soon as 1-day post-fire, with the workflow used in this study then potentially producing CVS estimates within days. Further, the high accuracy of the RGB models presents the possibility for management organizations to acquire reasonable-cost systems for this application.

However, several challenges and limitations should be considered when applying these model strategies to different sites and forest types. First, canopy structure and species composition can influence the accuracy of CVS predictions. Our study was conducted in an open-canopy pine forest, where individual tree crowns were relatively easy to delineate. In denser forests or mixed-species stands, overlapping crowns and variable leaf morphology could complicate segmentation and lead to greater model uncertainty. Additionally, spectral signatures of scorched foliage may vary by species, meaning models trained in one forest type may require recalibration before being applied elsewhere. Second, operational constraints of UAS technology present limitations in large-scale applications. Most UAS are limited in their spatial extent due to battery life, with the tested UAS system's 30 minute battery life providing ~20 ha flight extents. While multiple batteries or larger UAS platforms can extend coverage, surveying extensive burn areas remains a logistical challenge. Additionally, regulatory restrictions, such as flight altitude limitations and line-of-sight requirements, may influence data acquisition strategies in certain regions. Despite these challenges, integrating spectral and structural data, optimizing model transferability across forest types, and refining UAS deployment strategies could enhance the applicability of this approach. Future work should

focus on validating models across diverse forest conditions and exploring methods for improving scalability.

While this study demonstrates the utility of UAS for CVS prediction, future work could expand the applications. The models developed in this study demonstrate strong potential for classifying CVS class at the individual tree scale across a 17-ha site. However, prescribed fire in the southeastern US is applied to approximately 2.1 million hectares annually (Cummins et al., 2023). As such, the scaling of these models to larger areas could provide managers with valuable information on fire effects including scorched tree locations and landscape-scale patterns of scorch. Training satellite-based sensors from UAS observations of fire effects would substantially enhance spatial coverage and sample variation, allowing researchers to describe effects at broader scales, particularly larger prescribed fires (100s of hectares). Integrating multi-scale approaches, such as combining satellite remote sensing with field-based physiological assessments of fire impacts, could yield deeper insights into individual tree recovery and ecosystem processes.

5.5 Conclusion

This study underscores the potential of leveraging remote sensing technologies to improve post-fire vegetation assessments in fire-adapted forests. By integrating multitemporal and multispectral ultra-high-resolution imagery, we successfully modeled CVS and CVS class at multiple post-fire dates, providing a practical and scalable method for evaluating fire effects and severity to inform management strategies. Our findings bridge critical gaps in existing methods by offering consistent and cost-effective models of CVS that are not computationally difficult or costly. These advancements can be applied directly to forest management actions

and aid in prescribed fire prescription planning or wildfire recovery. Informed and adaptive management using our models will ensure that the ecological, economic, and cultural values of longleaf pine savannas remain. However, the transference of these models should be tested across different longleaf pine dominated forests and substrate soils to ensure reliable predictions can be made.

5.6 References

Abatzoglou, J.T., Williams, A.P., Boschetti, L., Zubkova, M., Kolden, C.A., 2018. Global patterns of interannual climate–fire relationships. *Global Change Biology* 24, 5164–5175. https://doi.org/10.1111/gcb.14405

Abdollahnejad, A., Panagiotidis, D., 2020. Tree Species Classification and Health Status Assessment for a Mixed Broadleaf-Conifer Forest with UAS Multispectral Imaging. *Remote Sensing* 12, 3722. https://doi.org/10.3390/rs12223722

Agee, J.K., Skinner, C.N., 2005. Basic principles of forest fuel reduction treatments. *Forest Ecology and Management* 211, 83–96. https://doi.org/10.1016/j.foreco.2005.01.034

Alonso-González, E., Fernández-García, V., 2021. MOSEV: a global burn severity database from MODIS (2000–2020). *Earth System Science Data* 13, 1925–1938. https://doi.org/10.5194/essd-13-1925-2021

Arkin, J., Coops, N.C., Daniels, L.D., Plowright, A., 2023. A novel post-fire method to estimate individual tree crown scorch height and volume using simple RPAS-derived data. *Fire Ecology* 19, 17. https://doi.org/10.1186/s42408-023-00174-7

Baston, D. exactextractr: fast extraction from raster datasets using polygons. R package version 0.10.0, https://github.com/isciences/exactextractr

Bechtold, W.A. (2003). Crown-diameter prediction models for 87 species of stand-grown trees in the eastern United States. *Southern Journal of Applied Forestry*, 27(4), 269–278.

Brooks, M. E., Kristensen, K., van Benthem, K. J., Magnusson, A., Berg, C. W., Nielsen, A., Skaug, H. J., Maechler, M., & Bolker, B. M. (2017). glmmTMB balances speed and flexibility among packages for zero-inflated generalized linear mixed modeling. *The R Journal, 9*(2), 378–400. https://doi.org/10.32614/RJ-2017-066

Cansler, C. A., Hood, S. M., Van Mantgem, P. J., & Varner, J. M. (2020). A large database supports the use of simple models of post-fire tree mortality for thick-barked conifers, with less support for other species. *Fire Ecology,* 16(1), 25. https://doi.org/10.1186/s42408-020-00082-0

Carvajal-Ramírez, F., Marques Da Silva, J.R., Agüera-Vega, F., Martínez-Carricondo, P., Serrano, J., Moral, F.J., 2019. Evaluation of Fire Severity Indices Based on Pre- and Post-Fire Multispectral Imagery Sensed from UAV. *Remote Sensing* 11, 993. https://doi.org/10.3390/rs11090993

Chuvieco, E., Deshayes, M., Stach, N., Cocero, D., Riaño, D., 1999. Short-term fire risk: foliage moisture content estimation from satellite data, in: Chuvieco, E. (Ed.), Remote Sensing of Large Wildfires: In the European Mediterranean Basin. Springer, Berlin, Heidelberg, pp. 17–38. https://doi.org/10.1007/978-3-642-60164-4_3

Chuvieco, E., Yue, C., Heil, A., Mouillot, F., Alonso-Canas, I., Padilla, M., Pereira, J.M., Oom, D., Tansey, K., 2016. A new global burned area product for climate assessment of fire impacts. *Global Ecology and Biogeography* 25, 619–629. https://doi.org/10.1111/geb.12440

Creasy, M.B., Tinkham, W.T., Hoffman, C.M., Vogeler, J.C., 2021. Potential for individual tree monitoring in ponderosa pine dominated forests using unmanned aerial system structure from motion point clouds. *Can. J. For. Res.* 51, 1093–1105. https://doi.org/10.1139/cjfr-2020-0433

Engber, E. A., & Varner, J. M. (2012). Predicting Douglas-fir Sapling Mortality Following Prescribed Fire in an Encroached Grassland. *Restoration Ecology*, *20*(6), 665–668. https://doi.org/10.1111/j.1526-100X.2012.00900.x

Escuin, S., Navarro, R., Fernández, P., 2008. Fire severity assessment by using NBR (Normalized Burn Ratio) and NDVI (Normalized Difference Vegetation Index) derived from LANDSAT TM/ETM images. *International Journal of Remote Sensing* 29, 1053–1073. https://doi.org/10.1080/01431160701281072

Fernández-Guisuraga, J.M., Sanz-Ablanedo, E., Suárez-Seoane, S., Calvo, L., 2018. Using Unmanned Aerial Vehicles in Postfire Vegetation Survey Campaigns through Large and Heterogeneous Areas: Opportunities and Challenges. *Sensors* (Basel) 18, 586. https://doi.org/10.3390/s18020586

Fowler, J. F., Sieg, C. H., McMillin, J., Allen, K. K., Negrón, J. F., Wadleigh, L. L., Anhold, J. A., & Gibson, K. E. (2010). Development of post-fire crown damage mortality thresholds in ponderosa pine. *International Journal of Wildland Fire*, *19*(5), 583–588. https://doi.org/10.1071/WF08193

Fox, J., Weisberg, S. (2019). _An R Companion to Applied Regression_, Third edition. Sage, Thousand Oaks CA. <https://socialsciences.mcmaster.ca/jfox/Books/Companion/>.

Fraser, B.T., Congalton, R.G., 2021. Monitoring Fine-Scale Forest Health Using Unmanned Aerial Systems (UAS) Multispectral Models. *Remote Sensing* 13, 4873. https://doi.org/10.3390/rs13234873

Frost, C., 2006. History and Future of the Longleaf Pine Ecosystem, in: Jose, S., Jokela, E.J., Miller, D.L. (Eds.), The Longleaf Pine Ecosystem: Ecology, Silviculture, and Restoration, Springer Series on Environmental Management. Springer, New York, NY, pp. 9–48. https://doi.org/10.1007/978-0-387-30687-2_2

Hanna, L., Tinkham, W. T., Battaglia, M. A., Vogeler, J. C., Ritter, S. M., & Hoffman, C. M. (2024). Characterizing heterogeneous forest structure in ponderosa pine forests via UAS-derived structure from motion. *Environmental Monitoring and Assessment*, 196(6), 530. https://doi.org/10.1007/s10661-024-12703-1

Hollingsworth, L.T., Kurth, L.L., Parresol, B.R., Ottmar, R.D., Prichard, S.J., 2012. A comparison of geospatially modeled fire behavior and fire management utility of three data sources in the southeastern United States. *Forest Ecology and Management*, Assessing wildland fuels and hazard mitigation treatments in the southeastern United States 273, 43–49. https://doi.org/10.1016/j.foreco.2011.05.020

Hood, S.M., Varner, J.M., Mantgem, P. van, Cansler, C.A., 2018. Fire and tree death: understanding and improving modeling of fire-induced tree mortality. *Environ. Res. Lett*. 13, 113004. https://doi.org/10.1088/1748-9326/aae934

Hudak, A.T., Freeborn, P.H., Lewis, S.A., Hood, S.M., Smith, H.Y., Hardy, C.C., Kremens, R.J., Butler, B.W., Teske, C., Tissell, R.G., Queen, L.P., Nordgren, B.L., Bright, B.C., Morgan, P., Riggan, P.J., Macholz, L., Lentile, L.B., Riddering, J.P., Mathews, E.E., 2018. The Cooney Ridge Fire Experiment: An Early Operation to Relate Pre-, Active, and Post-Fire Field and Remotely Sensed Measurements. *Fire* 1, 10. https://doi.org/10.3390/fire1010010

Jaiswal, R.K., Mukherjee, S., Raju, K.D., Saxena, R., 2002. Forest fire risk zone mapping from satellite imagery and GIS. *International Journal of Applied Earth Observation and Geoinformation* 4, 1–10. https://doi.org/10.1016/S0303-2434(02)00006-5

Johnstone, J.F., Allen, C.D., Franklin, J.F., Frelich, L.E., Harvey, B.J., Higuera, P.E., Mack, M.C., Meentemeyer, R.K., Metz, M.R., Perry, G.L., Schoennagel, T., Turner, M.G., 2016. Changing disturbance regimes, ecological memory, and forest resilience. *Frontiers in Ecology and the Environment* 14, 369–378. https://doi.org/10.1002/fee.1311

Knapp, B.O., Stephan, K., Hubbart, J.A., 2015. Structure and composition of an oak-hickory forest after over 60 years of repeated prescribed burning in Missouri, U.S.A. *Forest Ecology and Management* 344, 95–109. https://doi.org/10.1016/j.foreco.2015.02.009

Lad, L.E., Tinkham, W.T., Sparks, A.M., Smith, A.M.S., 2023. Evaluating Predictive Models of Tree Foliar Moisture Content for Application to Multispectral UAS Data: A Laboratory Study. *Remote Sensing* 15, 5703. https://doi.org/10.3390/rs15245703

Lake, F.K., Wright, V., Morgan, P., McFadzen, M., McWethy, D., Stevens-Rumann, C., 2017. Returning Fire to the Land: Celebrating Traditional Knowledge and Fire. *Journal of Forestry* 115, 343–353. https://doi.org/10.5849/jof.2016-043R2

Littell, J.S., Peterson, D.L., Riley, K.L., Liu, Y., Luce, C.H., 2016. A review of the relationships between drought and forest fire in the United States. *Global Change Biology* 22, 2353–2369. https://doi.org/10.1111/gcb.13275

McIver, J.D., Stephens, S.L., Agee, J.K., Barbour, J., Boerner, R.E.J., Edminster, C.B., Erickson, K.L., Farris, K.L., Fettig, C.J., Fiedler, C.E., Haase, S., Hart, S.C., Keeley, J.E., Knapp, E.E., Lehmkuhl, J.F., Moghaddas, J.J., Otrosina, W., Outcalt, K.W., Schwilk, D.W., Skinner, C.N., Waldrop, T.A., Weatherspoon, C.P., Yaussy, D.A., Youngblood, A., Zack, S., 2012. Ecological effects of alternative fuel-reduction treatments: highlights of the National Fire and Fire Surrogate study (FFS). *Int. J. Wildland Fire* 22, 63–82. https://doi.org/10.1071/WF11130

Moran, C.J., Hoff, V., Parsons, R.A., Queen, L.P., Seielstad, C.A., 2022. Mapping Fine-Scale Crown Scorch in 3D with Remotely Piloted Aircraft Systems. *Fire* 5, 59. https://doi.org/10.3390/fire5030059

Moreira, F., Ascoli, D., Safford, H., Adams, M.A., Moreno, J.M., Pereira, J.M.C., Catry, F.X., Armesto, J., Bond, W., González, M.E., Curt, T., Koutsias, N., McCaw, L., Price, O., Pausas, J.G., Rigolot, E., Stephens, S., Tavsanoglu, C., Vallejo, V.R., Wilgen, B.W.V., Xanthopoulos, G., Fernandes, P.M., 2020. Wildfire management in Mediterranean-type regions: paradigm change needed. *Environ. Res. Lett*. 15, 011001. https://doi.org/10.1088/1748-9326/ab541e

Noss, R.F. (2018). *Fire Ecology of Florida and the Southeastern Coastal Plain*. Gainesville: University Press of Florida.

O'Brien, R. M. (2007). A caution regarding rules of thumb for variance inflation factors. *Quality & Quantity, 41*(5), 673–690. https://doi.org/10.1007/s11135-006-9018-6

O'Brien, J.J., Kevin Hiers, J., Mitchell, R.J., Varner, J.M., Mordecai, K., 2010. Acute Physiological Stress and Mortality Following Fire in a Long-Unburned Longleaf Pine Ecosystem. *Fire Ecology* 6, 1–12. https://doi.org/10.4996/fireecology.0602001

Parresol, B.R., Blake, J.I., Thompson, A.J., 2012. Effects of overstory composition and prescribed fire on fuel loading across a heterogeneous managed landscape in the southeastern USA. Forest Ecology and Management, Assessing wildland fuels and hazard mitigation treatments in the southeastern United States 273, 29–42. https://doi.org/10.1016/j.foreco.2011.08.003

Pausas, J.G., Bond, W.J., 2020. On the Three Major Recycling Pathways in Terrestrial Ecosystems. *Trends in Ecology & Evolution* 35, 767–775. https://doi.org/10.1016/j.tree.2020.04.004

Pebesma, E., 2018. Simple Features for R: Standardized Support for Spatial Vector Data. The R Journal 10 (1), 439-446. https://doi.org/10.32614/RJ-2018-009
Plowright, A. (2024). _ForestTools: Tools for Analyzing Remote Sensing Forest Data_. R package version 1.0.2, <https://CRAN.R-project.org/package=ForestTools>.
R Core Team (2023). _R: A Language and Environment for Statistical Computing_. R Foundation for Statistical Computing, Vienna, Austria. <https://www.R-project.org/>.
Ravan, S.A., Roy, P.S., 1997. Satellite remote sensing for ecological analysis of forested landscape. *Plant Ecology* 131, 129–141. https://doi.org/10.1023/A:1009731608350
Robin, X., Turck, N., Hainard, A., Tiberti, N., Lisacek, F., Sanchez, J.-C., & Müller, M. (2011). pROC: An open-source package for R and S+ to analyze and compare ROC curves. *BMC Bioinformatics, 12*, 77. https://doi.org/10.1186/1471-2105-12-77
Roussel, J. (2024). _lasR: Fast and Pipeable Airborne LiDAR Data Tools_. R package version 0.5.6, https://github.com/r-lidar/lasR
Roussel, J. R., Auty, D. (2024). Airborne LiDAR Data Manipulation and Visualization for Forestry Applications. R package version 4.1.0. https://cran.r-project.org/package=lidR
Rowe, J.S., Scotter, G.W., 1973. Fire in the Boreal Forest. *Quaternary Research* 3, 444–464. https://doi.org/10.1016/0033-5894(73)90008-2
Ryan, K. C., Knapp, E. E., & Varner, J. M. (2013). Prescribed fire in North American forests and woodlands: History, current practice, and challenges. *Frontiers in Ecology and the Environment,* 11(s1), e15–e24. https://doi.org/10.1890/120329
Sader, S.A., Winne, J.C., 1992. RGB-NDVI colour composites for visualizing forest change dynamics. *International Journal of Remote Sensing* 13, 3055–3067. https://doi.org/10.1080/01431169208904102
Santos, F., Bailey, J.K., Schweitzer, J.A., 2023. The eco-evolutionary role of fire in shaping terrestrial ecosystems. *Functional Ecology* 37, 2090–2095. https://doi.org/10.1111/1365-2435.14387
Sayer, M.A.S., Tyree, M.C., Kuehler, E.A., Jackson, J.K., Dillaway, D.N., 2020. Physiological Mechanisms of Foliage Recovery after Spring or Fall Crown Scorch in Young Longleaf Pine (Pinus palustris Mill.). *Forests* 11, 208. https://doi.org/10.3390/f11020208
Staver, A.C., Archibald, S., Levin, S.A., 2011. The Global Extent and Determinants of Savanna and Forest as Alternative Biome States. *Science* 334, 230–232. https://doi.org/10.1126/science.1210465
Stow, D., Nichol, C. J., Wade, T., Assmann, J. J., Simpson, G., & Helfter, C. (2019). Illumination Geometry and Flying Height Influence Surface Reflectance and NDVI Derived from Multispectral UAS Imagery. *Drones*, *3*(3), Article 3. https://doi.org/10.3390/drones3030055
Swayze, N.C., Tinkham, W.T., Vogeler, J.C., Hudak, A.T., 2021. Influence of flight parameters on UAS-based monitoring of tree height, diameter, and density. *Remote Sensing of Environment* 263, 112540. https://doi.org/10.1016/j.rse.2021.112540
Tang, L., Shao, G., 2015. Drone remote sensing for forestry research and practices. *J. For. Res*. 26, 791–797. https://doi.org/10.1007/s11676-015-0088-y
Thonicke, K., Venevsky, S., Sitch, S., Cramer, W., 2001. The role of fire disturbance for global vegetation dynamics: coupling fire into a Dynamic Global Vegetation Model. *Global Ecology and Biogeography* 10, 661–677. https://doi.org/10.1046/j.1466-822X.2001.00175.x

Tinkham, W.T., Swayze, N.C., 2021. Influence of Agisoft Metashape Parameters on UAS Structure from Motion Individual Tree Detection from Canopy Height Models. *Forests* 12, 250. https://doi.org/10.3390/f12020250

Tinkham, W.T., Swayze, N.C., Hoffman, C.M., Lad, L.E., Battaglia, M.A. Modeling the missing DBHs: influence of model from on UAV DBH characterization. *Forests* 13(12), 2077. https://doi.org/10.3390/f13122077

van der Werf, G.R., Randerson, J.T., Giglio, L., van Leeuwen, T.T., Chen, Y., Rogers, B.M., Mu, M., van Marle, M.J.E., Morton, D.C., Collatz, G.J., Yokelson, R.J., Kasibhatla, P.S., 2017. Global fire emissions estimates during 1997–2016. *Earth System Science Data* 9, 697–720. https://doi.org/10.5194/essd-9-697-2017

van Mantgem, P.J., Caprio, A.C., Stephenson, N.L., Das, A.J., 2016. Does Prescribed Fire Promote Resistance to Drought in Low Elevation Forests of the Sierra Nevada, California, USA? *Fire ecol* 12, 13–25. https://doi.org/10.4996/fireecology.1201013

Walker, R.B., Coop, J.D., Parks, S.A., Trader, L., 2018. Fire regimes approaching historic norms reduce wildfire-facilitated conversion from forest to non-forest. *Ecosphere* 9, e02182. https://doi.org/10.1002/ecs2.2182

Westlind, D.J., Kerns, B.K., 2021. Repeated fall prescribed fire in previously thinned Pinus ponderosa increases growth and resistance to other disturbances. *Forest Ecology and Management* 480, 118645. https://doi.org/10.1016/j.foreco.2020.118645

White, J.D., Ryan, K.C., Key, C.C., Running, S.W., 1996. Remote Sensing of Forest Fire Severity and Vegetation Recovery. *Int. J. Wildland Fire* 6, 125–136. https://doi.org/10.1071/wf9960125

Willis, J.L., Self, A.B., Siegert, C.M., 2022. Proceedings of the 21st Biennial Southern Silvicultural Research Conference (No. SRS-GTR-268). U.S. Department of Agriculture, Forest Service, Southern Research Station, Asheville, NC. https://doi.org/10.2737/SRS-GTR-268

Wilson, L. A., Spencer, R. N., Aubrey, D. P., O'Brien, J. J., Smith, A. M. S., Thomas, R. W., & Johnson, D. M. (2022). Longleaf Pine Seedlings Are Extremely Resilient to the Combined Effects of Experimental Fire and Drought. *Fire*, 5(5), Article 5. https://doi.org/10.3390/fire5050128

Woolsey, G. (2024). cloud2trees: Point Cloud Data to Forest Inventory Tree List. R package version 0.1.0. Retrieved from https://CRAN.R-project.org/package=cloud2trees

Zhang, J., Hu, J., Lian, J., Fan, Z., Ouyang, X., Ye, W., 2016. Seeing the forest from drones: Testing the potential of lightweight drones as a tool for long-term forest monitoring. *Biological Conservation* 198, 60–69. https://doi.org/10.1016/j.biocon.2016.03.027

CHAPTER 6 – CONCLUSION

6.1 Conclusion

This dissertation addresses critical gaps in the application of uncrewed aerial system (UAS) imagery for forest health assessment while addressing challenges to forest management. As disturbances increase in their frequency, severity, and spatial coverage, adaptive forest management provides a critical tool to combat forest and biodiversity loss. By leveraging the high spatial and temporal resolution of UAS imagery with machine learning modeling and tree physiology, this body of work advances our knowledge of how to assess forest health and resilience in multiple forest types.

In Chapter 2, I use band-equivalent reflectance (BER) data to examine the feasibility of detecting physiological stress in saplings under a variety of controlled drought conditions. This study converted BER into spectral bands available on a consumer-grade UAS to model both drought class and foliar moisture content using a variety of machine-learning models. This chapter achieved high accuracy using both classification and regression models and demonstrated the theoretical ability of UAS sensors to describe drought-stress in saplings. By integrating BER data to physiological stress, this chapter underscores the potential for UAS data to monitor tree health non-destructively.

Chapter 3 extended the models from Chapter 2 into natural forest sites in northern Colorado to test the scalability of lab-based models of FMC. This chapter highlighted the difficulties in adapting lab-based models such as increased within-crown variability, crown-to-crown shading, and the importance of choosing appropriate crown summarization techniques.

This chapter successfully models relative FMC across two sites and four dates using field-developed models from a consumer-grade multispectral UAS. The findings of this chapter highlight the importance of species, collection timing, and site-based knowledge for applying these models. Further, the difficulty in translating controlled experiments to natural ecosystems underscores the challenges that exist in applying remote sensing data to diverse forest types. Our site-based models of relative tree stress could be adapted and applied in multiple forest types to provide managers with site-specific models that meet their management needs.

In Chapter 4, I investigate the compounded effects of pre-fire drought intensity and subsequent fire on the recovery and mortality of *Pinus monticola* and *Pseudotsuga menziesii* saplings. Utilizing a toxicological dose-response framework, this study elucidates how varying levels of drought stress before fire events influence post-fire physiological responses and survival rates. The findings reveal that saplings experiencing severe pre-fire drought conditions exhibit higher mortality and reduced recovery post-fire, underscoring the critical need to consider antecedent environmental stressors in fire management and post-fire recovery strategies. This research bridges the gap between controlled experimental insights and practical applications, offering valuable guidance for adaptive management in fire-frequent forests.

Lastly, Chapter 5 demonstrated the utility of applying UAS data to assess crown volume scorch (CVS) following a prescribed fire. Specifically, this study evaluates how the timing of post-fire scorch assessment, the inclusion of pre-fire reference imagery, and available spectral range impact model accuracy of CVS. Results demonstrate that the most accurate predictions of CVS should be made 1-day post-fire, but with minimal accuracy loss up to 35-days post-fire, and

that a variety of spectral bands and indices can be used. Additionally, the inclusion of pre-fire reference imagery showed little or no improvement over modeling from just post-fire imagery. The findings of this chapter underscore the ability of UAS data to assess physiological changes (i.e., crown volume scorch) before they are ocularly visible, providing a practical, cost-effective approach for adaptive forest management. The ability to classify CVS quickly could provide managers with actionable data that can be used to evaluate treatment effectiveness and to refine future prescription patterns.

This dissertation provides frameworks to produce actionable insights that can inform and evaluate site-based adaptive management decisions such as thinning and prescribed fire. UAS provide ultra-high spatial resolution data with a flexible temporal resolution that can be used to monitor forests by capturing dynamic indicators of tree stress. The models and approaches developed in this dissertation could be integrated into operational workflows wherein managers can better predict and mitigate the impacts of management actions on site resilience to both drought and fire. Ultimately, the application of the models in this work can be applied to improve forest resilience and reduce the likelihood of forest conversion following disturbances.

This research offers significant advancements in our understanding of forest health monitoring with UAS, while highlighting areas for future research and improvement. The transferability of lab-developed models to natural forests highlighted challenges with model scalability. Future research should consider testing additional species and lab-based assessments of tree physiological health, such as stomatal conductance and vapor pressure deficit, to better understand the relationships between sapling physiology and spectral

reflectance and how those relationships change through a tree's lifetime. The importance of species in the models from Chapter 3 underscores potential difficulties with applying these models to new sites or other forest types. Further work is needed to test the application of these models in other forest types and across additional dates to understand the variability of FMC through time so these models can be optimized to inform management decision-making. As these sensors advance, it will be a challenge for the field to overcome normalization and spatial matching issues to improve the reliability of multi-temporal UAS imagery for forest monitoring. The models in Chapters 3 and 5 could potentially be improved with the inclusion of hyperspectral, joint analysis of the three-dimensional structural and multispectral data, or by exploring how UAS can be used to train satellite imagery to provide landscape patterns of tree stress.

In summary, this dissertation demonstrates the potential of UAS data to inform forest management aiming to improve forest resilience. By integrating lab-based modeling with UAS and field data, this dissertation provides actionable insights to improve the ecological integrity of forest management. As forests are challenged by increasingly variable climatic conditions and face changing disturbance regimes, the combination of ecologically informed data collection and modeling approaches is an essential tool to protect forest integrity.